Petrology and Geochemistry of Cenozoic Volcanic Rocks from Northern Kyushu: Influence of Philippine Sea Plate on the Subarc Mantle Composition

Masaya Miyoshi

Doctoral Dissertation

Submitted to the Graduate School of

Science and Technology, Kumamoto University

March 25, 2008

To my parents

Abstract

Northern Kyushu, characterized by the subduction of Philippine Sea plate slab with different ages (a young Shikoku basin and a old West Philippine basin) beneath Eurasian plate, forms a complex portion of Southwestern Japan arc. In order to evaluate the spatial and temporal influences of slab-derived fluids from these two contrasting oceanic plates on the subarc mantle, the author addresses the following two topics for discussion.

1. Boron contents in basaltic rocks from northern Kyushu.

The author determined boron (B) contents in basaltic rocks from ten volcanoes and three old volcanic fields which erupted after 11 Ma until present. Since B is distinctly concentrated into slab-derived fluids among the earth's materials, the author attempted to estimate the spatial influences of subduction on the subarc mantle composition from the interpretation of B data in basaltic rocks.

Old (11-6 Ma) basaltic rocks represent low B/Sm (0.5-1.3), B/Zr (0.02-0.05) and B/Nb (0.2-0.5) ratios, suggesting little influence of slab-derived fluid on their source mantle. Back-arc basaltic rocks occurring throughout the observed period similarly show little influence of subduction. In contrast, volcanic products from young Aso volcano, located at the volcanic front, show a strong influence of slab-derived fluid on their source mantle, as indicated by high B/Sm (1.6-4.3), B/Zr (0.07-0.16) and B/Nb (1.4-3.7) ratios. After 6 Ma, the volcanic arc segment containing Aso volcano is associated with the subduction of cold West Philippine basin, thus B-rich fluid was probably added to the subarc mantle. Yufu, Tsurumi and Kuju volcanoes located at the same volcanic front, however show low B/Sm (0.9-1.9), B/Zr (0.04-0.07) and B/Nb (0.5-0.9) ratios. This implies that the subduction of hot Shikoku basin released B-rich fluids from the slab at the shallow depth; thereby it becomes depleted with B and other subduction components by the time it reaches the volcanic front.

2. Temporal changes of the composition of magma source beneath Aso area.

Aso volcano is located on the volcanic front of Kyushu arc. To investigate the temporal changes of subduction signatures, we analyzed B and other major and trace element compositions in volcanic products which erupted since 4 Ma in Aso area.

The author grouped the volcanic activities of Aso area into the following three stages on the basis of geochemistry of mafic magmas. 1) 4-3 Ma: those of High-magnesian andesites (HMA); 2) 2-0.4 Ma: those of Adakitic andesites, Island-arc-type andesites and high-alumina basalts (HAB); 3) 0.3-0 Ma: those of Island-arc-type andesites and HAB.

The ratios of B/Sm (0.4-1.0) and B/Zr (0.01-0.02) in the HMAs are significantly lower than those of the HABs (1.3-5.0 and 0.06-0.17, respectively). The B/Nb ratios in the HMAs (0.1-0.2) are similar to those of the mantle values (0.05-0.5). On the other hand, B/Nb ratios (1.4-4.0) in the HABs overlap with those of basalts from cool subduction zones (Kurile and NE-Japan) where fluid-induced melting of the mantle wedge dominantly occurs. The

existence of adakitic andesite probably indicates the subducted slab was partially molten beneath Aso area between 2 and 0.4 Ma.

These observations probably indicate the progressive metasomatism of the magma source. This temporal change was probably caused by the addition of fluid-flux to the mantle beneath Aso area which is associated with the initiation of subduction of the Philippine Sea plate between 4 and 2 Ma.

Contents

Chapter 1

Boron contents in basaltic rocks from northern Kyushu

Chapter 2

Temporal changes of the composition of magma source beneath Aso area

Chapter 1

Boron contents in basaltic rocks from northern Kyushu

1.1 Introduction

Boron is a key element in the evaluation of slab influences on the subarc mantle compositions in subduction zones because this element is enriched in altered oceanic crust and sea floor sediments (e.g., Ishikawa and Nakamura, 1993; Smith et al., 1995) and is selectively partitioned into fluid phase during fluid-flux melting at the base of the mantle wedge (e.g., Moran et al., 1992; Bebout et al., 1999). Thus, the high boron content observed in the arc basaltic rocks is a strong evidence for recycling of the oceanic slab to the arc crust. In contrast, OIB (oceanic island basalt) and MORB (mid-ocean ridge basalt) have low boron contents (Ryan and Langmuir, 1993; Ryan et al., 1996; Leeman and Sisson, 1996; Chaussidon and Jambon, 1994; Chaussidon and Marty, 1995; Sun and McDonough, 1989) because they have no interaction with the subducting slab.

In order to identify the involvement of the subduction components in the mantle wedge, we employ fluid-mobile/immobile element ratios (B/Sm, B/Zr, B/Nb and Ba/Nb). Previous studies (Leeman and Sisson, 1996; Ishikawa and Nakamura, 1994; Ishikawa and Tera, 1997; Ishikawa et al., 2001; Tonarini et al., 2004; Sano et al., 2001) indicate that B/Nb, B/Sm and B/Zr are sensitive indicators of slab involvement because of the following evidences: 1) Since B, Nb, Sm and Zr have similar solid/melt distribution coefficients under upper mantle and crustal conditions, B/Nb, B/Sm and B/Zr are not significantly affected by partial melting and crystal fractionation; 2) B and the other three elements have entirely different chemical behaviors in fluid-related processes. B has a significantly higher mobility than Nb; 3) The variation of B/Nb does

not reflect the crust assimilation process because the ratio of B/Nb in the crust is negligibly low (continental crust: 0.4–0.7; Wedepohl, 1995).

Across-arc variations of the B/Nb ratios in the basalts from the cool subduction zone are described as a smooth depletion trend (Ishikawa and Tera, 1997). Such continuous depletion trends of the B/Nb ratios reflect the gradual depletion of volatiles and fluid-mobile elements in the dehydrating slab during subduction zone metamorphism (Peacock and Herving, 1999). The continuous dehydration reaction of the subducted slab is demonstrated by the experimental study conducted by Wunder et al. (2005).

On the other hand, recent petrological and geochemical studies have reported the occurrence of arc basalts showing weak slab fluid contributions from the warm subduction zones (Leeman et al., 2004; Hochstaedter et al., 1996). The smooth depletion trend of the across-arc variation of B/Nb is not observed in such warm subduction zones. This indicates that the slab-derived fluid is not transported to the backarc region by the hot slab because large amounts of H_2O and fluid-mobile elements are expelled from the slab at shallow depths in the forearc due to the extremely high geotherm (Peacock and Wang, 1999; Iwamori, 2007; Leeman et al., 2004; Hochstaedter et al., 1996).

Japan arc is characterized by the subduction of two different oceanic plates (Fig. 1.1): the old and cold Pacific plate (130 Ma, Pitman et al., 1974), which is related to the subduction volcanism of NE-Japan, Kurile and Izu-Mariana arcs, and the Philippine Sea plate, which subducts beneath SW-Japan and Ryukyu volcanic arcs. The Philippine Sea plate is further divided into two different segments by the NW-SE trending Kyushu-Palau ridge. The northern segment (= Shikoku basin) is young and hot (15–26 Ma; Okino et al., 1994), whereas the southern segment is old and cold (37–115 Ma; Shibata et al., 1977; Hilde and Lee, 1984; Hickey-Vargas, 2006) (Fig. 1.1). Northern Kyushu, our study area (Fig. 1.2), is characterized by the subduction of these two segments of the Philippine Sea plate (Kimura et al., 2005).

In northern Kyushu, the subduction of the Philippine Sea plate commenced at 6–4 Ma (Kamata and Kodama, 1994). Prior to the subduction event, the volcanism in northern

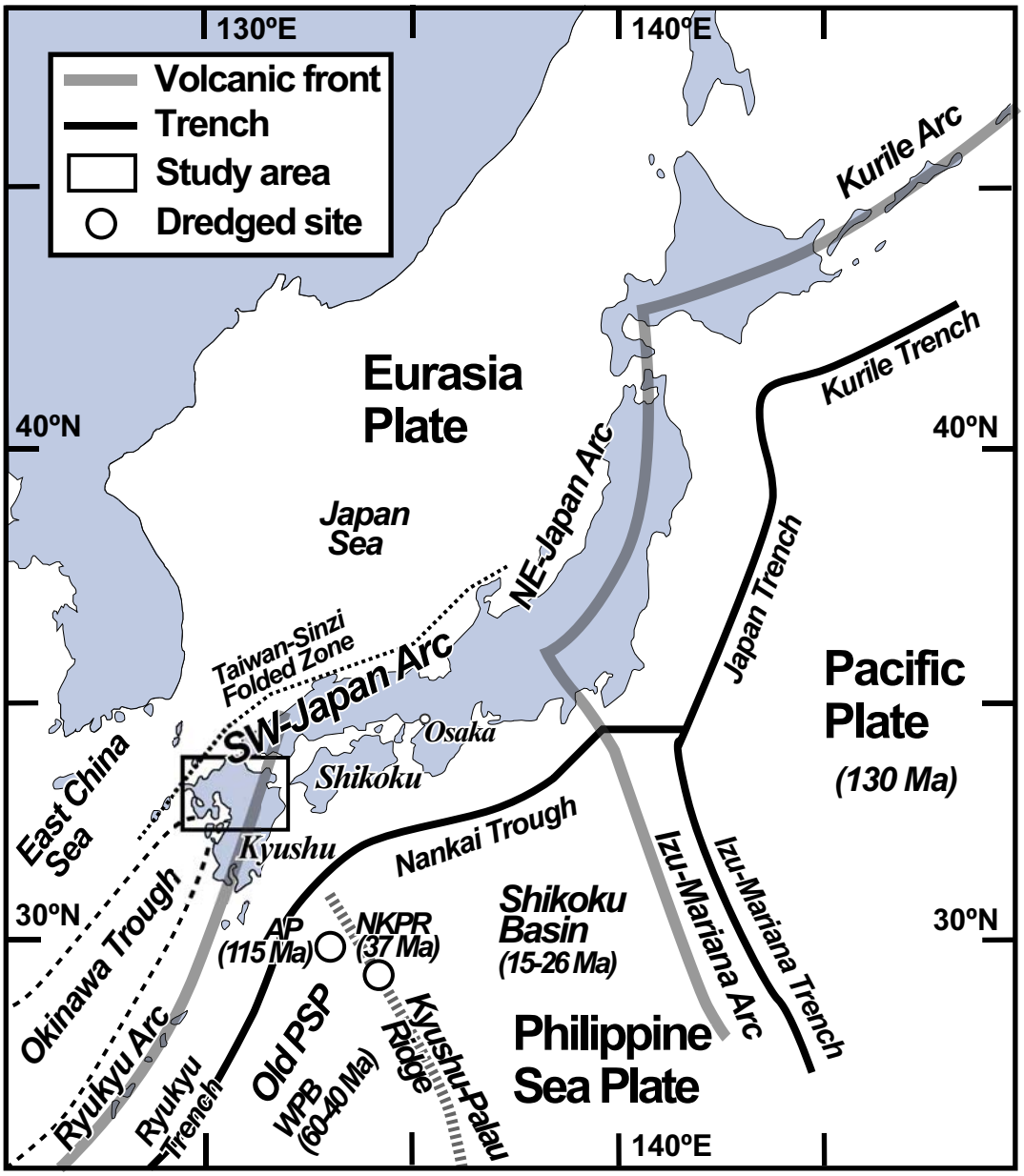

Fig. 1.1

Index map of the Japanese Islands and tectonic settings. Data for age of Pacific plate is from Pitman et al. (1974), and those of Philippine Sea plate are from Okino et al. (1994), Shibata et al. (1977), Hilde and Lee (1984) and Hickey-Vargas (2006). PSP: Philippine Sea plate, AP: Amami Plateau, NKPR: Northern Kyushu-Palau ridge.

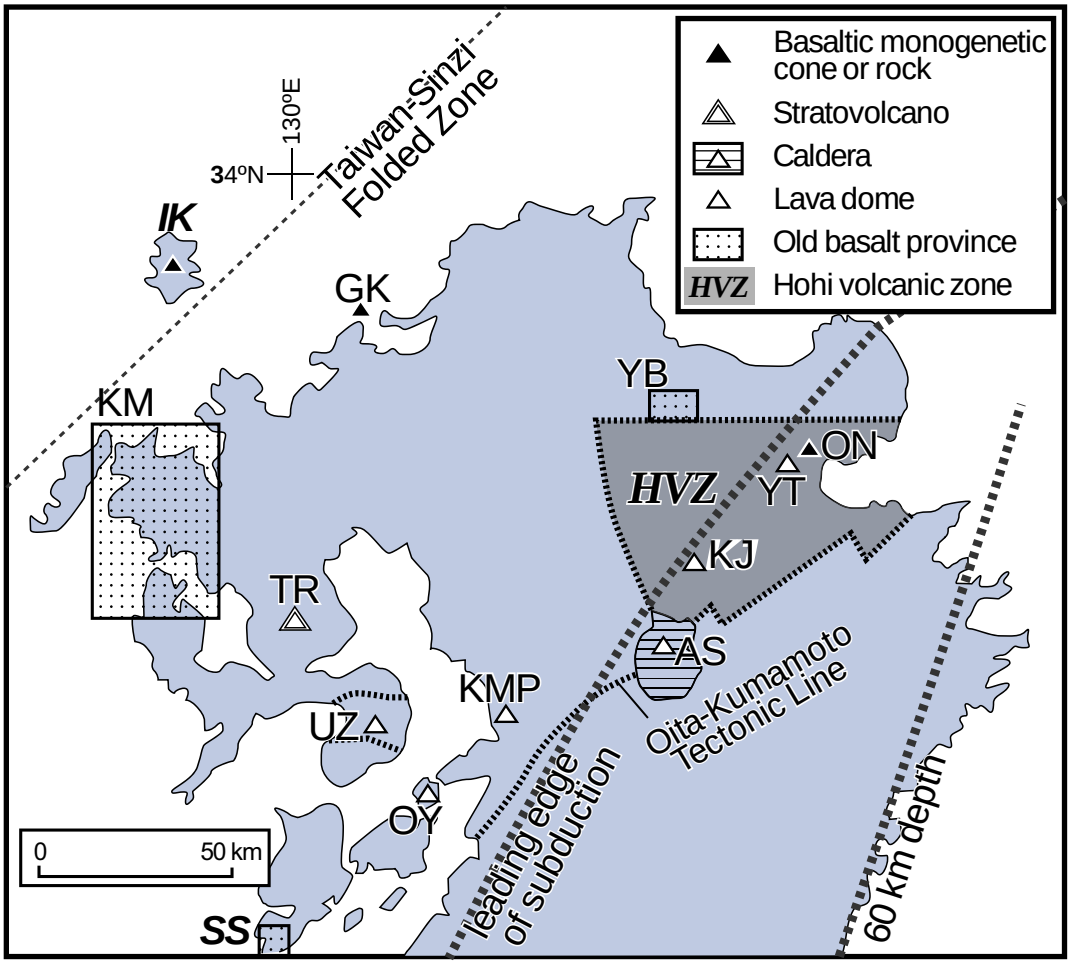

Fig. 1.2

Sample Location and main tectonic setting of the northern Kyushu (modified from Kamata and Kodama, 1994). HVZ (gray) = Hohi volcanic zone (Kamata, 1989). The leading edge of the subducted Philippine Sea plate is from Nakada and Kamata (1991). Dotted line labeled 60 km depth represents the depth contour of the Wadati-Benioff zone (Ishida, 1992). The Taiwan-Sinzi Folded Zone is from Uto et al. (2004). KM: Kita-Matsuura, SS: Shimoshima, YB: Yabakei, IK: Iki, GK: Genkai, TR: Tara-dake, UZ: Unzen, OY: Oyano, KMP: Kimpo, AS: Aso, KJ: Kuju, YT: Yufu, Tsurumi, ON: Oninomi.

Kyushu was dominated by the activity of OIB-like basalt (Nakada and Kamata, 1991). The subduction of the Philippine Sea plate from 6 Ma caused the development of a large graben system (HVZ in Fig. 1.2) and the activity of the arc-type magma in the frontal arc region (Kamata, 1989). Nakada and Kamata (1991) suggested that the arc-type basaltic products in the frontal arc that are younger than 6 Ma are associated with the subduction of the Philippine Sea plate. However, the oceanic slab contribution of these two contrasting segments to the arc-type magma genesis in the northern Kyushu area is still debatable. Although Zhao et al. (2000) and Iwamori (2007) indicated the existence of a descending young Shikoku basin beneath northern Kyushu on the basis of geophysical and petrochemical data; this is remain incompletely examined by the petrological and geochemical data. Therefore, I present a new boron data for the northern Kyushu basalts for the investigation of the subduction contributions of the two contrasting segments to the arc-type magma genesis.

1.2 Tectonic settings in northern Kyushu

Kyushu is characterized by the subduction of Philippine Sea plate. This oceanic plate descends into the mantle beneath Kyushu with a dipping angle of approximately 30°, and then suddenly steepens at a depth of 70 km (Wang and Zhao, 2006). In northern Kyushu, the Wadati-Benioff Zone (WBZ) is detected at a depth of 140 km beneath the volcanic front (Nagamune and Tashiro, 1989). However, the WBZ is not detected beneath the backarc volcano area.

Two pronounced low-velocity anomaly zones are visible in the mantle wedge beneath Kyushu: One zone exists beneath the active volcanoes in northern Kyushu, and the other exists beneath those in southern Kyushu. The low-velocity anomaly zone in the mantle wedge extends to the forearc side of the volcanic front in northern Kyushu; however, this does not happen into southern Kyushu (Zhao et al., 2000). Iwamori (2007) interpreted this tomographic feature as follows. The geotherm in the forearc beneath northern Kyushu is higher than that in southern Kyushu due to the subduction of the young (and hot) Shikoku basin (<26 Ma). On the other hand, southern Kyushu is

characterized by the subduction of the old (and cold) West Philippine basin. In northern Kyushu, dehydration probably occurs on the forearc side due to a high geotherm along the young slab (Zhao et al., 2000). The descending slab releases a large amount of H_2O when the hydrated metabasalt transforms to eclogite at approximately 500 °C (Peacock and Wang, 1999). The estimated temperature along the slab/mantle interface is 500 °C at a 50-km depth for SW Japan (Peacock and Wang, 1999). These geophysical studies indicate that a significant amount of H_2O is expelled from subducted slab on the forearc side in northern Kyushu because of the young (and hot) slab subduction.

A tomographic low-velocity anomaly zone is also observed beneath the backarc of Kyushu. This low-velocity zone under the west of Kyushu indicates a mantle upwelling around the northeastern edge of the extending Okinawa trough (Fig. 1.1; Sadeghi et al., 2000). Previous studies (Nakada and Kamata, 1991; Uto et al., 2004; Kimura et al., 2005) suggested that the backarc volcanism in Kyushu was not related to the subduction of the Philippine Sea plate but was related to an extensive mantle upwelling due to the opening of the Okinawa Trough (Sibuet et al., 1995) along the eastern Asian margin during the Cenozoic; this is because the backarc volcanism is characterized by OIB-type basalt activity (Kimura et al., 2005). This is consistent with the absence of WBZ beneath the backarc volcano area (Nagamune and Tashiro, 1989). However, a tomographic low-velocity anomaly is observed in the depth range of 20–120 km beneath Unzen volcano, which is located on the backarc side (UZ in Fig. 1.2) (Wang and Zhao, 2006). This low-velocity zone obliquely extends from the frontal seismic slab to under UZ. This suggests a possibility of slab components released from the subducting slab in addition to a widely accepted mantle upwelling for the magma origin of UZ (Wang and Zhao, 2006).

1.3 Volcanisms in northern Kyushu

The modern SW Japan volcanism closely relates to the reinitiation of subduction associated with backarc basin opening that commenced at 17 Ma, and it is

characterized by the complex activity of OIB, IAB (Island arc basalt), HMA (high-magnesian andesite) and adakite-type magmas (Kimura et al., 2005) from 15 to 0 Ma as follows: In the northern Kyushu frontal arc, OIB-like basalt lavas erupted in the Yabakei area (Fig. 1.2) at 8 Ma (Kakubuchi and Matsumoto, 1990; Fig. 1.3). Volcanism related to the Philippine Sea plate subduction commenced at 6–4 Ma in the northern Kyushu (Kamata, 1989; Kamata and Kodama, 1994). This coincided with the resumption of the arc-type volcanic activity in the Ryukyu arc (Shinjo et al., 2000). The change in the direction of subduction (NNW to NW) caused a dextral fault movement along the Oita-Kumamoto tectonic line (Fig. 1.2) and formed a graben system of 70 by 40 km (Hohi volcanic zone, HVZ in Fig. 1.2; Kamata, 1989) that was extended in the N-S direction (Kamata and Kodama, 1994). The HVZ is filled with voluminous volcanic materials (>5000 km^3) erupted since approximately 6 Ma (Kamata, 1989; Kamata and Kodama, 1994). Calc-alkalic HMAs erupted at 6–3 Ma in the northern and southern edges of the HVZ (Nakada and Kamata, 1991; Kakubuchi et al., 1995). The northern Kyushu HMA volcanism may be related to the melting of subducted Philippine Sea plate sediments (Kita et al., 2001; Nakada and Kamata, 1991) by the addition of heat from the upwelling backarc asthenospheric mantle associated with the opening of the Okinawa Trough (Kimura et al., 2005). Yufu-Tsurumi volcanoes (Fig. 1.2) produced adakite-like andesites (Sugimoto et al., 2006) at 35–6 ka (Kobayashi, 1984; Fig. 1.3). This probably indicates that the subducting Philippine Sea plate is partially molten beneath northeast Kyushu (Sugimoto et al., 2006). High-alumina IAB-like basalts erupted from Kuju and Aso volcanoes (KJ and AS in Fig. 1.2) at 2–0 Ma (Nakada and Kamata, 1991; Fig. 1.3). Nakada and Kamata (1991) indicated that the composition of the basaltic rocks from the HVZ entirely varied from the OIB-type to the IAB-type with time. However, the OIB-type Oninomi basalt exceptionally erupted in the frontal arc at 22–6 ka (Ohta et al., 1992; ON in Fig. 1.2).

In the northern Kyushu backarc, OIB-like basalt activity commenced at 15 Ma. The activity of the northwestern Kyushu basalts relates to the backarc opening of the East China and Japan Seas at 15 Ma (Uto et al., 2004), and has occurred independent of the Philippine Sea plate subduction. These basalts align as islands along the Taiwan-Sinzi

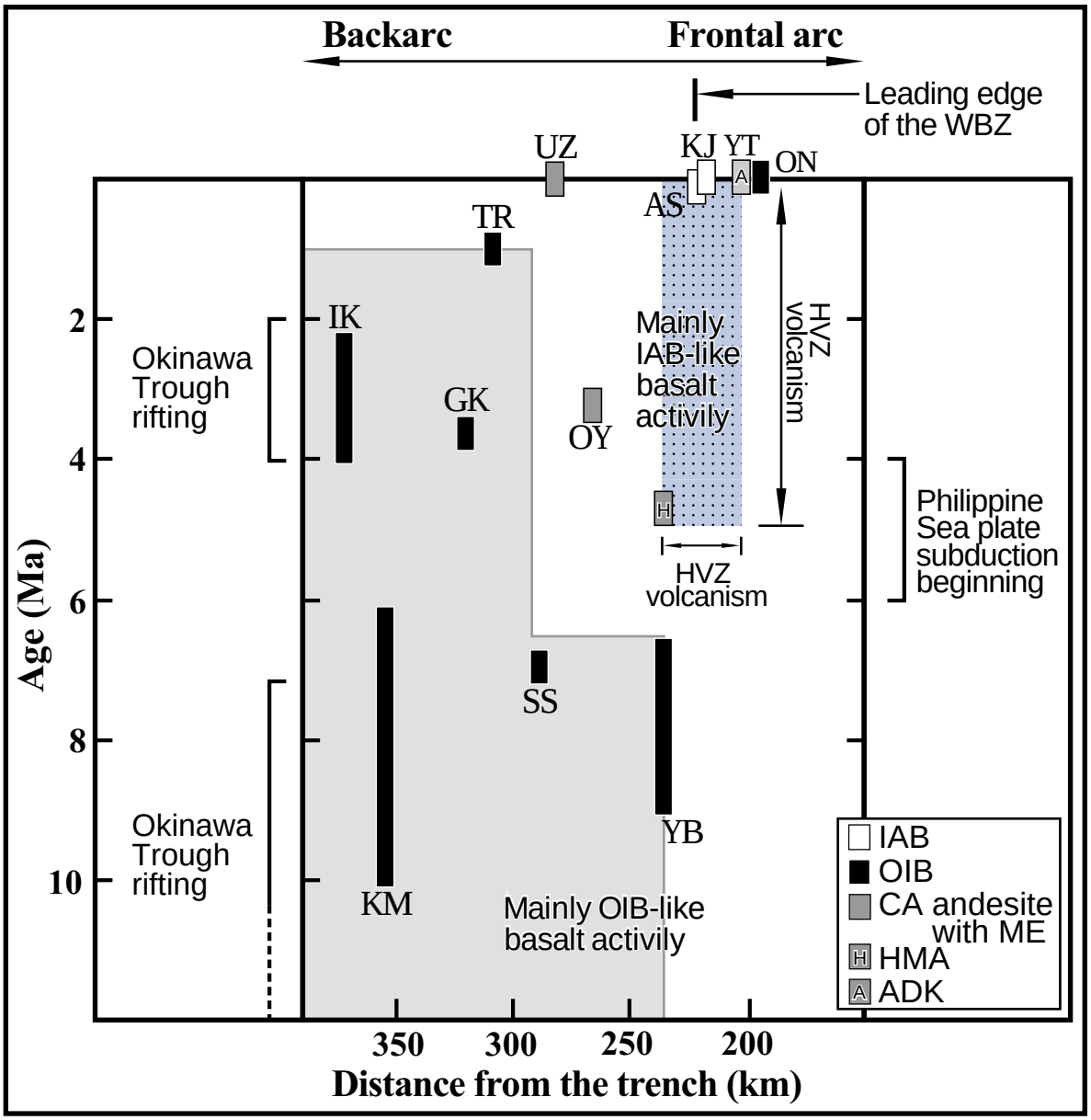

Fig. 1.3

Spatial and temporal distributions of the northern Kyushu basalts since 11 Ma. Each shaded and dotted areas show OIB and IAB-like basalt activities, respectively. Data for volcanism are from the following sources: Matsui and Shibata (1976), Nagao et al. (1992), Kakubuchi and Matsumoto (1992), Yokose et al. (1999), Matsumoto et al. (1992), Sano (1995), Ogata and Takaoka (1991), Ono and Watanabe (1985), Kamata and Kobayashi (1997), Ohta et al. (1990, 1992); and for tectonics: Kamata and Kodama (1994), Uto et al. (2004), Sibuet et al. (1995). Vertical bars with bold italics indicate the samples which analyzed in this study and with 'A' and 'H' show adakite (Sugimoto et al., 2006) and high-Mg andesite (Kakubuchi et al., 1995), respectively. IAB: Island Arc-type Basalt, OIB: Oceanic Island-type Basalt, CA: Calc-alkaline, ME: Mafic Enclave, HMA: High-Magnesium Andesite, ADK: Adakite, WBZ: Wadati-Benioff Zone. Other abbreviations are the same as in Fig. 1.1 and 1.2.

Folded Zone (Fig. 1.1, 1.2); which is a Miocene extensional graben (Uto et al., 2004). The OIB-like basalts from Kita-Matsuura (KM) area and Iki (IK) island (Fig. 1.2) erupted at 11–6 Ma (Matsui and Shibata, 1976) and 4–2 Ma (Sano, 1995), respectively (Fig. 1.3). The monogenetic volcanoes of the OIB-like basalts, which are scattered along the northern Kyushu coastal area, erupted at 4–1 Ma (Hoang and Uto, 2003). The OIB-like basalts erupted from Genkaijima (GK in Fig. 1.2) at 4–3 Ma (Matsumoto et al., 1992; Fig. 1.3) Minor amounts of OIB-like basalts erupted between 10 and 7.5 Ma on the Kyushu backarc side (Nagao et al., 1999; Kimura et al., 2005). In the Shimoshima (SS) area, OIB-like basalts erupted at 7 Ma (Nagao et al., 1992; Fig. 1.3). During this time, the Philippine Sea plate subduction was very slow (<1 cm/year; Kimura et al., 2005) or almost ceased (Kamata and Kodama, 1994). The subduction of the Philippine Sea plate accelerated (4 cm/year) at 6–4 Ma, and the opening of the Okinawa Trough (4–2 Ma; Sibuet et al., 1995) coincided during this time. The OIB-like basalts coexisted with the island-arc-type calc-alkalic andesites at 5–1 Ma in the southwestern part of northern Kyushu (Yokose et al., 1999). The OIB-like basalts and island-arc-type calc-alkaline andesites erupted from Tara-dake volcano (TR in Fig. 1.2) at 1 Ma (Ikawa and Nagao, 1996; Fig. 1.3). Oyano (OY), Unzen (UZ) and Kimpo (KMP) volcanoes (Fig. 1.2) produced island-arc-type calc-alkalic andesite lavas at 3–0 Ma (Yokose et al., 1999; Takai et al., 1984; Fig. 1.3).

1.4 Samples and Methods

Sixty-four samples were collected from a wide region of northern Kyushu (Fig. 1.2). They included fifty basaltic rocks which erupted at 11–0 Ma. The basalts which erupted before the Philippine Sea plate subduction (11-6 Ma) are as follows: Backarc basalts = KM (10.6–6.1 Ma; Matsui and Shibata, 1976) and SS (6.79–6.99 Ma; Nagao et al., 1992); Frontal arc basalts = YB (7.91 ± 1.38 Ma; Kakubuchi and Matsumoto, 1990). The basalts which erupted after the Philippine Sea plate subduction (6–0 Ma) are as follows: Backarc basalts = OY (5–3 Ma, Yokose et al., 1999), GK (3–4 MA; Matsumoto et al., 1992), IK (2.1–4.3 Ma; Sano, 1995), TR (1–0.45 Ma; Ogata and

Takaoka, 1991) and UZ (1990–1994); Frontal arc basalts = AS (<90 ka; Ono and Watanabe, 1985; Miyoshi et al., 2005), KJ (7–11 ka; Kamata and Kobayashi, 1997), YT (<6 ka; Ohta et al., 1990) and ON (22–6 ka; Ohta et al., 1992).

The samples from YT, UZ and OY are mafic enclaves (>50 mm) included in andesitic host rocks, and those from KJ are scoria and mafic enclaves. Six crustal xenoliths (gneiss, gabbroic and granitic rocks; Yokose and Yamamoto, 1996) included in the host andesite lava (<1.12 Ma; Takai et al., 1984) were sampled from KMP (Fig. 1.2).

The data for boron and the other elements are presented in Table 1.1. All the analyzed samples were fresh because phenocryst phases do not show alterations into secondary minerals. Thus, the influence of sample alteration on these data appears negligibly small.

The whole-rock chemical compositions of the samples were determined by X-ray fluorescence (XRF) on flux-fused disks with a Rigaku RIX2100 spectrometer at Fuji Tokoha University and a Philips PANalytical MagiX PRO spectrometer at Kitakyushu Museum of Natural History and Human History. An acceptable accuracy of analysis is maintained using the nine Japanese (JB-1a, JB-2, JB-3, JA-2, JA-3, JR-1, JG-1a, JG-2 and JGb-1) standards and seven international standards (GS-N, DR-N, BCR-2, DNC-1, DTS-2b, BHVO-2 and AGV-2) for calibration. The details of the analytical procedures are described by Sano (2002) and Mori and Mashima (2005).

Boron and other selected trace elements (Sm, Gd) were determined by neutron-induced prompt gamma-ray analysis (PGA) at the thermal neutron beam guide of the JRR-3M reactor, Japan Atomic Energy Research Institute by using the facilities described by Yonezawa (1993). The powdered samples (0.8 g) were dried for more than 24 h at 110 °C in an oven and cold-pressed into disks (12 mm in diameter and 2–3 mm in thickness). These disks were heat-sealed in 25-μm thick fluorinated ethylenepropylene resin films with sizes smaller than 14 × 14 mm^2. A Compton suppression PGA spectrum was accumulated for 1000–7200 s. Geological Survey of Japan standards JB-1 and JB-2 were used to calibrate the determination of the B, Sm and Gd contents. To correct the variations in the count rate caused by neutron flux

fluctuation and sample geometry, all the count rates of B, Sm and Gd were corrected by the Si factor (i. e. the Si count rate divided by the Si content of the same sample). The details of the analytical procedures have been described by Sano et al. (1999), (2004).

1.5 Results

1.5.1 Major and trace element compositions of the northern Kyushu basalts

The major and trace element contents and phenocryst assemblages obtained in this study are listed in Table 1.1. The northern Kyushu basalts are divided into two types of magmas based on their SiO_2 and total alkali compositions (Fig. 1.4): alkalic and tholeiitic basalts. In NW-Kyushu, the older (11–6 Ma) KM basalts are classified into both alkalic and tholeiitic affinities (Fig. 1.4a). We call them KM-A basalts and KM-T basalts hereafter. The younger (6–0 Ma) IK and GK basalts have alkalic compositions (Fig. 1.4b). On the central Kyushu backarc side, the older SS basalts exhibit tholeiitic compositions (Fig. 1.4c). The younger UZ and OY basalts exhibit the tholeiitic compositions, although their host andesites exhibit calc-alkalic compositions (Fig. 1.4d). In Fig. 1.4d, the TR basalts are classified into both alkalic and tholeiitic affinities. Hereafter, we will call them TR-A basalts and TR-T basalts. On the frontal arc side, the older YB basalts are plotted in the tholeiitic field (Fig. 1.4e). The younger YT, ON, KJ and AS basaltic lavas and enclaves are plotted in the tholeiitic field. The host andesite lavas of YT have calc-alkalic compositions (Fig. 1.4f).

The trace element characteristics of the basalts are simply illustrated by normalizing their trace element contents to those of the normal-MORB (Fig. 1.5; Sun and McDonough, 1989). In NW-Kyushu, the old basalts (KM) exhibit patterns that are similar to those of OIB. The KM-T basalts have poorer HFSE and LILE compositions and richer B contents than the KM-A basalts (Fig. 1.5a). Both the young basalts (GK and IK) exhibit patterns that are similar to those of OIB (Fig. 1.5b, c). In central Kyushu, the old basalts (SS) show OIB-like patterns (Fig. 1.5d). In the younger stages,

both TR-T and TR-A basalts exhibit patterns similar to those of OIB (Fig. 1.5e). These TR-T basalts are slightly enriched in B and depleted in Nb as compared with the TR-A basalts. UZ basalts exhibit OIB-like patterns (Fig. 1.5f). Although the patterns of the host andesites of UZ are similar to those of UZ, they are slightly enriched in B compared with the latter. The patterns of the UZ basalts are similar to those of the TR-T basalts (Fig. 1.5e, f). OY basalts represent OIB-like patterns. In contrast, their host andesites represent IAB-like patterns (Fig. 1.5f). On the frontal arc side, the old basalts (YB) have the compositions similar to OIB (Fig. 1.5g). In the younger stages, the ON basalts exhibit OIB-like patterns (Fig. 1.5h). On the other hand, AS, YT and KJ basalts exhibit patterns similar to the IAB (Fig. 1.5h, i). The host andesites of YT also exhibit IAB-like patterns.

Most of the backarc basalts are plotted in the OIB-MORB array (Leeman et al., 1990; Leeman et al., 2005; Fig. 1.6). The KM-T and TR-T basalts have lower Nb/Zr ratios than the KM-A and TR-A basalts. On the other hand, all the frontal arc basalts except for the YB and ON are slightly enriched in the subduction components, as illustrated by the low Nb/Zr and elevated Ba/Zr ratios. Although YB and ON basalts are also distributed in the frontal arc region, they have Nb/Zr and Ba/Zr ratios similar to the backarc basalts, which have no slab contribution (Fig. 1.6). As an exception, the UZ basalts exhibit both the backarc and frontal arc features of the Nb/Zr and Ba/Zr ratios (Fig. 1.6).

1.5.2 Across-arc variations in subduction components

Between 11 and 6 Ma, the volcanism in northern Kyushu was dominated by OIB-like basalt activities. The across-arc variations in B/Sm, B/Zr, B/Nb and Ba/Nb ratios for these old basalts are subdued (Fig. 1.7). The backarc KM-T basalts have higher values and wider ranges of B/Sm (0.5–1.3), B/Zr (0.02–0.05) and B/Nb (0.2–0.5) as compared with those of KM-A (<0.5; <0.01; <0.1). All the old basalts have similar B/Sm, B/Zr, B/Nb and Ba/Nb ratios (Fig. 1.7). The B/Nb values of these basalts are similar to the mantle values (0.05–0.5; Ryan et al., 1996; Fig. 1.7).

Table 1.1
Major and trace element contents of basaltic rocks from northern Kyushu

Sample No.	KM02	KM03	KM05	KM06	KM07	KM08	KM09	GG01
Location [a]	KM	KM	KM	KM	KM	KM	KM	SS
Sample type [b]	LV	LV	LV	LV	LV	LV	LV	LV
D (km) [c]	203	203	203	203	203	203	203	137
Phenocryst assemblage [d]	OlCpPl	OlCpPl	OlCpPl	OlCpPl	OlCpPl	OlCpPl	OlCpPl	OlCp
SiO_2 (wt. %)	51.01	48.05	51.13	48.42	50.89	47.56	47.92	52.70
TiO_2	1.42	1.97	1.30	1.20	1.37	2.57	2.31	1.24
Al_2O_3	15.13	16.78	14.57	13.59	14.43	14.98	16.73	14.92
Fe_2O_3	10.18	12.13	12.94	11.44	12.26	13.84	10.88	10.46
MnO	0.15	0.16	0.17	0.16	0.19	0.17	0.17	0.16
MgO	8.62	6.01	6.97	11.20	7.63	6.58	6.29	8.44
CaO	8.49	9.66	8.06	9.09	9.16	8.62	7.44	9.19
Na_2O	2.87	2.97	2.66	2.40	2.47	3.08	3.14	2.95
K_2O	1.10	0.82	1.14	0.72	0.50	1.20	2.53	0.68
P_2O_5	0.22	0.36	0.15	0.17	0.16	0.33	0.53	0.25
Total	99.19	98.90	99.07	98.39	99.06	98.94	97.92	100.98
V (ppm)	199	172	187	182	237	209	196	208
Cr	106	225	553	300	136	73	94	549
Ni	61	141	242	87	75	47	61	162
Rb	29	18	26	18	17	22	59	8
Sr	345	458	187	357	231	365	579	355
Y	31	21	22	19	59	25	23	34
Zr	136	123	114	93	88	171	274	118
Nb	15	18	13	10	9	28	41	11
Ba	276	271	171	233	119	357	683	258
B (ppm) [e]	6.7	1.0	4.5	1.6	1.9	0.1	2.6	1.4
error	0.2	0.1	0.2	0.1	0.1	0.1	0.4	0.1
Sm [e]	5.31	4.32	3.59	3.42	5.79	5.56	5.64	5.54
error	0.22	0.16	0.17	0.14	0.23	0.17	0.65	0.28
Gd [e]	22.50	16.20	14.10	13.30	31.50	21.30	22.40	6.25
error	0.80	0.55	0.52	0.47	1.10	0.69	1.48	0.18
XRF lab. [f]	1	1	1	1	1	1	1	2

Table 1.1
Continued

Sample No.	GG02	YB01	YB02	YB03	IK218	IK565	IK790	GK01
Location [a]	SS	YB	YB	YB	IK	IK	IK	GK
Sample type [b]	LV	LV	LV	LV	LV	LV	LV	LV
D (km) [c]	137	86	86	86	221	221	221	319
Phenocryst assemblage [d]	OlCp	OlCpPl	OlCpPl	OlCpPl	Ol	OlCpPl	OlPl	OlCpPl
SiO_2 (wt. %)	52.46	52.01	51.88	52.50	46.61	48.75	51.05	50.51
TiO_2	1.21	0.77	0.77	0.78	2.77	2.25	1.81	1.87
Al_2O_3	14.68	15.99	15.90	16.01	16.05	16.81	17.07	16.88
Fe_2O_3	10.23	8.63	8.53	8.09	9.64	10.41	9.39	11.07
MnO	0.16	0.15	0.15	0.14	0.17	0.17	0.14	0.16
MgO	8.38	9.59	10.06	9.56	7.95	5.77	6.03	4.62
CaO	9.00	9.32	9.40	9.18	9.22	9.83	7.53	8.18
Na_2O	2.92	2.63	2.64	2.78	4.30	3.35	3.98	4.04
K_2O	0.72	0.57	0.57	0.51	1.04	1.12	1.61	1.36
P_2O_5	0.25	0.16	0.16	0.17	0.74	0.31	0.45	0.67
Total	100.00	99.82	100.06	99.71	98.49	98.77	99.06	99.36
V (ppm)	204	189	191	173	-	-	-	209
Cr	528	577	577	528	-	-	-	91
Ni	158	183	186	182	112	23	58	26
Rb	13	12	11	11	111	26	39	24
Sr	353	334	330	377	725	924	438	877
Y	31	18	16	21	28	36	76	26
Zr	118	74	69	78	282	-	216	216
Nb	10	10	9	10	52	18	26	24
Ba	246	194	194	187	621	387	342	334
B (ppm) [e]	2.2	2.5	3.0	2.8	3.6	1.9	1.5	6.3
error	0.1	0.1	0.1	0.1	0.2	0.1	0.2	0.3
Sm [e]	5.08	2.47	2.46	3.70	9.07	6.79	13.15	7.84
error	0.26	0.14	0.14	0.20	0.37	0.23	0.48	0.42
Gd [e]	5.75	2.87	2.81	4.18	32.70	28.50	64.40	6.92
error	0.17	0.10	0.10	0.14	1.24	0.96	2.33	0.29
XRF lab. [f]	2	2	2	2	1	1	1	2

Table 1.1
Continued

Sample No.	TRD01	TRD03	TRD05	TRD06	TRD07	TRD08	TRD09	TRD10
Location [a]	TR	TR	TR	TR	TR	TR	TR	TR
Sample type [b]	LV	LV	LV	LV	LV	LV	LV	LV
D (km) [c]	308	308	308	308	308	308	308	308
Phenocryst assemblage [d]	OlCpPl	OlCpPl	OlCpPl	OlCpPl	OlCpPl	OlCpPl	OlCpPl	OlCpPl
SiO_2 (wt. %)	49.70	53.10	53.97	52.56	48.82	47.09	47.72	51.42
TiO_2	1.10	1.25	1.25	1.12	1.41	1.82	1.92	1.86
Al_2O_3	15.46	18.34	18.86	16.19	15.17	16.15	16.77	17.64
Fe_2O_3	9.27	9.50	9.23	9.70	10.60	11.42	11.46	10.98
MnO	0.17	0.18	0.17	0.17	0.18	0.20	0.20	0.18
MgO	10.38	4.02	3.54	6.37	10.43	8.24	6.83	3.92
CaO	9.97	8.40	7.89	9.65	9.51	10.28	10.50	8.60
Na_2O	2.78	3.36	3.41	2.98	2.89	2.95	2.91	3.75
K_2O	1.10	1.52	1.60	1.18	1.06	1.22	1.26	1.29
P_2O_5	0.28	0.27	0.28	0.20	0.27	0.35	0.35	0.41
Total	100.21	99.95	100.19	100.12	100.32	99.70	99.89	100.05
V (ppm)	208	246	237	230	202	239	254	300
Cr	439	16	14	139	468	253	167	7
Ni	179	6	5	35	212	82	52	2
Rb	25	34	36	25	20	24	26	24
Sr	427	590	585	456	371	449	456	562
Y	21	28	35	25	24	32	33	30
Zr	107	134	138	107	112	126	130	141
Nb	17	14	15	9	21	27	27	18
Ba	301	376	403	264	275	377	372	282
B (ppm) [e]	5.0	4.4	6.2	6.5	2.6	1.9	2.1	3.8
error	0.3	0.3	0.4	0.4	0.2	0.2	0.1	0.2
Sm [e]	3.33	3.90	9.78	3.60	3.71	4.38	4.14	4.88
error	0.24	0.25	0.53	0.26	0.22	0.23	0.21	0.26
Gd [e]	5.08	5.66	3.04	5.56	5.56	6.97	6.80	7.04
error	0.24	0.23	0.18	0.26	0.22	0.24	0.23	0.26
XRF lab. [f]	2	2	2	2	2	2	2	2

Table 1.1
Continued

Sample No.	KDI-02	KDI-06	KDI-07	UZ-MN	UZ01	UZ02	KDI-03	KDI-03B
Location [a]	UZ	UZ	UZ	UZ	UZ	UZ	OY	OY
Sample type [b]	ME	ME	ME	LV	LV	LV	ME	LV
D (km) [c]	131	131	131	281	281	281	263	263
Phenocryst assemblage [d]	HbBtPl	HbBtPl	HbBtPl	HbBtPl	HbBtPl	HbBtPl	CpHbPl	HbBtPl
SiO_2 (wt. %)	55.05	56.67	56.28	63.75	64.55	64.76	52.48	63.12
TiO_2	1.05	0.91	0.94	0.68	0.64	0.61	1.32	0.65
Al_2O_3	16.96	18.05	18.01	15.80	15.98	15.82	16.67	16.95
Fe_2O_3	8.05	8.39	7.59	5.22	4.85	5.27	8.76	5.40
MnO	0.15	0.17	0.16	0.10	0.09	0.08	0.13	0.08
MgO	6.85	3.48	4.18	2.45	2.33	2.26	6.22	1.91
CaO	7.05	7.54	7.40	4.79	4.54	4.58	9.06	5.80
Na_2O	2.71	4.38	3.65	3.63	3.74	3.82	3.29	3.96
K_2O	1.55	1.47	2.16	2.37	2.57	2.24	0.70	1.27
P_2O_5	0.29	0.20	0.21	0.14	0.13	0.12	0.31	0.18
Total	99.70	101.27	100.56	98.92	99.42	99.56	98.93	99.31
V (ppm)	166	209	172	89	86	220	285	155
Cr	182	8	33	24	30	245	124	39
Ni	78	2	14	15	21	64	28	11
Rb	48	42	70	84	90	79	14	30
Sr	333	415	391	327	352	311	674	520
Y	26	31	23	18	15	17	26	16
Zr	151	116	114	161	158	168	131	115
Nb	16	13	11	13	13	11	11	8
Ba	328	300	470	425	503	389	285	456
B (ppm) [e]	7.9	6.9	9.8	16.5	9.1	17.0	2.7	4.8
error	0.3	0.2	0.3	0.4	0.3	0.4	0.1	0.2
Sm [e]	4.65	4.82	3.71	3.54	3.38	3.86	5.20	3.07
error	7.18	0.21	0.17	0.18	0.18	0.18	0.23	0.20
Gd [e]	5.18	5.14	3.97	13.60	12.90	12.80	5.30	2.96
error	0.16	0.15	0.12	0.51	0.49	0.48	0.15	0.12
XRF lab. [f]	2	2	2	1	1	1	2	2

Table 1.1
Continued

Sample No.	YT01	YT02	YT07	YT09	YT05A	YT05B	YT06A	YT06B
Location [a]	YT	YT	YT	YT	YT	YT	YT	YT
Sample type [b]	LV	LV	LV	LV	ME	ME	ME	ME
D (km) [c]	202	202	202	202	202	202	202	202
Phenocryst assemblage [d]	OlCpOp HbPl	OlCpOp HbPl	OlCpOp HbPl	OlCpOp HbPl	OlCpHbPl	OlCpHbPl	OlCpHbPl	OlCpHbPl
SiO_2 (wt. %)	62.73	58.74	59.46	59.89	53.99	51.38	50.37	49.67
TiO_2	0.64	0.71	0.78	0.75	0.87	0.97	1.10	1.12
Al_2O_3	16.12	17.55	16.70	16.79	17.50	18.65	18.43	18.65
Fe_2O_3	5.80	6.84	6.95	6.84	8.27	9.12	9.73	10.12
MnO	0.13	0.13	0.13	0.13	0.15	0.15	0.17	0.18
MgO	2.51	3.21	3.23	3.24	4.89	4.78	5.14	5.15
CaO	5.34	5.74	6.61	6.02	9.34	9.64	9.73	9.61
Na_2O	3.61	3.28	3.51	3.55	3.37	2.96	3.06	2.98
K_2O	2.12	1.46	1.73	1.71	1.03	1.10	1.03	1.05
P_2O_5	0.13	0.14	0.14	0.15	0.16	0.22	0.06	0.07
Total	99.11	97.78	99.24	99.06	99.56	98.97	98.81	98.58
V (ppm)	158	181	155	103	247	255	304	304
Cr	20	154	24	21	55	16	13	12
Ni	8	53	12	15	11	6	4	6
Rb	62	32	47	41	25	27	25	25
Sr	485	425	497	514	493	535	615	634
Y	18	18	17	18	18	20	22	23
Zr	148	124	123	145	76	58	81	84
Nb	8	9	7	10	6	6	6	7
Ba	507	488	433	461	264	247	269	267
B (ppm) [e]	10.1	5.3	6.5	6.8	4.9	3.9	3.4	3.4
error	0.3	0.2	0.2	0.2	0.2	0.2	0.1	0.1
Sm [e]	3.55	3.22	2.81	3.75	2.78	2.02	3.30	3.64
error	0.18	0.16	0.15	0.18	0.13	0.06	0.14	0.15
Gd [e]	12.30	11.60	10.40	13.60	3.12	4.27	3.83	4.09
error	0.47	0.44	0.39	0.51	0.09	0.07	0.11	0.11
XRF lab. [f]	1	1	1	1	2	2	2	2

Table 1.1
Continued

Sample No.	YT05	YT06	KDI-01	KJ04-S	AS028	AS049	AS065	ASYS46
Location [a]	ON	ON	KJ	KJ	AS	AS	AS	AS
Sample type [b]	LV	LV	ME	SC	LV	LV	LV	LV
D (km) [c]	195	195	218	218	220	220	220	220
Phenocryst assemblage [d]	OlCpHbPl	OlCpHbPl	HbPl	OlOpCpPl	OlOpCpPl	OlOpCpPl	OlOpCpPl	OlOpCpPl
SiO_2 (wt. %)	52.85	51.29	56.86	52.52	50.98	52.02	50.91	52.04
TiO_2	1.87	2.01	0.88	1.00	0.93	1.02	0.85	0.81
Al_2O_3	15.41	15.53	17.58	18.29	17.24	17.44	18.60	18.02
Fe_2O_3	10.20	10.84	8.40	9.93	11.06	11.36	9.65	9.82
MnO	0.15	0.15	0.16	0.19	0.17	0.17	0.17	0.15
MgO	5.67	6.05	3.84	4.49	5.20	4.27	3.66	4.23
CaO	7.42	7.98	7.22	8.80	9.43	8.18	10.28	9.30
Na_2O	3.50	3.49	3.08	3.10	2.72	3.04	2.92	2.97
K_2O	1.52	1.40	1.33	1.10	1.44	1.86	1.49	1.60
P_2O_5	0.40	0.42	0.16	0.24	0.19	0.23	0.20	0.21
Total	98.99	99.17	99.52	99.66	99.36	99.58	98.70	99.16
V (ppm)	200	182	251	309	303	283	269	255
Cr	178	19	8	10	26	23	30	24
Ni	50	3	2	-	11	10	11	8
Rb	35	29	37	25	40	52	42	45
Sr	641	654	533	826	568	600	628	662
Y	19	19	22	20	20	22	18	19
Zr	190	187	122	79	112	137	112	116
Nb	20	20	9	5	7	6	5	5
Ba	381	384	410	342	325	351	288	353
B (ppm) [e]	4.8	3.5	7.3	5.0	17.2	22.6	12.1	15.7
error	0.2	0.1	0.3	0.2	0.7	1.0	0.6	0.7
Sm [e]	6.10	5.74	4.18	4.24	4.11	5.24	3.94	4.38
error	0.23	0.22	0.27	0.25	0.27	0.38	0.29	0.32
Gd [e]	18.70	17.70	4.26	4.15	4.03	4.80	3.92	4.06
error	0.67	0.63	0.17	0.15	0.19	0.25	0.21	0.22
XRF lab. [f]	1	1	2	2	1	1	1	1

Table 1.1
Continued

Sample No.	AS039	AS046	AS054	AS082B	AS057	AS034	AS047	AS051
Location [a]	AS	AS	AS	AS	AS	AS	AS	AS
Sample type [b]	LV	LV	LV	LV	SC	LV	LV	LV
D (km) [c]	220	220	220	220	220	220	220	220
Phenocryst assemblage [d]	OlOpCpPl	OlOpCpPl	OlOpCpPl	OlOpCpPl	OlOpCpPl	OlOpCpPl	OlOpCpPl	OlOpCpPl
SiO_2 (wt. %)	47.64	51.16	51.46	52.69	49.94	48.18	53.52	51.13
TiO_2	0.93	0.90	0.99	0.90	0.91	0.87	1.15	0.93
Al_2O_3	18.39	16.83	16.74	19.93	17.38	17.63	18.13	17.75
Fe_2O_3	11.25	10.83	10.65	7.36	11.24	11.52	8.98	10.89
MnO	0.17	0.18	0.17	0.11	0.17	0.16	0.17	0.17
MgO	5.71	5.38	5.72	2.70	5.44	6.06	4.33	4.80
CaO	11.62	9.74	9.34	10.16	9.96	11.78	8.38	9.41
Na_2O	2.19	2.70	2.62	3.00	2.63	2.17	3.16	2.82
K_2O	0.75	1.42	1.49	1.62	1.18	0.86	1.25	1.51
P_2O_5	0.22	0.22	0.22	0.22	0.18	0.18	0.20	0.19
Total	98.87	99.36	99.40	98.69	99.01	99.41	99.27	99.60
V (ppm)	341	283	291	261	301	327	241	294
Cr	36	39	44	27	28	35	18	24
Ni	13	12	10	1	13	16	2	9
Rb	20	37	43	49	31	25	35	42
Sr	621	620	517	688	583	545	481	593
Y	16	19	20	21	19	16	22	18
Zr	84	105	113	126	97	71	114	116
Nb	4	5	6	6	5	4	8	7
Ba	193	333	326	341	292	158	290	303
B (ppm) [e]	6.2	14.5	15.6	17.1	13.6	5.6	14.0	13.8
error	0.2	0.4	0.5	0.5	0.4	0.2	0.5	0.4
Sm [e]	3.23	4.29	4.44	5.25	4.04	2.92	4.68	4.54
error	0.15	0.20	0.22	0.27	0.22	0.19	0.27	0.24
Gd [e]	3.18	3.99	4.09	4.45	3.54	2.86	4.63	4.37
error	0.13	0.16	0.18	0.15	0.13	0.11	0.17	0.15
XRF lab. [f]	1	1	1	1	1	1	1	1

Table 1.1
Continued

Sample No.	AS077	AS021		01X	KMP02	KMP07	KMP08	KMP10	KMP11
Location [a]	AS	AS		KMP	KMP	KMP	KMP	KMP	KMP
Sample type [b]	LV	LV		XL	XL	XL	XL	XL	XL
D (km) [c]	220	220							
Phenocryst assemblage [d]	OlOpCpPl	OlOpCpPl	Rock type	Gneiss	Gabbro	Gabbro	Gneiss	Granitic rock	Gneiss
SiO_2 (wt. %)	53.33	50.80		50.36	50.35	49.91	55.71	75.01	45.94
TiO_2	0.99	0.96		1.11	0.79	1.09	1.56	0.04	1.78
Al_2O_3	17.50	19.78		19.61	19.89	17.14	19.52	14.33	15.68
Fe_2O_3	10.06	10.24		8.57	7.25	9.50	6.56	0.06	11.50
MnO	0.16	0.23		0.16	0.19	0.15	0.13	0.00	0.22
MgO	4.00	2.93		4.92	6.20	6.89	3.75	0.09	9.22
CaO	8.09	9.09		9.48	10.97	10.05	6.88	1.15	11.22
Na_2O	3.30	3.70		3.06	2.42	2.27	3.35	4.13	1.80
K_2O	1.77	1.04		0.49	0.54	1.06	1.08	4.33	0.54
P_2O_5	0.20	0.17		0.30	0.09	0.10	0.24	0.03	0.06
Total	99.41	98.93		98.06	98.70	98.17	98.79	99.17	97.96
V (ppm)	257	205		224	278	371	258	-	385
Cr	23	16		65	59	29	72	-	425
Ni	3	-		16	18	8	45	19	99
Rb	48	25		15	20	29	37	101	16
Sr	543	552		657	538	378	621	105	315
Y	23	22		13	18	18	24	24	21
Zr	135	128		186	70	76	179	41	74
Nb	7	5		6	3	3	13	4	5
Ba	358	261		210	211	252	245	157	97
B (ppm) [e]	15.0	7.1		1.8	4.1	2.0	3.5	1.9	3.0
error	0.4	0.3		0.1	0.2	0.1	0.2	0.1	0.2
Sm [e]	5.09	4.45		2.42	3.86	5.70	5.40	0.96	5.79
error	0.27	0.23		0.13	0.18	0.23	0.22	0.08	0.23
Gd [e]	4.61	3.59		2.35	4.04	2.37	5.73	1.94	6.79
error	0.15	0.12		0.09	0.14	0.09	0.18	0.09	0.20
XRF lab. [f]	1	1		1	1	1	1	1	1

(a) Sampling locations are: KM (Kita-Matsuura); SS (Shimoshima); YB (Yabakei); IK (Iki); GK (Genkai); TR (Taradake); UZ (Unzen); OY (Oyano); ON (Oninomi); YT (Yufu, Tsurumi); KJ (Kuju); AS (Aso); KMP (Kimpo). (b) LV: lava; ME: mafic enclave; SC: scoria; XL: crustal xenolith. (c) D: distance from the trench (Ishida, 1992). (d) Pl: plagioclase, Ol: olivine, Op: orthopyroxene, Cp: clinopyroxene, Hb: hornblende, Bt: biotite, -: Not analyzed. (e) B, Sm and Gd contents are determined by the PGA. Error shows the standard deviation (one sigma). The contents of other element are determined by XRF. (f) XRF lab: 1. Fuji Tokoha University, 2. Kitakyushu Museum of Natural History and Human History.

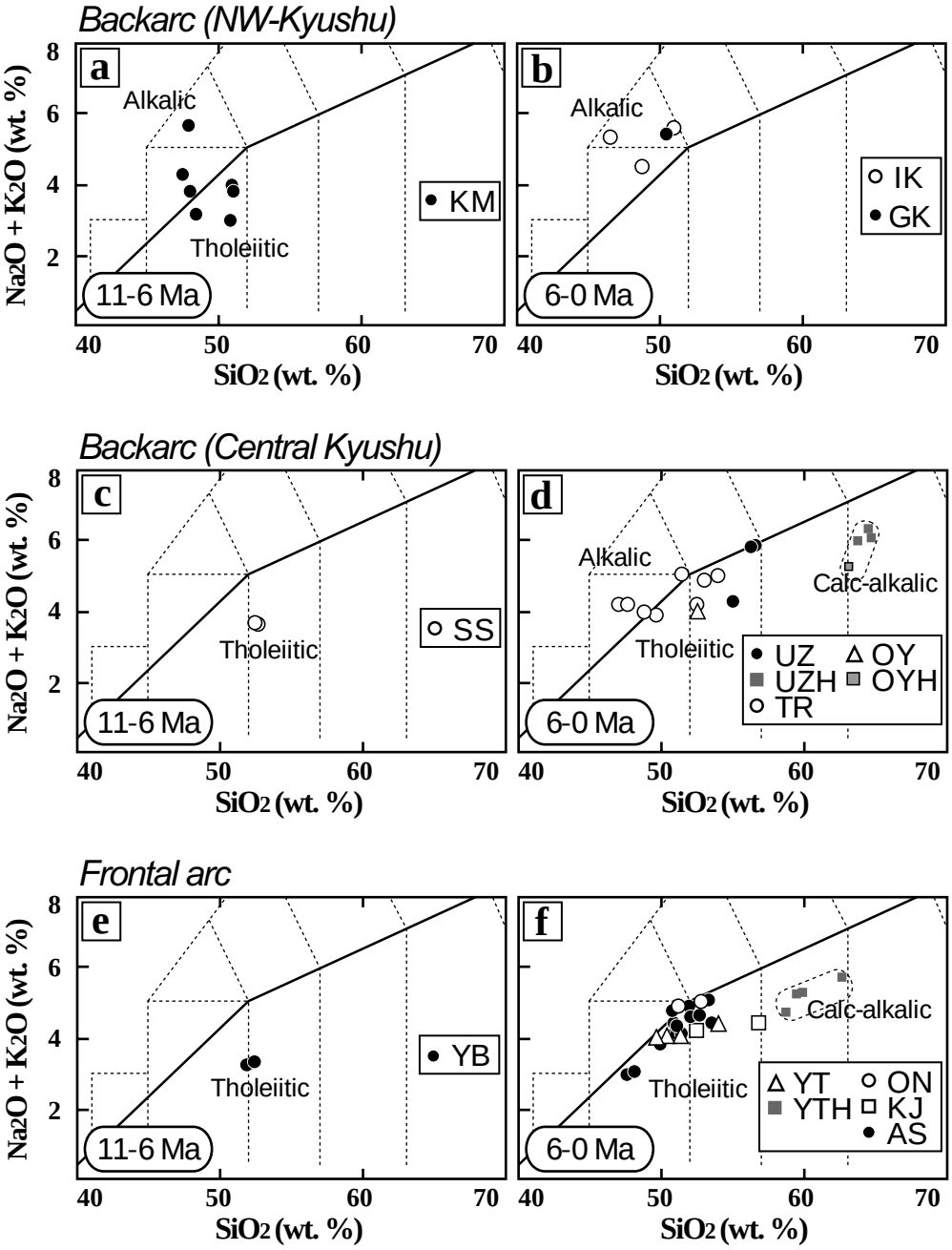

Fig. 1.4

Total alkali versus silica plots for the northern Kyushu volcanic products. Thick lines indicate alkali-tholeiitic rocks suite boundary (LeMaitre et al., 1989; MacDonald and Katsura, 1964). UZ (H): Unzen host andesite, OY (H): Oyano host andesite, YT (H): Yufu, Tsurumi host andesite. Other abbreviations are the same as in Fig. 1.2.

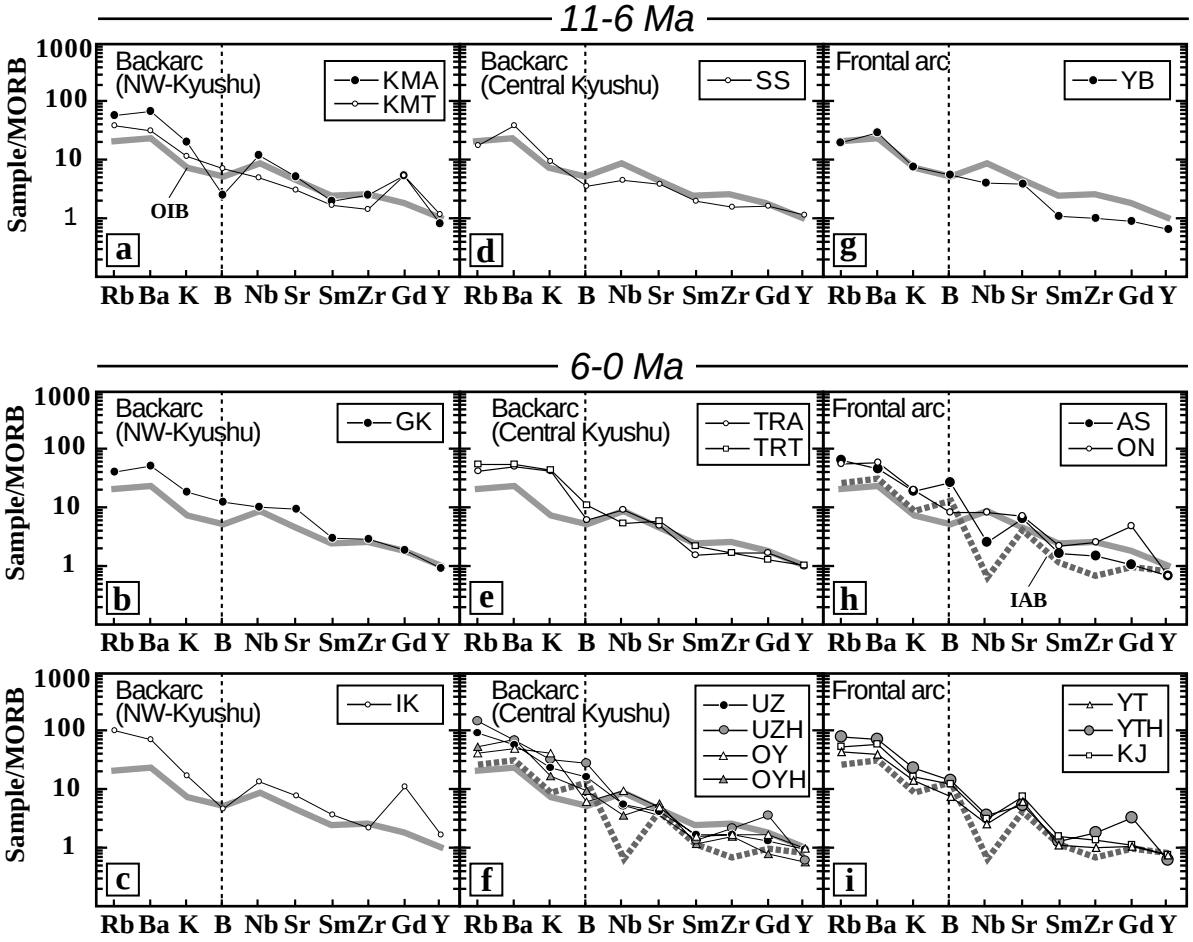

Fig. 1.5

Spider diagrams of averaged incompatible elements for northern Kyushu volcanic rocks. Data for OIB are obtained from Abbey (1982), Flanagan (1976), Govindaraju (1994), and the data for IAB are obtained from Moriguti et al. (2004). Abundances are normalized by n-MORB values: Rb (0.56), Ba (6.3), K (600), B (0.5), Nb (2.33), Sr (90), Sm (2.63), Zr (74), Gd (3.68), Y (28) (Sun and McDonough, 1989). KM-A: Kita-Matsuura Alkalic basalt, KM-T: Kita-Matsuura Tholeiitic basalt, TR-A: Tara-dake Alkalic basalt, TR-T: Tara-dake Tholeiitic basalt. Other abbreviations are the same as those defined in Fig. 1.2.

On the other hand, wide ranges in the B/Sm, B/Zr, B/Nb and Ba/Nb ratios are observed in the young basalts since 6 Ma (Fig. 1.7). The present leading edge of the WBZ (dashed line in Fig. 1.7) is observed beneath AS; however, it is not revealed under the backarc region (Nagamune and Tashiro, 1989). The smooth and continuous decline trends of these ratios, such as those represented in the cool subduction zone (Ishikawa and Tera, 1997), are not observed in the young basalts. The across-arc variations in B/Nb observed in the case of the young basalts are similar to those of the warm subduction zone basalts (Leeman et al., 2004).

On the backarc side, the IK, GK, TR-A and OY basalts exhibit low B/ fluid-immobile element ratios. The B/Nb ratios of these basalts fall in the mantle value range (0.05–0.5; Ryan et al., 1996). Although the TR-T and UZ basalts are also distributed in the backarc region, they have higher B/Sm (1.1–1.8 for TR; 1.4–2.6 for UZ), B/Zr (0.03–0.06; 0.05–0.09) and B/Nb (0.3–0.7; 0.5–0.9) ratios than those of the other backarc OIB-like basalts. The andesitic host rocks of UZ and OY have slightly higher B/Zr and B/Nb ratios and higher B/Sm ratios than those of the UZ and OY basalts (mafic enclaves) (Fig. 1.7).

In the frontal arc region, B and fluid-immobile element ratios are most pronounced among AS basalts (B/Sm = 1.6–4.3; B/Zr = 0.07–0.16; B/Nb = 1.4–3.7). Although the KJ and YT are located in the frontal arc (Fig. 1.2), their basalts have lower B/Sm (<2.0), B/Zr (<0.08) and B/Nb (<1.0) ratios than those of AS basalts. The andesitic host rocks of YT show slightly elevated B/Nb and higher B/Sm ratios than those of the YT basalts (mafic enclaves). In contrast, the ON basalts have low B/Sm (0.6–0.8), B/Zr (0.02–0.03) and B/Nb (0.2) ratios; these are similar to those of the backarc OIB-like basalts. The B/Nb ratios in ON basalts fall in the mantle value range (0.05–0.5; Ryan et al., 1996) (Fig. 1.7).

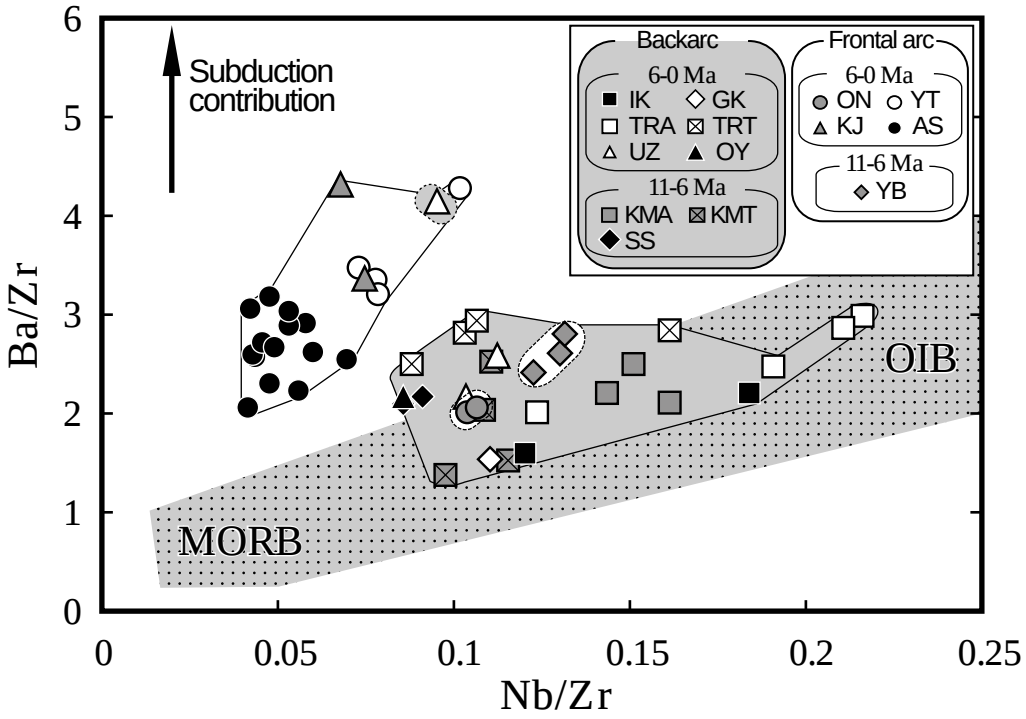

Fig. 1.6

Ba/Zr versus Nb/Zr diagram in the northern Kyushu basalts. Dark dotted field shows MORB-OIB array (Leeman et al., 1990; Leeman et al., 2005). Up-arrow indicates involvement of subduction components. Abbreviations are the same as those in Fig. 1.2, 1.4 and 1.5.

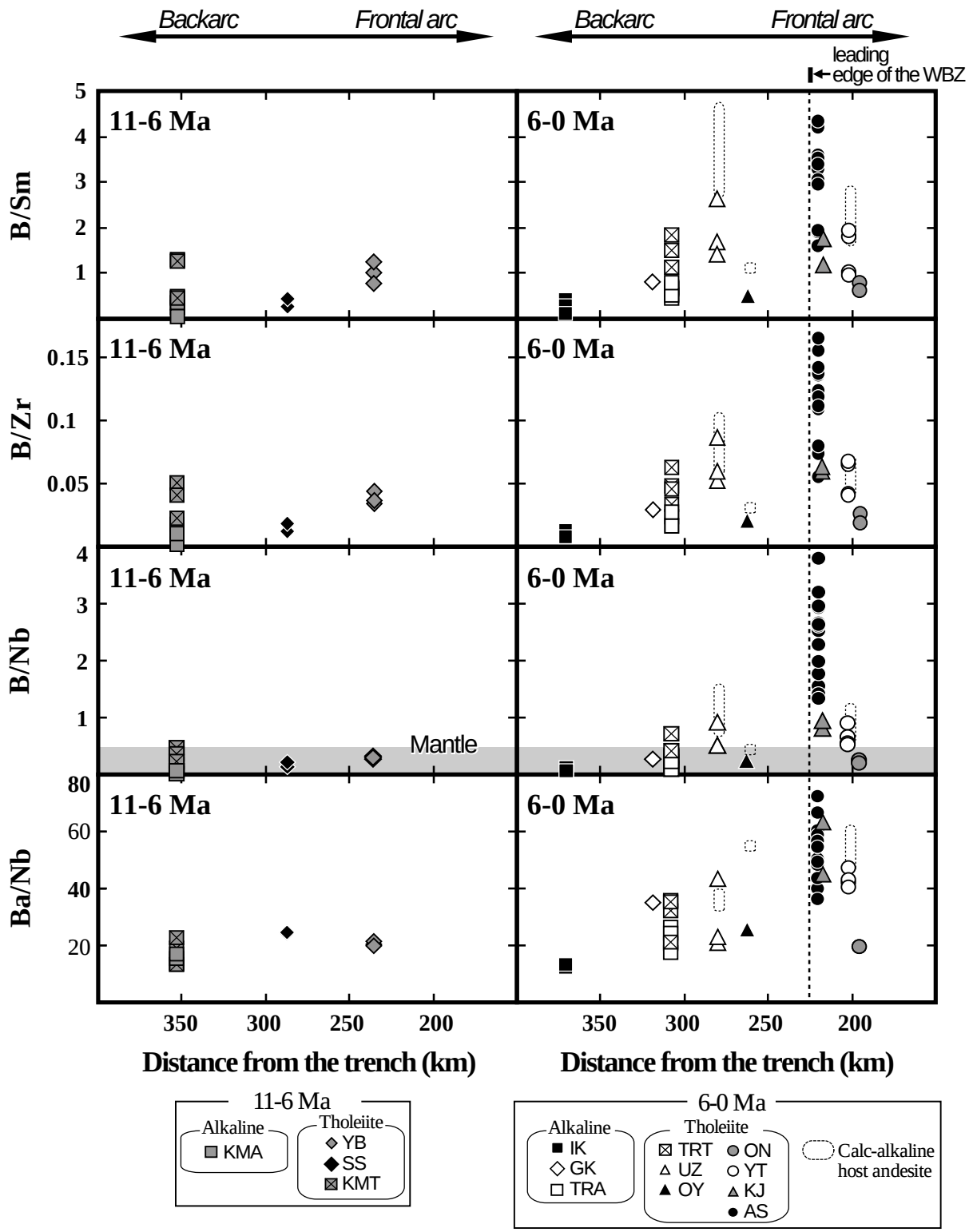

Fig. 1.7

Plots of element ratios for across-arc transects in the northern Kyushu. The shaded field on B/Nb diagram represents ranges for MORB and OIB compositions (Ryan et al., 1996). Abbreviations are the same as those in Fig. 1.2, 1.3, 1.4 and 1.5.

1.6 Discussions

1.6.1 Boron enrichment of the northern Kyushu basalts

Fig. 1.8 shows the process that is cause of the compositional variations observed in each unit. The lateral variation of Zr (ppm) shows the crystallization and/or partial melting control. The vertical variation of the B/Zr ratio shows the subduction contribution.

In the backarc region, at 11–6 Ma, significantly diverse B/Sm, B/Zr and B/Nb ratios were observed in the KM basalts (Fig. 1.7). Kakubuchi et al. (1994) suggested that the source mantle compositions of the primitive magmas of both KM-T and KM-A basalts are similar, and the alkalic and tholeiitic basalts are derived from deeper (10–15 kbar) and shallower (5–10 kbar) mantles, respectively. Most of the KM basalts have similar B/Zr ratios (<0.02) with varying Zr contents (88–274 ppm), as shown in Fig. 1.8a. This probably reflects the partial melting control suggested by Kakubuchi et al. (1995). However, a few KM-T basalt samples show slightly elevated B/Zr ratios (0.04–0.05) (Fig. 1.8a). This elevated B/Zr ratios are not caused by the crystallization and/or partial melting. Contamination by the crustal materials is unlikely to be the cause of the enhanced B/Zr ratios because these ratios are extremely low (0.01-0.06) in crustal xenoliths. These elevated B/Zr ratios observed in the KM-T basalts indicate the subduction contributions which modified their source mantle compositions.

In the backarc region, at 6–0 Ma, TR basalts exhibit a wide range in their B/Zr ratios (0.02–0.06) (Fig. 1.8b). TR-T basalts show higher B/Zr ratios (0.03–0.06) than the TR-A basalts (0.02–0.03). Ikawa and Nagao (1996) suggested that the primitive magmas of both tholeiitic and alkalic basalts are derived from the same source mantle. However, the high B/Zr ratios observed in the TR-T basalts are unlikely to have been caused by partial melting, crystallization controls and crustal contamination. The source mantle of the TR-T basalts is probably modified by the subduction components.

The UZ and OY basalts (mafic enclaves) exhibit B/Zr ratios (0.05–0.09 and 0.02, respectively) that are similar to those of their host andesites (0.06–0.1; 0.03).

Therefore, although it is not clear whether they (basalt and their host andesite) are co-genetic (Nakada and Motomura, 1997) or not (Chen et al., 1993) from these data, the assimilation of the UZ and OY basaltic magmas into the andesitic host does not modify the original B/Zr ratios of the assimilated basaltic enclaves.

In the frontal arc region, at 6–0 Ma, the AS basalts exhibit a significantly high and wide range in the B/Zr ratios (0.05–0.16) (Fig. 1.8b). These elevated B/Zr ratios observed in the AS basalts apparently indicate the subduction contribution to their source mantle.

The assimilation of YT basaltic magmas into the andesitic host does not modify the original B/Zr ratios of the assimilated basaltic enclaves because both of them show the similar B/Zr ratios (0.04–0.07). A similar relationship is found between the mafic enclave and the scoria from KJ (B/Zr = 0.06). Therefore, this indicates that B/fluid-immobile element ratios do not vary among the basaltic products.

1.6.2 Origin of the elevated B/fluid-immobile element ratios observed in the old basalts.

The Philippine Sea plate did not subduct beneath northern Kyushu when the KM, SS and YB basalts were active at 11–7 Ma. Hence, their source mantle compositions are not metasomatized by the subduction components from the Philippine Sea plate (Kakubuchi et al., 1994; Kakubuchi and Matsumoto, 1990; Nagao et al., 1992). They all show OIB-like compositions (Fig. 1.5, 1.6). However, the KM-T basalts are slightly enriched in B/Sm, B/Zr and B/Nb ratios than the KM-A alkalic basalts (Fig. 1.7). The B/Nb ratios of the KM-T basalts are similar to those of the IAB-like basalts from the warm subduction zones (Leeman et al., 2004; Hochstaedter et al., 1996; Fig. 1.9a). On the other hand, the B/Nb ratios of the KM-A basalts overlap with the OIB-like values (Fig. 1.9a). This probably indicates that the source mantle of the KM-T basalts is slightly enriched in B/Sm, B/Zr and B/Nb ratios as compared with the KM-A basalts. The source mantle of the KM-T basalts is possibly slightly modified by the subduction component.

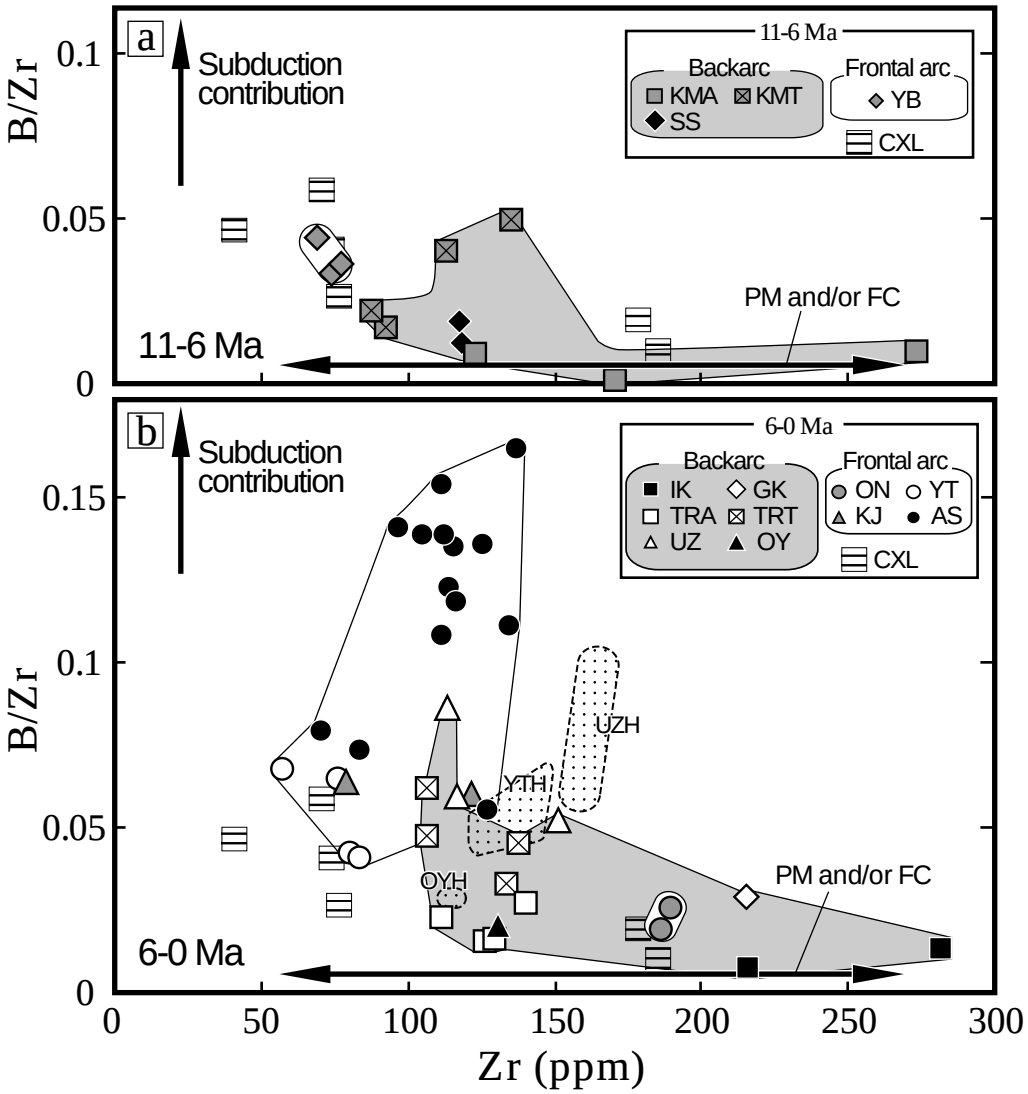

Fig. 1.8

Zr versus B/Zr diagrams for old (a) and young (b) basaltic rocks from northern Kyushu. Up-arrows indicate involvement of subduction components. Right and left arrows show partial melting (PM) and/or fractional crystallization (FC)-controlled processes. CXL: Crustal Xenoliths from KMP. Other abbreviations are the same as those in Fig. 1.2, 1.4 and 1.5.

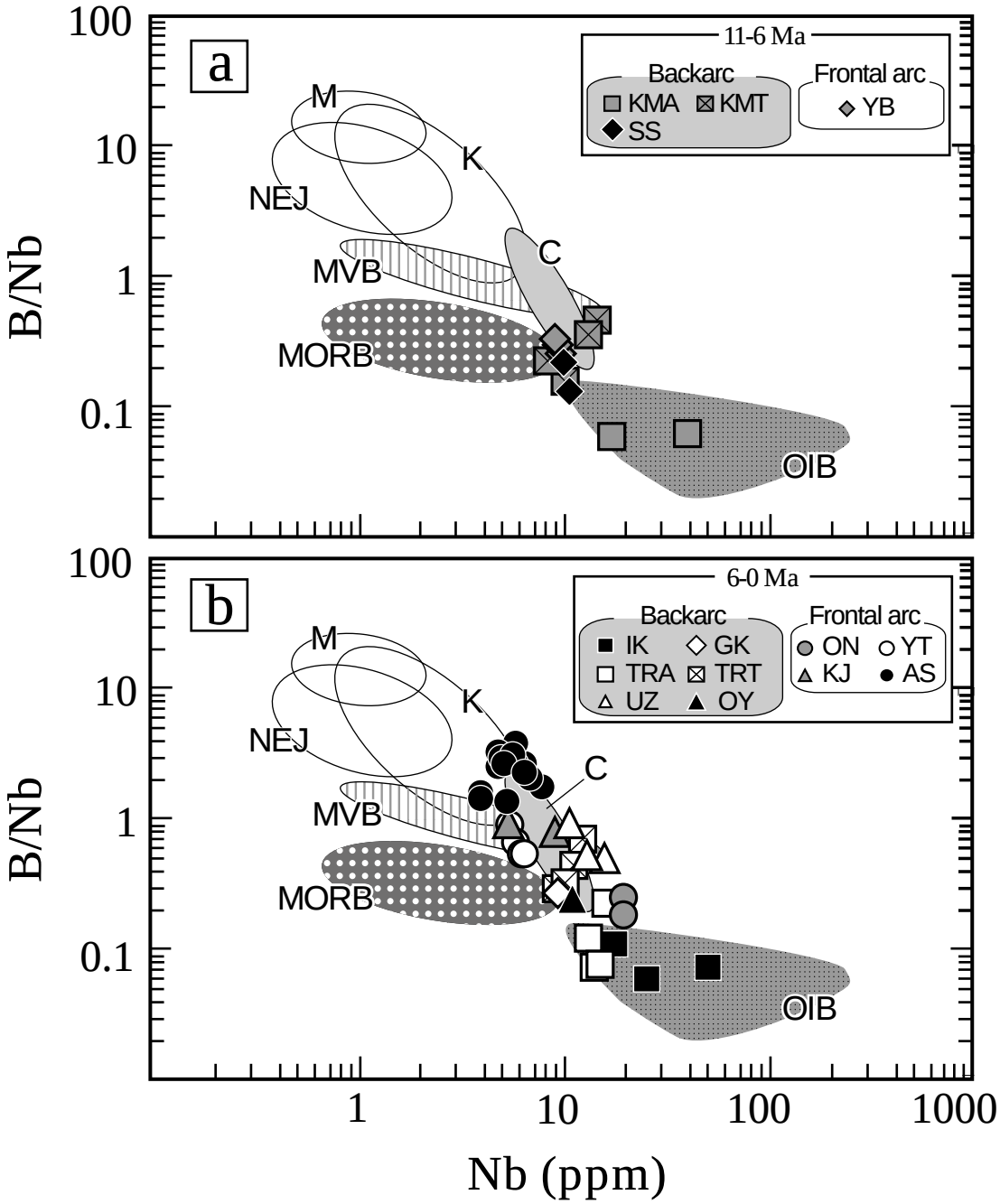

Fig. 1.9

B/Nb versus Nb diagram for old (a) and young (b) basaltic rocks from northern Kyushu and other volcanic arcs. MORB and OIB compositions are plotted for comparison. K: Kurile (Ishikawa and Tera, 1997); M: Mariana (Ishikawa and Tera, 1999); NEJ: NE-Japan (Moriguti et al., 2004); MVB: Mexican volcanic belt (Hochstaedter et al., 1996 and Hasenaka et al., 1993); C: Cascade (Leeman et al., 2004); MORB and OIB: Ryan et al. (1996). Other abbreviations are the same as those defined in Fig. 1.2, 1.4 and 1.5.

The activities of the tholeiitic to alkalic basalts in northwest Kyushu is closely related to the East China Sea opening in the Cenozoic age (Uto et al., 2004). The older syn-opening and younger post-opening basalts are tholeiitic and alkalic, respectively. Uto et al. (2004) argued that the older tholeiitic basalts are derived from the depleted lithospheric mantle based on their geochemical characteristics. Similar depleted lithospheric mantles are assumed beneath the KM area. Thus, it is reasonable that the KM-T basalts, which enriched in B/Sm, B/Zr and B/Nb ratios, are derived from the sub-arc lithospheric mantle. The KM-A basalts appear to be derived from the deeper OIB-source mantle.

Both SS and YB basalts also show B/Sm, B/Zr and B/Nb ratios similar to those of the KM-T basalts (Fig. 1.7, 1.9a). Therefore, the slightly elevated B/Sm, B/Zr and B/Nb ratios observed in these old OIB-like basalts may represent the sub-arc lithospheric background beneath northern Kyushu.

1.6.3 Subduction influences of the Philippine Sea plates on the mantle beneath northern Kyushu

The subduction of the Philippine Sea plate initiated at 6–4 Ma in the northern Kyushu frontal arc (Kamata and Kodama, 1994). Hence, the source mantle of young basalts may be metasomatized by the subduction components from the Philippine Sea plate.

A slight enrichment of the boron and fluid-immobile element ratios is revealed in the YT, KJ, UZ and TR-T basalts. These ratios are relatively high and wide ranging in AS basalts (Fig. 1.7). The B/Nb ratios of the YT, KJ, UZ and TR-T basalts are similar to those of the basalts from the warm subduction zones (Leeman et al., 2004; Hochstaedter et al., 1996; Fig. 1.9b). These basalts from the warm subduction zones show lower subduction signatures than those from the cool subduction zones (Ishikawa and Tera, 1997; Moriguti et al., 2004; Ishikawa and Tera, 1999; Fig. 1.9b).

Leeman et al. (2004) explained the cause of the weak subduction signature revealed in the Cascade basalts as follows: The mantle beneath the Cascade arc is divided into two layers (upper layer: both IAB and OIB sources; lower layer: OIB source) on the

basis of the petrologic data (estimated segregation temperatures and pressures of these basalts by using geothermometers and barometers; Leeman et. al., 2005). The upper B-enriched domain (IAB source) could develop as a consequence of melt migration and intrusion that are related to the previous subduction magmatism. The modern slab inputs are negligibly small because a large amount of H_2O and fluid-mobile elements are released from the slab before it descends beneath the volcanic front due to the high geotherm in the forearc. The origin of B-rich magma could involve remelting of the fossil subduction component-enriched domains in the shallow lithospheric mantle. The remelting of the lithospheric mantle is caused by the infiltration of hot OIB magmas.

The Cascade arc and northern Kyushu show the following similar tectonic settings: 1) Subduction of the young oceanic plate; 2) Development of a graben system; 3) Coexistence of the IAB and OIB; 4) The estimated occurrence of slab dehydration in the shallow depth (<50 km) beneath the forearc. The detailed tectonic setting and evidences are as follows:

1) The subduction of the young oceanic plate is still controversial because northern Kyushu is a critical area where the Shikoku basin and old Philippine Sea plate meet (Kimura et al., 2005). However, the adakitic andesite from YT (Sugimoto et al., 2006) and high-Mg andesite from YB (Kakubuchi et al., 1995) reflect the young (and hot) plate subduction. This is because the slab melts which are involved in the origin of adakite and high-Mg andesite magmas could occur in the warm subduction zones (Defant and Drummond, 1990). These evidences probably indicate that the subduction of the young plate occurred in the north and northeast part of frontal arc region.

2) Kamata (1989) indicated the existence of a large graben system in the frontal arc region (HVZ in Fig. 1.2).

3) Kita et al. (2001) suggested that the IAB-like AS, KJ, YT basalts coexist with the OIB-like ON basalts in the graben.

4) Zhao et al. (2000) argued the occurrence of the early dehydration of the young Shikoku basin by using the tomographic geophysical data. All these factors imply that the addition of modern fluids from the subducting slab to the mantle beneath northern Kyushu is extremely small, the same as the Cascade arc.

Slightly elevated B/Sm, B/Zr and B/Nb ratios are commonly observed in the backarc UZ and TR-T basalts (Fig. 1.7; Fig. 1.9b). This may suggest the involvement of the pre-existing sub-arc lithospheric mantle, because the WBZ does not reach beneath the backarc region. In addition, their B/Sm, B/Zr and B/Nb ratios are similar to those of the old tholeiitic basalts, which probably involve the composition of a pre-existing lithospheric background (as mentioned in chapter 5-2.). The considerable thermal source of remelting of the backarc lithospheric mantle is the ascending asthenospheric mantle, which is caused by the opening of Okinawa trough (Kimura et al., 2005). The ascending asthenospheric mantle beneath the backarc region is also indicated by tomographic studies (Sadeghi et al., 2000).

In contrast, a recent tomographic study suggested that the close relationship between the UZ magma genesis and the slab components derived from the subducting Philippine Sea plate (Wang and Zhao, 2006). Wang and Zhao (2006) argued that the low-velocity zones observed from a depth of 120 to 20 km beneath UZ volcano indicate the oblique ascending of magma generated by the fluid-flux melting of the mantle.

However, this interpretation does not agree with the low B/fluid-immobile element ratios revealed in the UZ basalts. In addition, the discontinuous decline trends of across-arc variations in the B/fluid-immobile element ratios (Fig. 1.7) do not appear to indicate the continuous dehydration of the oceanic slab, but reflect its early dehydration. Thus, it is skeptical that H_2O is transported to a 120-km depth beneath northern Kyushu. It possibly does not indicate the fluid-induced melting of the mantle, but may indicate the melting of the slab. The petrographic characteristics of hornblende andesite, incompatible element compositions (Y = 15–18 ppm, Sr/Y = 18–23; this study) and $^{87}Sr/^{86}Sr$ ratios (0.70438–0.70479; Chen et al., 1993) of the host andesites of UZ are similar to those of adakitic host andesites of YT (Y = 14–27 ppm, Sr/Y = 20–42, and $^{87}Sr/^{86}Sr$ = 0.703892–0.704880; this study and Sugimoto et al., 2006). Sugimoto et al. (2006) indicated that the YT andesites are the products of the mixture of slab melt and arc-type magma.

However, the slab melt is unlikely to generate the UZ and TR-T basalts because the

slab melts have siliceous compositions (Defant and Drummond, 1990). Hence, the slight enrichment of the B/fluid-immobile element ratios observed in the UZ and TR-T basalts probably represents the sub-arc lithospheric mantle compositions.

The frontal arc YT and KJ basalts show similar B/Sm, B/Zr and B/Nb ratios as the backarc UZ and TR-T basalts (Fig. 1.7). This probably indicates that the subduction contribution of the Philippine Sea plate to the source mantle of YT and KJ are extremely small. This small slab contribution to the mantle beneath the frontal arc well agrees with the tomographic data (Zhao et al., 2000). This may represent that the origin of the YT and KJ basalts is not the fluid-induced melting of the mantle but the remelting of the pre-existing sub-arc lithospheric mantle.

On the other hand, only AS basalts have higher and wider B/Sm, B/Zr and B/Nb ratios than the YT, KJ, UZ and TR-T basalts. The lower values of B/Sm and B/Zr in the AS basalts overlap with those of the YT, KJ, UZ and TR-T basalts (Fig. 1.7). The B/Nb ratios observed in the AS basalts are same or more than those of the warm subduction zone basalts, while they are similar to those of the cool subduction zone basalts (Fig. 1.9b). The low B/Sm, B/Zr and B/Nb ratios observed in the AS basalts may show the involvement of the pre-existing sub-arc lithospheric mantle composition; This is same as the YT, KJ, UZ and TR-T basalts. In contrast, the high B/Sm, B/Zr and B/Nb ratios observed in the AS basalts probably reflect the contribution of the slab-derived fluid released from the old segment of the Philippine Sea plate to the mantle. This suggests that the subduction influences of both young and old plates are observed in the AS basalts. This also implies that the boundary between the young Shikoku basin (15–26 Ma) and the old segment of the Philippine Sea plate (37–115 Ma) exists under the AS. The varied B/Sm, B/Zr and B/Nb ratios observed in the AS basalts may be caused by the response between the pre-existing sub-arc lithospheric mantle and the basaltic magma generated by the fluid-induced melting of the mantle.

1.7 Conclusions

Slightly elevated B/Sm, B/Zr and B/Nb ratios observed in the old (11–6 Ma) KM-T

basalts are not associated with the Philippine Sea plate subduction. Their B/Nb ratios also overlap with those of the IAB-like basalts from warm subduction zones such as the Cascade and Mexican volcanic belt. The compositions of the KM-T basalts probably involve the pre-existing sub-arc lithospheric mantle.

Various B/Sm, B/Zr and B/Nb ratios are observed in the young (6–0 Ma) basalts. The YT, KJ, UZ and TR-T basalts show slight enrichments of the B/Sm, B/Zr and B/Nb ratios. These ratios are similar to those of the old KM-T basalts. In addition, their B/Nb ratios overlap with those from the warm subduction zones such as the Cascade and Mexican volcanic belt. These weak slab signatures observed in the YT, KJ basalts are probably due to the subduction of the relatively young and hot Shikoku basin, which had released a large amount of hydrous fluid before reaching the frontal arc region. The compositions of the UZ and TR-T basalts do not show the influence of the fluid released from the currently subducting slab, but by the pre-existing sub-arc lithospheric mantle because the WBZ does not extend under UZ and TR volcanoes. Therefore, the subduction influence of the young Shikoku basin on the composition of the mantle beneath northern Kyushu appears to be extremely small.

Only the AS basalts show significantly high and wide ranges in their B/Sm, B/Zr and B/Nb ratios. The B/Nb ratios overlap with those in the basalts from the cool subduction zones. This may reflect that the slab influence of the old segment of the Philippine Sea plate is limited in the mantle beneath AS volcano in northern Kyushu.

Chapter 2

Temporal changes of the composition of magma source beneath Aso area

2.1 Introduction

The volcanic products from Aso area are suitable to investigate the relationship between the subduction of Philippine Sea plate and the temporal change of the source mantle composition. This is because the initiation of volcanism in Aso area (3.8 Ma; Shinmura, unpublished data) partly overlaps with the commencement of the subduction of Philippine Sea plate (6–4Ma; Kamata and Kodama, 1994).

The volcanism of Aso is divided into the following two stages on the basis of the eruption-style: caldera-forming and post-caldera stages (Ono and Watanabe, 1985). In the caldera-forming stage, four large plinian eruptions (Aso-1 to Aso-4) occurred from 270 ka to 90 ka (Ono and Watanabe, 1985; Watanabe, 2001). These four times eruptions formed a large caldera (18 km × 25 km) in this area. The pre- and post-caldera volcanism of Aso is characterized by effusive lava flow eruption (Ono and Watanabe, 1985).

The pyroclastic flow deposits from the caldera-forming stage show the compositional cycle from rhyolite to basalt in each unit (Ono and Watanabe, 1985; Hunter, 1998). This compositional cycle observed in these deposits indicates the magma-chamber beneath Aso was probably zoned in this period (Ono and Watanabe, 1983). Hunter (1998) argued the compositionally diversity observed in these pyroclastic products are caused by the intra-crustal processes (fractional crystallization, magma mixing and crustal assimilation) on the basis of their petrological and isotopic data.

In contrast, the reported petrological and geochemical data of the volcanic products

from pre- and post-caldera stages are limited (Ono and Watanabe, 1985). These data are important to investigate the origin of diverse magma types observed in Aso area and the relationship between the temporal change of magma source composition and the subduction of Philippine Sea plate. In this chapter, therefore, the author reports the petrographies, major- and trace-element compositions of the pre- and post-caldera volcanic products from Aso area.

2.2 Geology of Aso volcano

2.2.1 Tectonic settings in and around Aso volcano area

Aso volcano is located in the volcanic front associated with the subducting Philippine Sea Plate in central Kyusyu, southwest Japan (Fig.1.1, 1.2). In the SW-Japan arc, the subduction of Philippine Sea Plate initiated at about 6-4Ma in the direction of W-NW at the rate of 4cm/yr (Kamata, 1992; Kamata and Kodama, 1994). The seismic slab of Philippine Sea plate exists 150-200 km below Aso volcano (Nagamune and Tashiro, 1989). Aso volcano is also in the southwestern end of large graben system in the northern Kyushu (Hohi volcanic zone) where is the intersection point of Oita-Kumamoto tectonic line and Kokura-Tagawa fault zone (Kamata, 1989).

2.2.2 Volcanic history of Aso volcano

Aso volcano, situated in central Kyusyu, Japan is characterized by two different types of volcanism; the caldera-forming explosive plinian eruptions (Aso-1 to Aso-4) and the post-caldera extrusive volcanic activities (Ono and Watanabe, 1985) (Fig. 2.1).

Detailed geological works of Ono and Watanabe (1983) indicates that the compositional cycles of volcanic products from rhyolitic to basaltic or the reverse were recognized in the caldera-forming pyroclastic flow deposits (from 270ka to 90ka) (Fig. 2.1). They suggested a single-zoned magma chamber model to explain the compositional cycles observed in the pyroclastic flow deposits. Hunter (1998)

supported the single zoned-magma chamber model by major and trace elements and isotopic data.

In the post-caldera stage (after 90ka), the diverse magma types were extruded from more than seventeen observable vents in the caldera (Watanabe, 2001) (Fig. 2.3). Ono and Watanabe (1985), Watanabe (2001), Masuda et al. (2004) and Miyabuchi et al. (2004) indicate that more than thirty units of lava flows are distributed in the present surface. Although the compositional cycles of volcanic products as observed in the caldera-forming stage are not recognized in this stage, the basaltic lava activities are prominent after 29 ka (Aira-Tanzawa tephra: Okuno, 2002) (Fig. 2.1). Ono and Watanabe (1983) suggested a multiple-magma chambers model for the post-caldera volcanism that formed by the single magma chamber fracturing when the caldera collapsed on the basis of their geological data.

The pre-caldera volcanisms (2.2–0.43 Ma; Fig. 2.1, 2.2) are characterized by the extrusive eruptions of large volume of andesitic and small volume of rhyolitic, dacitic and basaltic lava flow units (Ono, 1965; Ono and Watanabe, 1985; Watanabe et al., 1989; Kaneoka and Ojima, 1970; Kamata, 1985). Kamata (1985) argued that the pre-caldera volcanic activities coincided with Pliocene large fissure eruptions in the north-central Kyushu which formed extensive lava plateaus. In addition, Shinmura (unpublished data) indicated that high-magnesium andesite lava erupted at 3.8 Ma in the western area of Aso caldera (Fig. 2.2). The pre-caldera volcanic stage is not recognized as a part of Aso volcanism, because the petrographic and geochemical characteristics of the volcanic products are different from those of volcanic products from both caldera-forming and post-caldera stages (Ono and Watanabe, 1985; Watanabe, 2001). For example, the pre-caldera volcanic products show significantly lower K_2O contents than those of the Aso volcanic products (Ono and Watanabe, 1985). The detailed sequence of the pre-caldera volcanic products is not established by previous studies. The distribution of the post- and pre-caldera volcanic products which represent the diverse geochemical compositions is shown in Fig. 2.3 and 2.4.

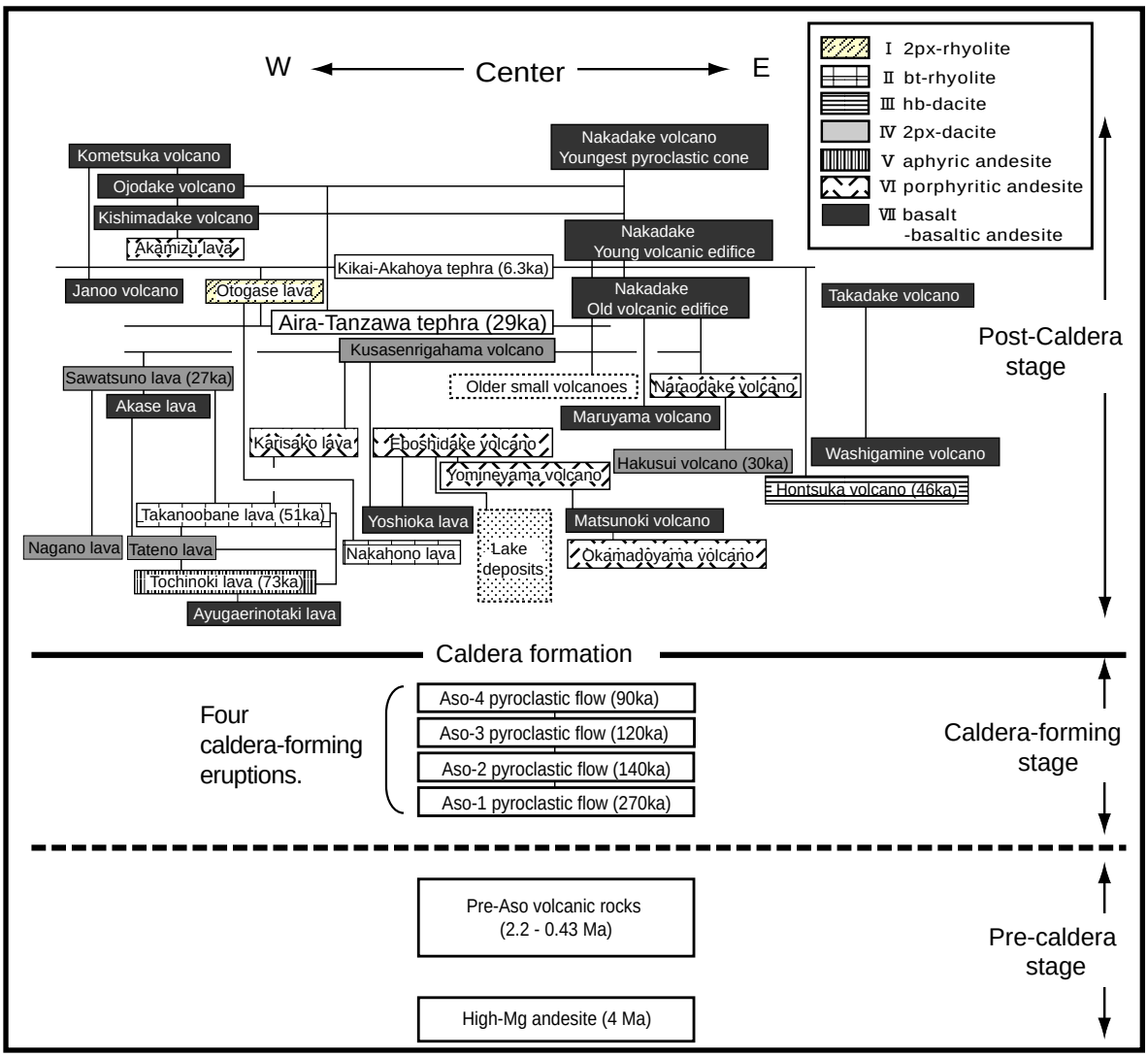

Fig. 2.1

Block diagram showing the history of the development of Aso volcano. This diagram is based on Ono (1965), Ono and Watanabe (1985), Kaneoka and Ojima (1970), Kamata (1985), Watanabe (1989), Watanabe (2001), Masuda et al. (2004) and Miyabuchi et al. (2004).

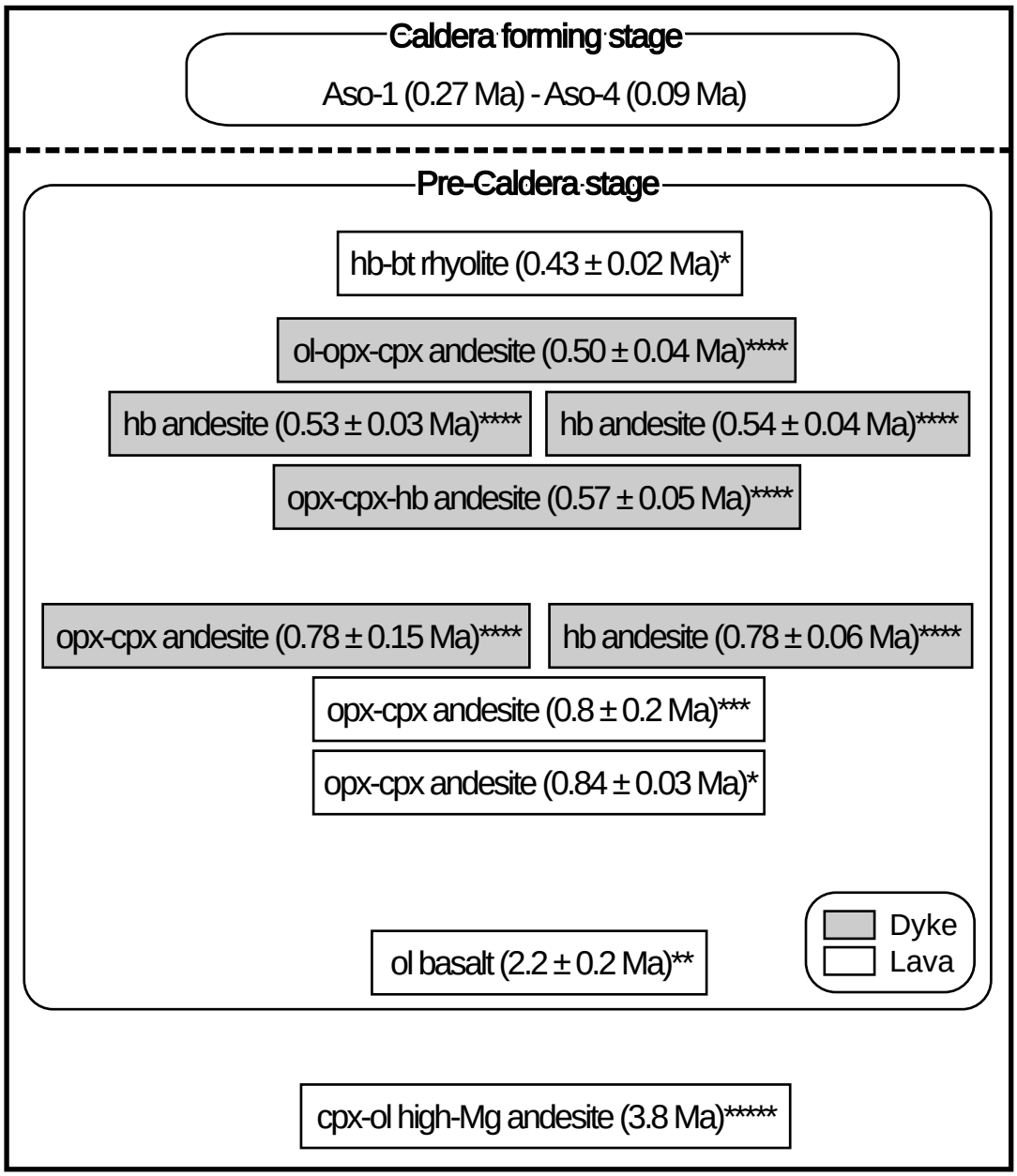

Fig. 2.2

Block diagram showing the history of the pre-caldera volcanic products in Aso area. Data sources of K-Ar ages of the volcanic products are: *Kaneoka and Ojima (1970); **Ono et al. (1982); ***Kamata (1985); ****Watanabe et al. (1989); *****Matsumoto et al. (1991); *****Shinmura (unpublished data).

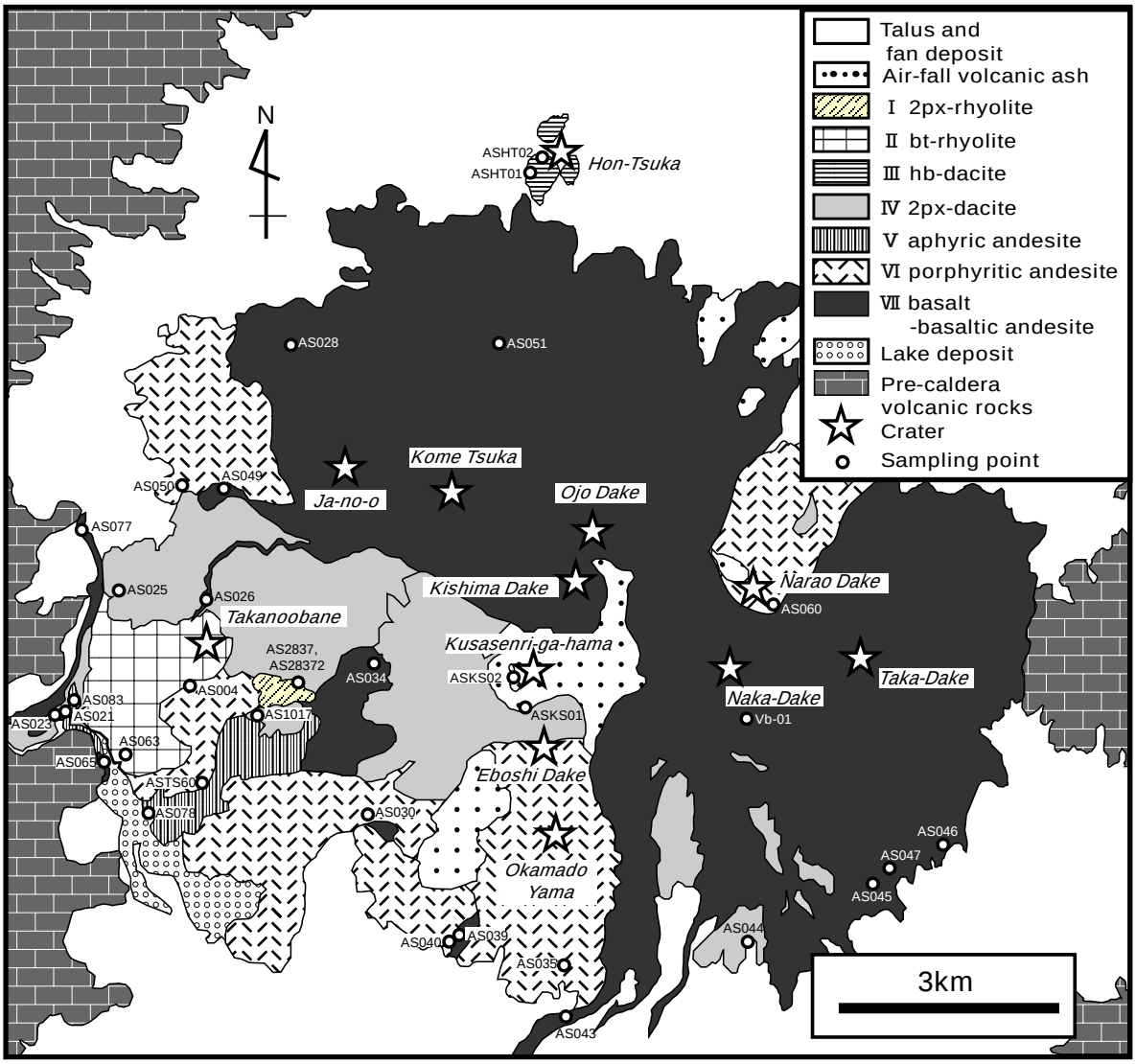

Fig. 2.3

Simplified distribution map of the post- caldera volcanic products of Aso volcano (adapted from Geological Survey of Japan Map Series 1:50,000, Ono and Watanabe, 1985).

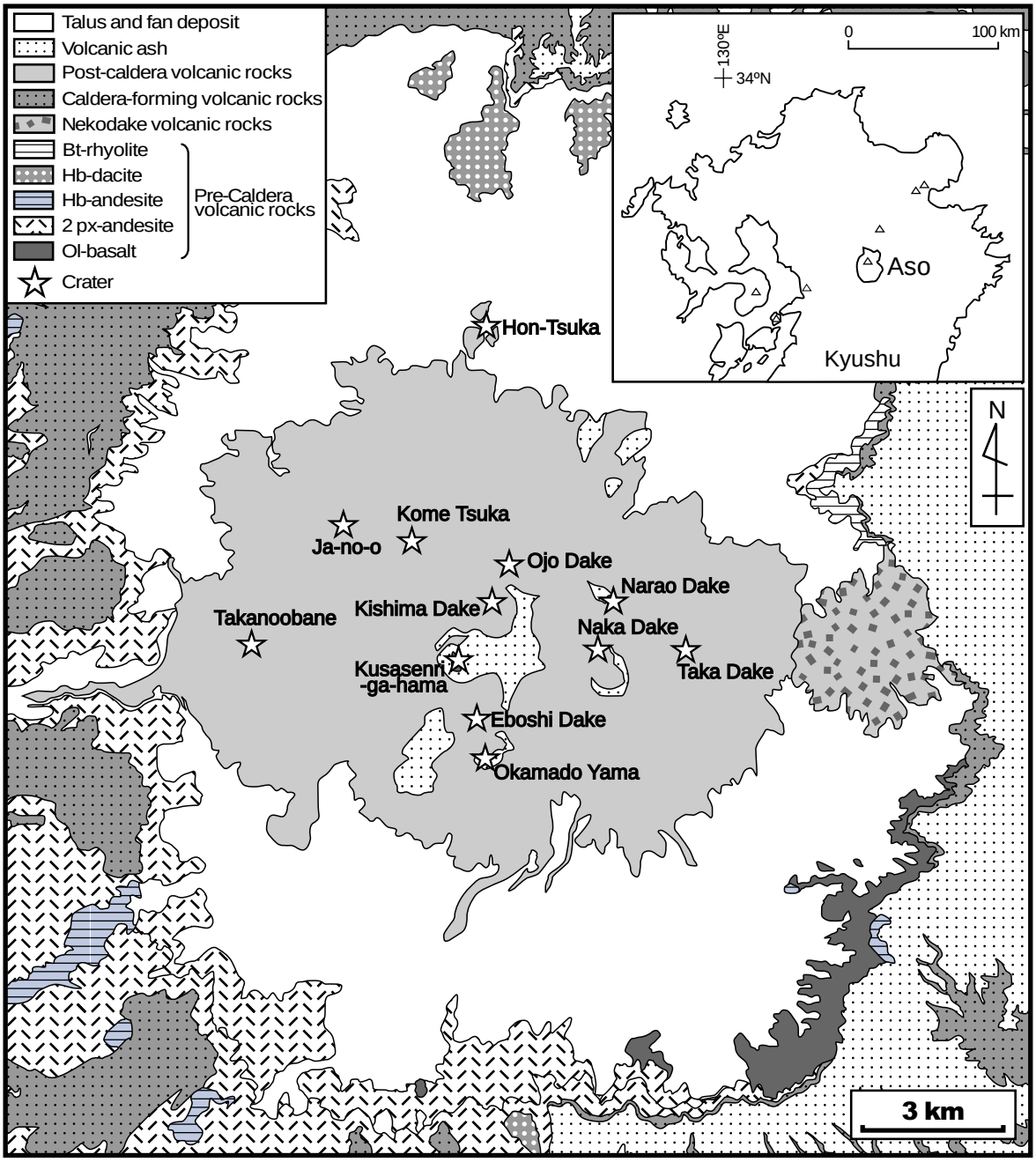

Fig. 2.4

Simplified distribution map of the pre- caldera volcanic products of Aso volcano (adapted from Geological Survey of Japan Map Series 1:50,000, Ono and Watanabe, 1985).

2.3 Samples and Methods

The samples of forty-three pre-caldera lavas and seventy-six post-caldera volcanic products were collected from a wide region of Aso area (Fig. 2.3 and 2.4). The modal abundances of phenocrysts in the representative samples of the pre- and post-caldera volcanic products are presented in Table 2.1.1 and 2.1.2, respectively.

The whole-rock chemical compositions of the samples were determined by X-ray fluorescence (XRF) on flux-fused disks with a Rigaku RIX2100 spectrometer at Fuji Tokoha University and a Philips PANalytical MagiX PRO spectrometer at Kitakyushu Museum of Natural History and Human History. The data for major and trace elements of all samples of the pre- and post-caldera volcanic products are presented in Table 2.2.1 and 2.2.2, respectively. Boron and other selected trace elements (Sm, Gd) were determined by neutron-induced prompt gamma-ray analysis (PGA) at the thermal neutron beam guide of the JRR-3M reactor, Japan Atomic Energy Research Institute. The detailed sample procedures are shown in Chapter 1.3. The data for B, Sm and Gd are presented in Table 2.2.3.

In addition, this study analyzed the modal abundances of phenocrysts, whole-rock and mineral compositions of samples of Tochinoki lava. These data are presented in Table 2.3 and 2.4.

2.4 Petrological characteristics of the pre-caldera lavas

The remnants of the pre-caldera lavas are observed in the caldera-wall and around caldera (Fig. 2.4). The several flow units of lavas and pyroclastic rocks were probably distributed in Aso area in the pre-caldera stage (Watanabe, 2001); however the most of them were disappeared by the following four huge plinian eruptions in the caldera-forming stage (Ono and Watanabe, 1985).

This study divided the pre-caldera lavas into following eight groups on the basis of their phenocryst assemblages and SiO_2 contents: A) ol-cpx basalt; B) ol-opx-cpx andesite; C) opx-cpx andesite; D) ol-hb-opx-cpx andesite; E) hb-opx-cpx andesite; F)

hb andesite; G) hb-opx-cpx dacite; H) hb-bt rhyolite. The detailed petrological characteristics of each group are shown in the following Chapter 2.4.1 and 2.4.2.

2.4.1 Petrography

Group A: Ol-cpx basalt

The basaltic lavas distributed in the southeastern part of the caldera-rim (Takamori, Nagaono and Nihonmatsu areas) are included in this group.

It includes 46–50 vol. % crystal content, as plagioclase (35–46 vol. %; < 2.5 mm), clinopyroxene (< 5 vol. %; < 0.8 mm), olivine (< 6 vol. %; < 1.6 mm) plus minor (< 1 vol. %) opaque minerals (< 0.5 mm). Most of plagioclase phenocrysts have sieve textures. Clinopyroxene phenocrysts are subhedral. Olivine phenocrysts in the samples from Takamori and Nagaono areas are fresh whereas those from Nihonmatsu area are altered into chlorite. Plagioclase, orthopyroxene, clinopyroxene and opaque minerals commonly form glomeroporphyritic aggregates. Groundmass shows intergranular or intersertal texture with many olivine, pyroxene plagioclase and opaque mineral microlites. (Fig. 2.5A)

Group B: Ol-opx-cpx andesite

The andesitic lavas distributed in the western and southwestern part of the caldera-rim (Tateno and Ichinomine areas) are included in this group. One of the andesitic dykes (0.50±0.04 Ma) reported by Watanabe et al. (1989) probably is included in this group, because the reported petrographic characteristics of the dyke sample is similar to that of the lava sample in this group.

It includes 40–42 vol. % crystal content, as plagioclase (28–30 vol. %), clinopyroxene (< 8 vol. %; < 2.0 mm), orthopyroxene (< 3 vol. %; < 2.0 mm) plus minor (< 1 vol. %) olivine (< 1.5 mm) and opaque minerals (< 0.5 mm). The following two types of plagioclase phenocrysts (< 2.5 mm) are coexisted: 1) phenocryst which

has clear core and rim; 2) phenocryst which has corroded rims and/or sieve textures. Both clinopyroxene and orthopyroxene phenocrysts are subhedral. The orthopyroxene phenocryst rarely has the reaction rim of clinopyroxene. Olivine phenocrysts are subhedral. Plagioclase, orthopyroxene, clinopyroxene and opaque minerals commonly form glomeroporphyritic aggregates. Groundmass shows intersertal or hyaloophitic texture with many pyroxene plagioclase and opaque mineral microlites. (Fig. 2.5B)

Group C: Opx-cpx andesite

The andesitic lavas widely distributed from the northern to southern part of the caldera-rim (Daikanbo, Tateno, southern Shirogatake and northern Gongenyama areas) are included in this group. Daikanbo lava (0.8±0.2 Ma; Kamata, 1985), lavas distributed in Saishigahana area (0.84±0.03 Ma; Kaneoka and Kojima, 1970) and an andesitic dyke (0.78±0.15 Ma; Watanabe et al., 1989) are included in this group, because the reported petrographic characteristics of these samples are similar to those of the lava samples in this group.

It includes 28–40 vol. % crystal content, as plagioclase (22–31 vol. %; < 4 mm), clinopyroxene (< 8 vol. %; < 2mm), orthopyroxene (< 2 vol. %; < 2 mm) and opaque minerals (< 2 vol. %; < 0.5 mm). The clear plagioclase is coexisted with dusty plagioclase which has corroded rims and/or sieve textures. Both clinopyroxene and orthopyroxene phenocrysts are subhedral. The orthopyroxene phenocryst rarely has the reaction rim of clinopyroxene. Plagioclase, orthopyroxene, clinopyroxene and opaque minerals commonly form glomeroporphyritic aggregates. Groundmass shows hyaloophitic texture with many pyroxene plagioclase and opaque mineral microlites. (Fig. 2.5C)

Group D: Ol-hb-opx-cpx andesite

The andesitic lavas distributed from the northwestern to southern part of the caldera-rim (Kario, Matoishi and Yabe areas) are included in this group.

It includes 39–49 vol. % crystal content, as plagioclase (29–37 vol. %; < 4 mm), clinopyroxene (< 11 vol. %; < 2mm), orthopyroxene (< 3 vol. %; < 2 mm) plus minor (< 1 vol. %) olivine (< 1.5 mm), hornblende (< 3mm) and opaque minerals (< 0.5 mm). The clear plagioclase is coexisted with the plagioclase which has corroded rim. Both clinopyroxene and orthopyroxene phenocrysts are subhedral. The orthopyroxene phenocryst rarely has the reaction rim of clinopyroxene. Olivine phenocrysts are subhedral. Hornblende phenocrysts are subhedral to anhedral, and have opacite rims. Plagioclase, orthopyroxene, clinopyroxene and opaque minerals commonly form glomeroporphyritic aggregates. Groundmass shows intersertal or hyaloophitic texture with many pyroxene plagioclase and opaque mineral microlites. (Fig. 2.5D)

Group E: Hb-opx-cpx andesite

The andesitic lavas distributed from the southwestern to southern part of the caldera-rim (southeastern Ichinomine and Yabe area) are included in this group. An andesitic dyke (0.57±0.05 Ma; Watanabe et al., 1989) is probably included in this group, because the reported petrographic characteristics of these samples are similar to those of the lava samples in this group.

It includes 30–42 vol. % crystal content, as plagioclase (27–35 vol. %; < 2 mm), clinopyroxene (< 4 vol. %; < 2mm), orthopyroxene (< 2 vol. %; < 2 mm) plus minor (< 1 vol. %) hornblende (< 3 mm) and opaque minerals (< 0.5 mm). The clear plagioclase is coexisted with dusty plagioclase which has sieve texture. Both clinopyroxene and orthopyroxene phenocrysts are subhedral. The orthopyroxene phenocryst rarely has the reaction rim of clinopyroxene. Hornblende phenocrysts are subhedral to anhedral, and have opacite rims. Plagioclase, orthopyroxene, clinopyroxene and opaque minerals commonly form glomeroporphyritic aggregates. Groundmass shows intersertal or hyaloophitic texture with many pyroxene plagioclase and opaque mineral microlites. (Fig. 2.5E)

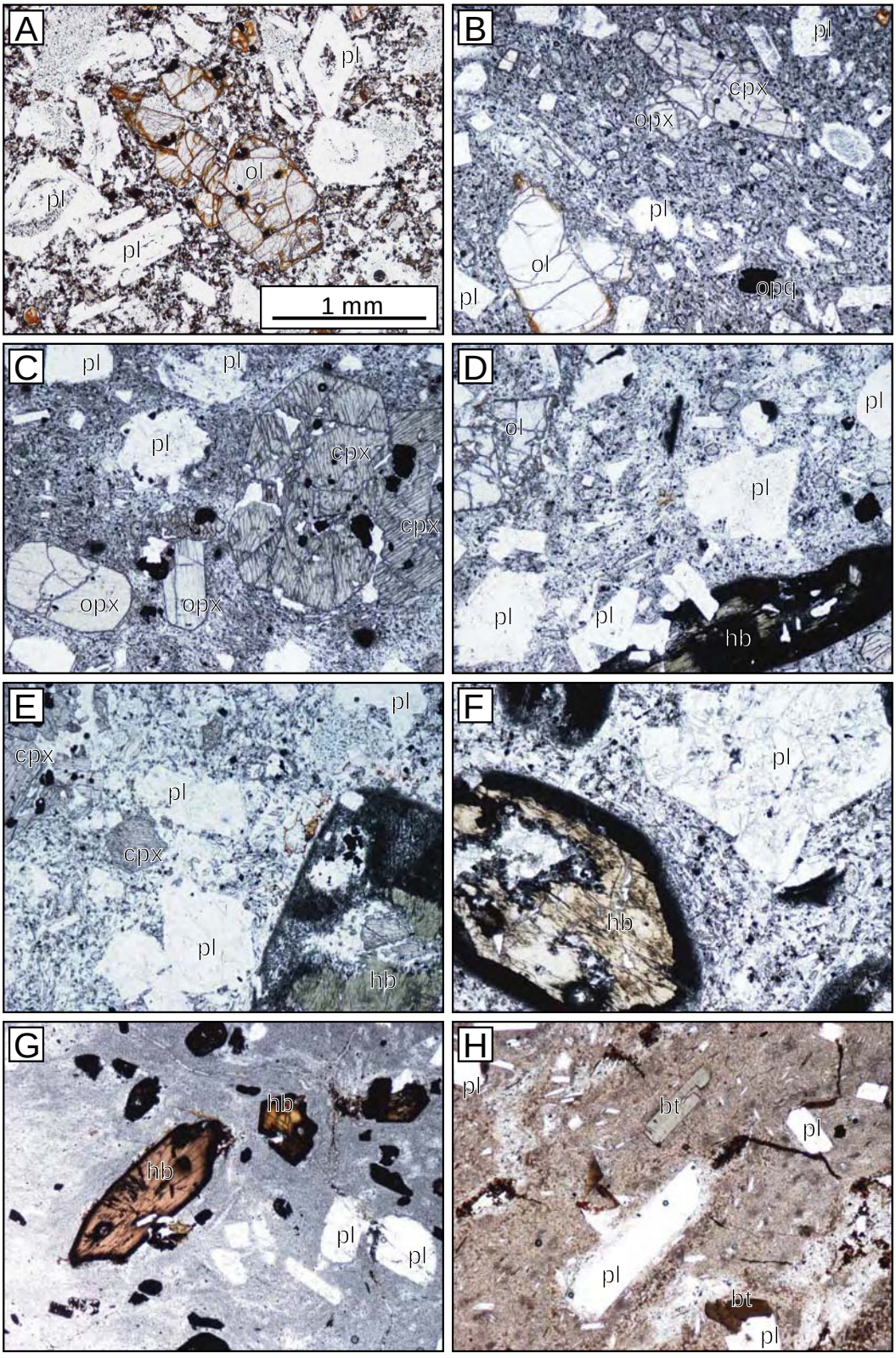

Fig. 2.5

Microscopic photographs of the pre-Aso volcanic rocks: (A) ol-cpx basalt; (B) ol-cpx-opx andesite; (C) cpx-opx andesite; (D) ol-cpx-opx-hb andesite; (E) cpx-opx-hb andesite; (F) hb andesite; (G) cpx-opx-hb dacite; (H) hb-bt rhyolites. Abbreviations: ol = olivine; cpx = clinopyroxene; opx = orthopyroxene; hb = hornblende; bt = biotite; pl = plagioclase; opq = opaque minerals.

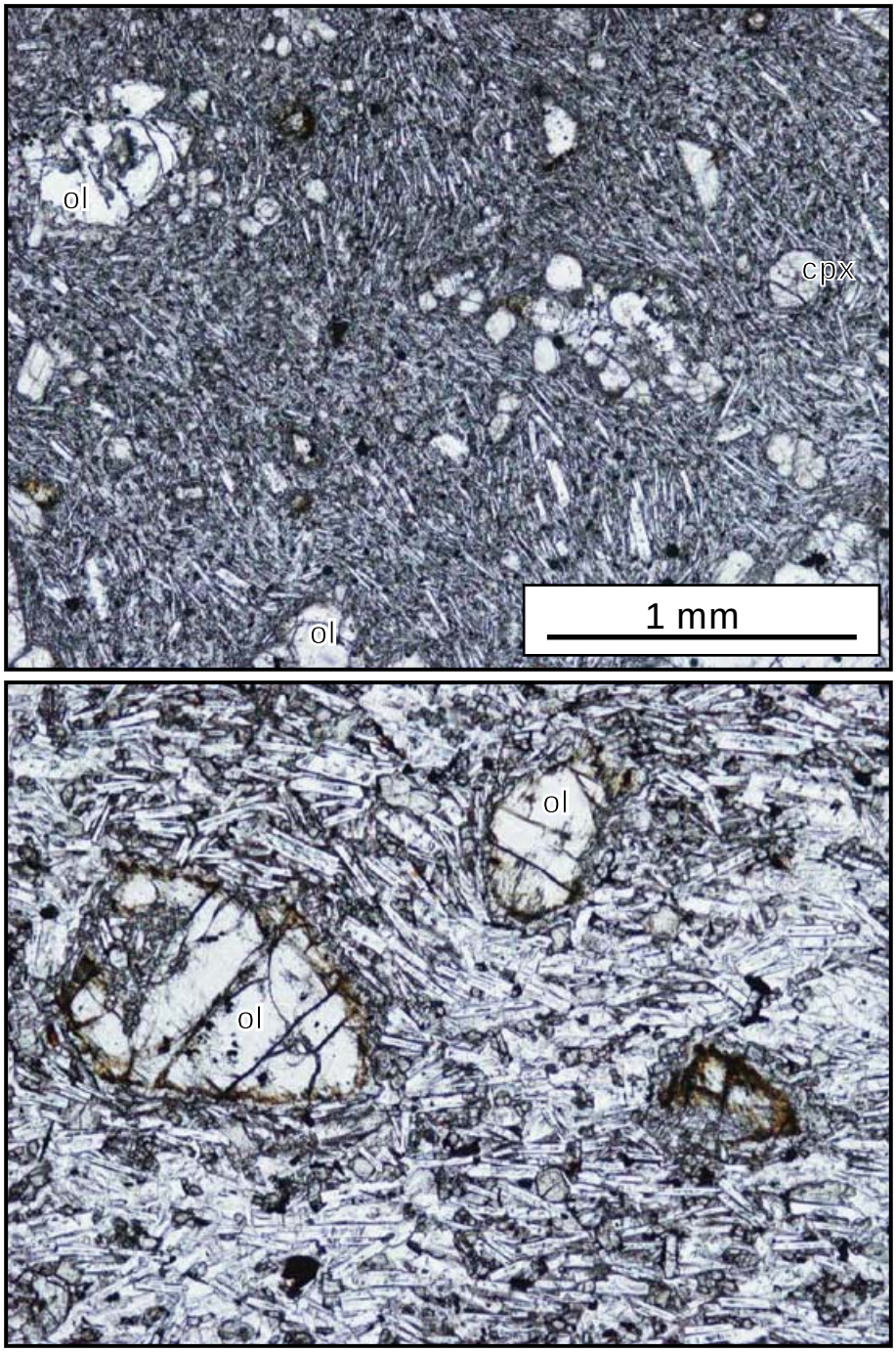

Fig. 2.6

Microscopic photographs of the pre-caldera high-magnesian andesite lava which is distributed in Haidoko area. Abbreviations: ol = olivine; cpx = clinopyroxene.

Group F: Hb andesite

The andesitic lavas distributed in the southwestern part of the caldera-rim (southeastern Ichinomine area) are included in this group. An andesitic dyke (0.54±0.04 Ma; Watanabe et al., 1989) is probably included in this group, because the reported petrographic characteristics of these samples are similar to those of the lava samples in this group.

It includes 22–26 vol. % crystal content, as plagioclase (19–26 vol. %; < 2 mm) plus minor (< 1 vol. %) hornblende (< 2 mm) and opaque minerals (< 0.5 mm). The clear plagioclase is coexisted with dusty plagioclase which has sieve texture. Hornblende phenocrysts are subhedral to anhedral, and have opacite rims. Plagioclase, hornblende and opaque minerals commonly form glomeroporphyritic aggregates. Groundmass shows hyaloophitic or hyalopilitic texture with many pyroxene plagioclase and opaque mineral microlites. (Fig. 2.5F)

Group G: Hb-opx-cpx dacite

The dacitic lavas distributed in the southern part of the caldera-rim (Takajoya area) are included in this group.

It includes vol. % crystal content, as plagioclase (vol. %; < 2 mm), clinopyroxene (vol. %; < 1 mm), orthopyroxene (vol. %; < 1 mm) and hornblende (< 1 mm) and opaque minerals (< 0.5 mm). The almost all plagioclase phenocrysts have corroded rims and/or sieve textures. Both clinopyroxene and orthopyroxene phenocrysts rarely have corroded rims. Hornblende phenocrysts are subhedral to anhedral, and have opacite rims. Groundmass is glassy, and shows hyaloophitic texture with many plagioclase and opaque mineral microlites. (Fig. 2.5G)

Group H: Hb-bt rhyolite

The rhyolitic lavas distributed in the eastern part of the caldera-rim (Sakanashi and

Saishigahana) are included in this group. Sakanashi rhyolite lava (0.43±0.02 Ma; Kaneoka and Ojima, 1970) is probably included in this group, because the reported petrographic characteristics of these samples are similar to those of the lava samples in this group.

It includes < 7 vol. % crystal content, as plagioclase (< 5 vol. %; < 2 mm) plus minor (< 1 vol. %) hornblende (< 2 mm), biotite (< 1 mm) and opaque minerals (< 0.4 mm). The plagioclase phenocrysts are euhedral to subhedral, and have clear rims. Hornblende phenocrysts are subhedral to anhedral, and have opacite rims. Biotite phenocrysts are subhedral. Plagioclase, hornblende and opaque minerals commonly form glomeroporphyritic aggregates. Groundmass is glassy, and shows flow band. (Fig. 2.5H)

Cpx-ol-high-magnesian andesite

The andesitic lavas distributed in the southwestern part of the caldera-rim (Haidoko) are included in this group. These andesites are reported as the high-MgO andesites by Shiraki et al. (1995).

It includes < 20 vol. % crystal content, as olivine (15–20 vol. %; < 2 mm) plus minor (< 1 vol. %) clinopyroxene (< 0.5 mm) and opaque minerals (< 0.4 mm). The olivine phenocrysts are occasionally surrounded by the thin pyroxene reaction-rims. Groundmass is devitrified, and shows intergranular textures with many plagioclase and pyroxene microlites. (Fig. 2.6)

2.4.2 Major and trace element compositions

On a total alkali vs. silica diagram (Fig. 2.7) the pre-caldera lava samples plot in the range from basalt to rhyolite, and plot around the boundary between alkalic and sub-alkalic rock series.

The geochemical trends of the pre-caldera lavas are depicted through the use of the Harker diagrams (Fig. 2.8, 2.9). With the exception of TiO_2, Na_2O, P_2O_5, Ni, Nb, Y and

Cr which show no apparent trend, Al_2O_3, Fe_2O_3, MgO, CaO, MnO, Sr and V display well defined negative, whereas K_2O, Ba, Rb and Zr display positive correlation with SiO_2. The andesitic groups of B, C, D, E and F have the wide range in compositions, and overlap each other. The high-magnesian andesite shows entirely different trend from the other pre-caldera lavas.

In MgO vs. Al_2O_3 diagram (Fig. 2.10), the basalt samples in group A are plotted in the field of low-magnesium high-alumina basalt which is suggested by Kuno (1960) and Sisson and Grove (1993b). This low-Mg high-Al basalt is the most typical type of basalt observed in the Island-arc setting around the world (Kuno, 1960; Sisson and Grove, 1993b). The andesitic products (group B, C, D, E and F) are also plotted in the compositional range of the low-Mg high-Al basalt. However, the high-Mg andesites are not plotted in this range.

Fig. 2.11 shows adakite field in the Y vs. Sr/Y diagram. The adakitic magma, which has high Sr/Y ratio and low Y contents, is interpreted as a partial melt of the oceanic slab with a garnet residue (Defant and Drummond, 1990). The andesite samples of group E are plotted in the adakite field suggested by Defant and Drummond (1993). On the other hand, the other andesite, dacite and rhyolite samples are plotted in the field of the typical Island-arc andesite, dacite and rhyolite (ADR) in the Fig. 2.11.

The trace element characteristics of the basalts and andesites from the pre-caldera stage are simply illustrated by normalizing their trace element contents to those of the normal-MORB (Fig. 2.12; Sun and McDonough, 1989). The incompatible elements of the basalts (group A) represent the IAB-like patterns which are characterized by their positive B and negative Nb. However the basalts have lower B and higher Rb, K, Nb, Sr, Sm and Zr than those of the typical IAB (JB-2: basalt from Izu-Bonin arc). The andesites (group B, C, D, E and F) represent the patterns which are similar to the typical Island-arc andesites (JA-1: Hakone volcano; JA-3: Asama volcano). The andesites have higher Rb, K, Nb, Sr, Sm and Zr and lower B contents than those of the typical arc-type andesites. The adakitic andesites (group E) have lower Nb, Sm, Zr, Gd and Y contents than those of the other pre-caldera andesites (Fig. 2.12).

The high-Mg andesites represent the different patterns from the typical arc-type

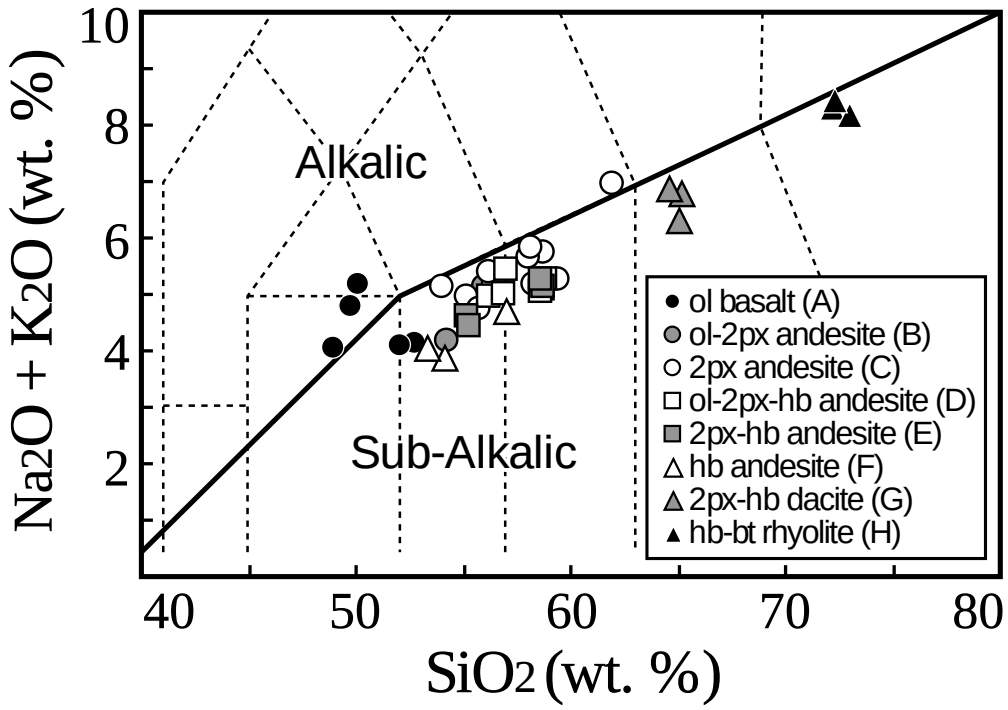

Fig. 2.7

Total alkali versus silica plots for the pre-caldera volcanic products. Thick lines indicate alkali-tholeiitic rocks suite boundary (LeMaitre et al., 1989; MacDonald and Katsura, 1964).

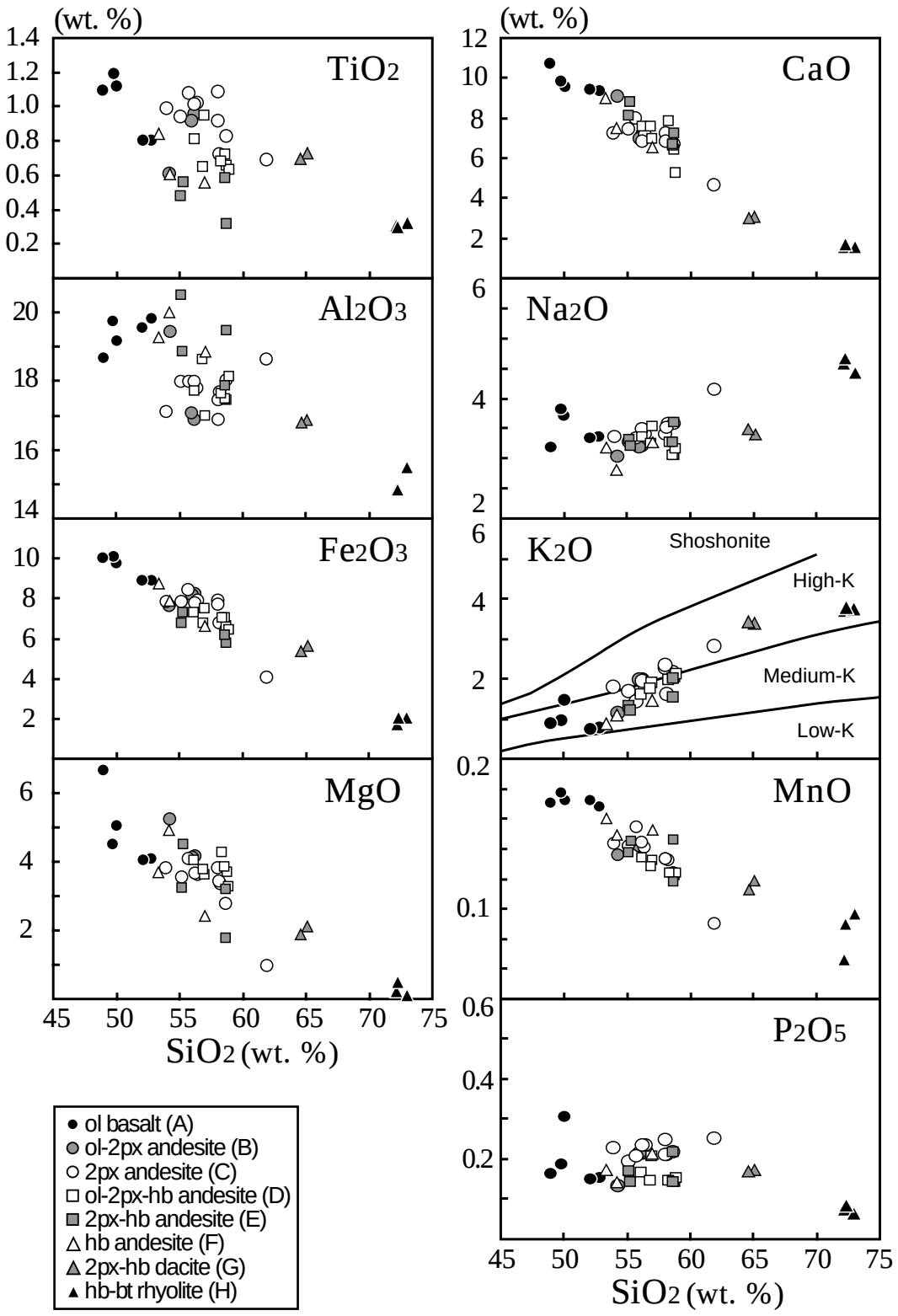

Fig. 2.8

Major elements (TiO_2, Al_2O_3, Fe_2O_3, MgO, CaO, Na_2O, K_2O and P_2O_5) vs. SiO_2 for the pre-Aso volcanic rocks. Thick lines indicate Low-K, Medium-K, High-K and Shoshonite rock series boundary (LeMaitre et al., 1989; Rickwood, 1989).

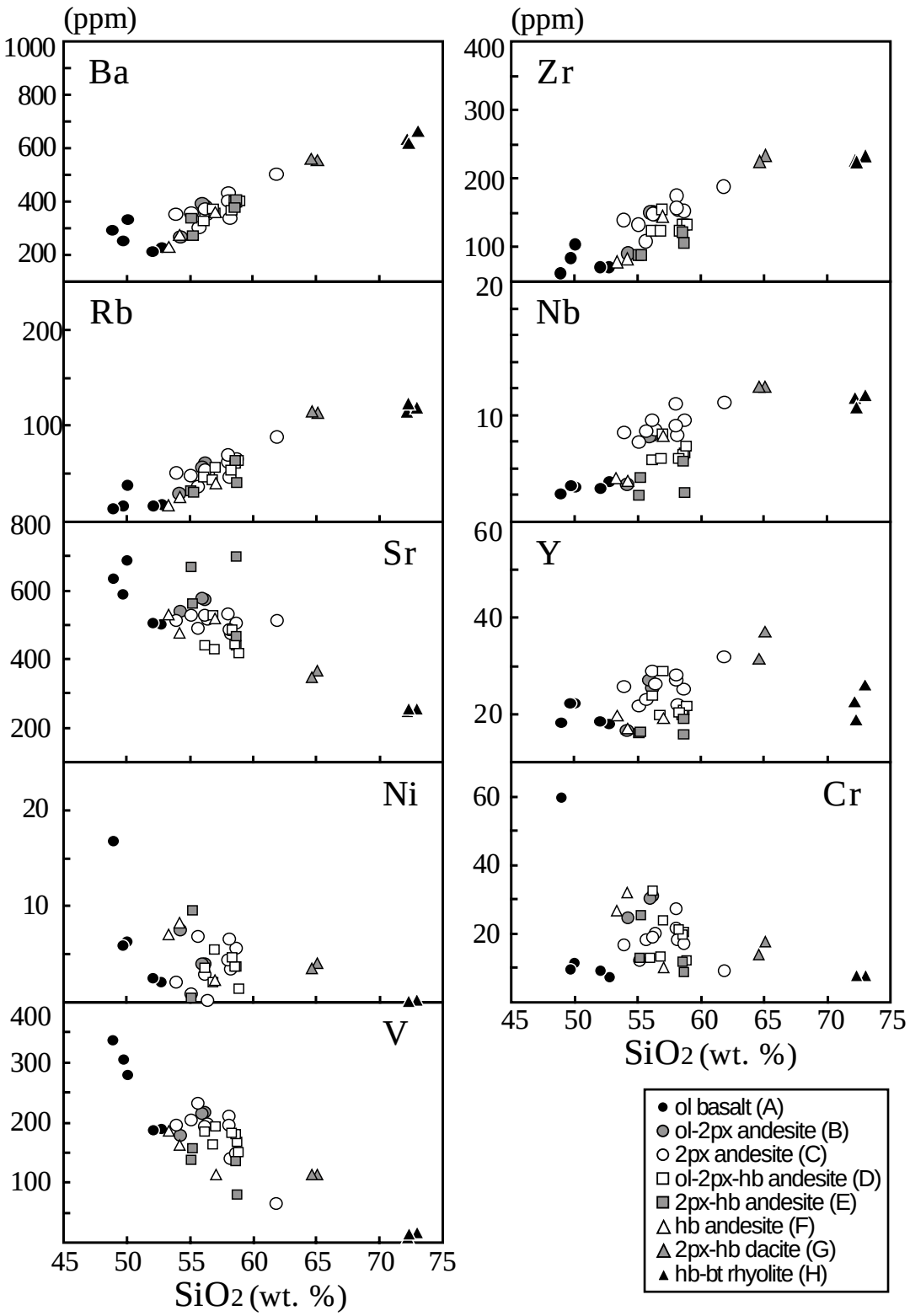

Fig. 2.9

Trace elements (Ba, Rb, Sr, Ni, V, Zr, Nb, Y, Cr) vs. SiO2 for the pre-Aso volcanic rocks.

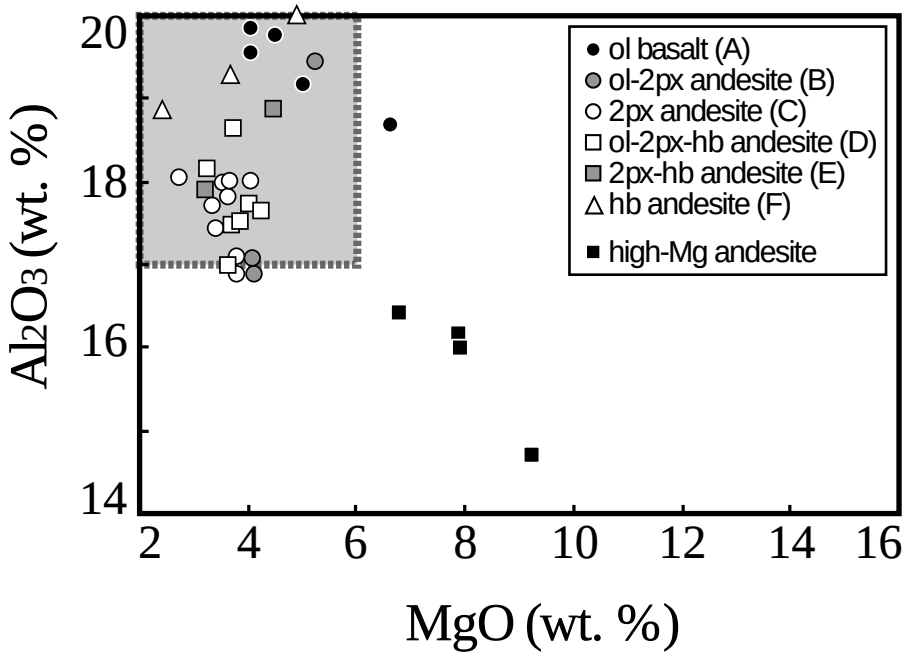

Fig. 2.10

MgO vs. Al_2O_3 diagram for the pre-caldera basaltic rocks. Shaded area shows the compositional range of low-MgO high-Alumina basalt (Kuno, 1960; Sisson and Grove, 1993b).

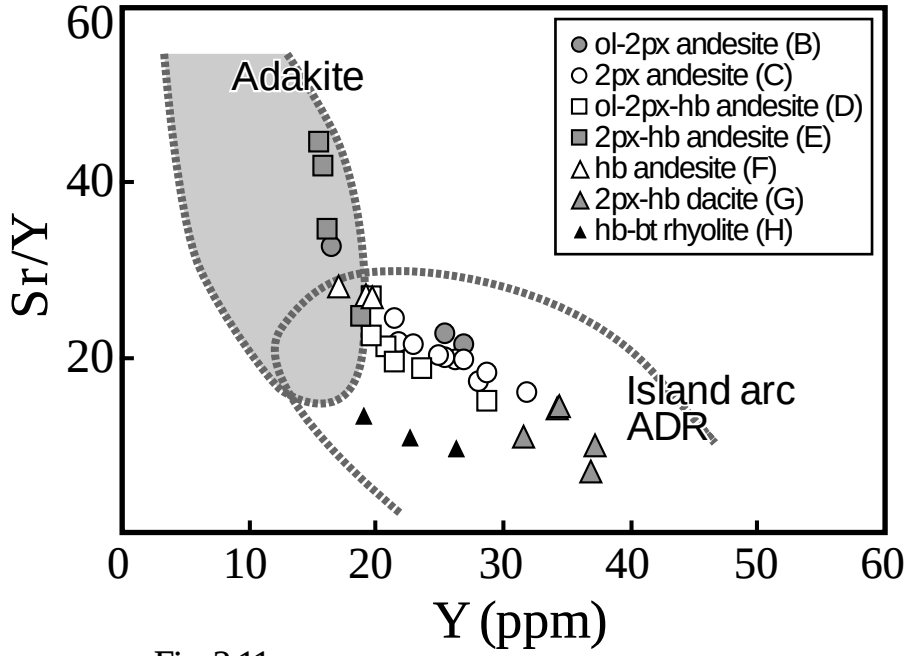

Fig. 2.11

Y vs. Sr/Y diagram for the pre-Aso volcanic rocks. The adakite and island arc ADR (andesite, dacite and rhyolites) fields are given by Defant and Drummond (1993).

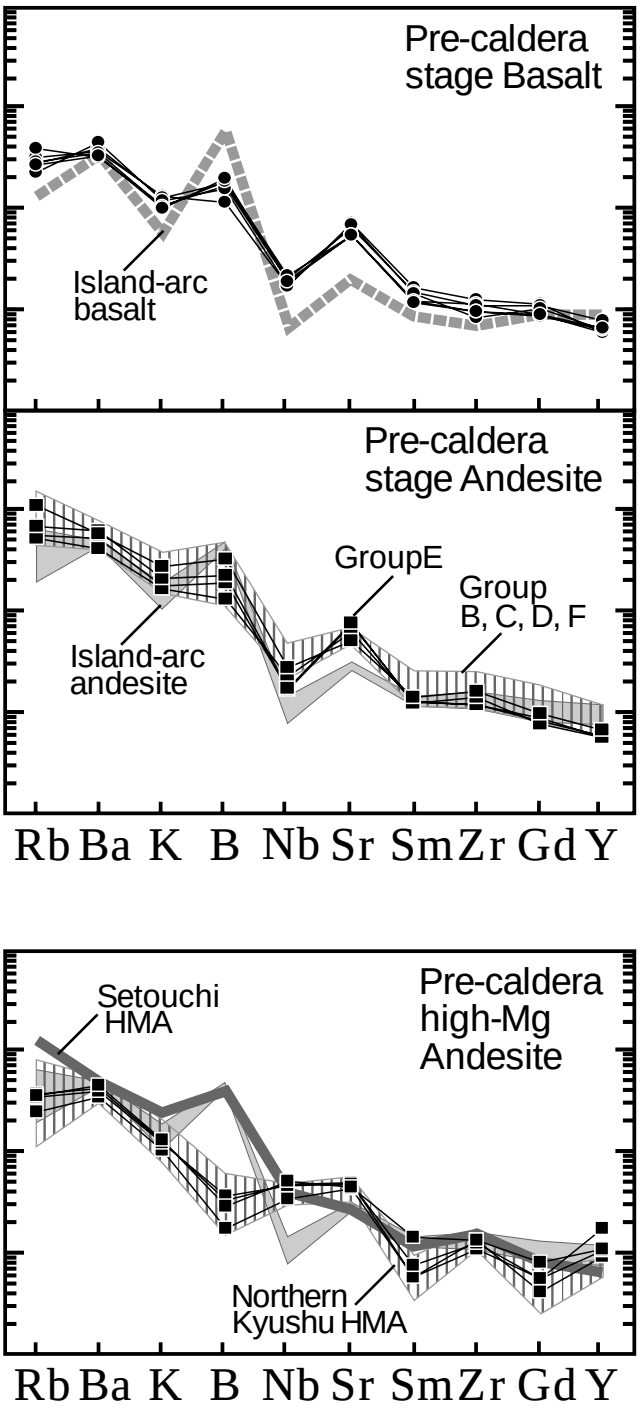

Fig. 2.12

Spider diagrams of incompatible elements for pre-caldera mafic rocks. Data for Island-arc basalt, andesite and Setouchi high-Ng andesite (HMA) are from the database of GSJ standard samples (JB-2, JA-1, JA-2 and JA-3). Abundances are normalized by n-MORB values: Rb (0.56), Ba (6.3), K (600), B (0.5), Nb (2.33), Sr (90), Sm (2.63), Zr (74), Gd (3.68), Y (28) (Sun and McDonough, 1989).

andesites and Setouchi high-Mg andesite. The high-Mg andesites have lower Rb, K, B, Sm and Gd and higher Sr and Y contents than those of the Setouchi high-Mg andesite. In particular, the B contents of the high-Mg andesites are significantly lower than those of the typical arc-type andesites and Setouchi high-Mg andesites (Fig. 2.12).

2.5 Petrological characteristics of the post-caldera volcanic products

Approximately thirty units of the post-caldera lavas are reported by Ono and Watanabe (1985). These flow units were distinguished by their topographies and volcanic stratigraphies. In order to discuss the origin of these volcanic products, this study divided the post-caldera volcanic products into following seven groups on the basis of their phenocryst assemblages, abundances and SiO_2 contents: I) two-px rhyolite; II) bt rhyolite; III) hb dacite; IV) two-px dacite; V) aphyric andesite; VI) porphyritic andesite; VII) basalt-basaltic andesite. The criteria of this grouping are presented in Table 2.5. The detailed petrological characteristics are shown in the following Chapter 2.5.1 and 2.5.2.

2.5.1 Petrography

Group I: Two pyroxene rhyolite

Otogase lava (Masuda et al., 2004) applies to this group. All samples are fresh obsidian lavas. It includes 5-10 vol. % crystal content, as plagioclase (4-9 vol. %) plus minor (< 1 vol. %) orthopyroxene, clinopyroxene and opaque minerals. Most of plagioclase phenocrysts (< 0.6 mm) have corroded rims, and/or sieve textures. Both orthopyroxene (< 0.2 mm) and clinopyroxene (< 0.3 mm) are subhedral to anhedral. Plagioclase, orthopyroxene, clinopyroxene and opaque minerals commonly form glomeroporphyritic aggregates. Groundmass is clear and glassy with few microlites. (Fig. 2.13-I)

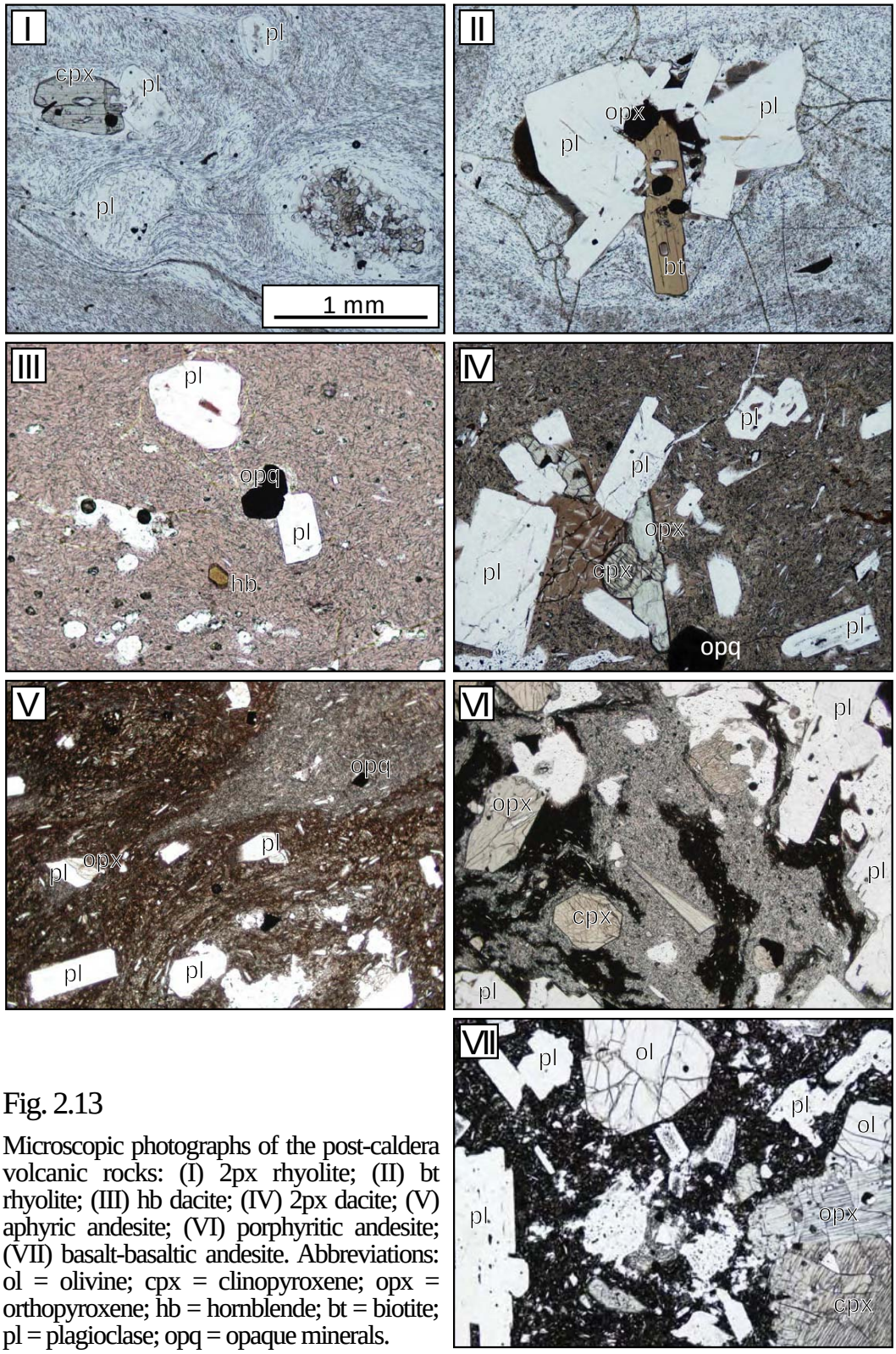

Fig. 2.13

Microscopic photographs of the post-caldera volcanic rocks: (I) 2px rhyolite; (II) bt rhyolite; (III) hb dacite; (IV) 2px dacite; (V) aphyric andesite; (VI) porphyritic andesite; (VII) basalt-basaltic andesite. Abbreviations: ol = olivine; cpx = clinopyroxene; opx = orthopyroxene; hb = hornblende; bt = biotite; pl = plagioclase; opq = opaque minerals.

Group II: Biotite rhyolite

Takanoobane lava applies to this group. All samples are aphyric obsidian lavas, with 10-12 vol. % crystal content as plagioclase (5-10 vol. %), biotite (1-2 vol. %) plus minor (< 1%) orthopyroxene, clinopyroxene and opaque minerals. Plagioclase phenocrysts (< 0.5 mm) are often twinned and surrounded by clear rims. Both orthopyroxene (< 0.3 mm) and clinopyroxene (< 0.2 mm) phenocrysts are subhedral to anhedral. Both clino- and ortho-pyroxene phenocrysts are usually surrounded by weakly corroded rims. Biotite phenocrysts (< 0.3 mm) are subhedral to euhedral. Some biotite phenocrysts have opacite rims or include plagioclase or opaque microlites. There are two types of glomeroporphyritic aggregates; Plagioclase + orthopyroxene + clinopyroxene + opaque mineral and plagioclase + biotite + opaque mineral. Groundmass textures are from glassy with few microlites to spherulitic. (Fig. 2.13-II)

Group III: Hornblende dacite

This group includes Hontsuka lava. All samples are aphyric lavas, with 5-10 vol. % crystal content as plagioclase (4-7 vol. %) plus minor (< 1 vol. %) hornblende, orthopyroxene, clinopyroxene and opaque minerals. Plagioclase phenocrysts (< 0.5 mm) are subhedral to euhedral, and are twinned and zoned. Both orthopyroxene (< 0.2 mm) and clinopyroxene (< 0.4 mm) are subhedral to anhedral, and usually have weakly corroded rims. Most of hornblende phenocrysts (< 0.1 mm) are oxidized. Plagioclase, orthopyroxene, clinopyroxene, hornblende and opaque minerals commonly form glomeroporphyritic aggregates. Groundmass is glassy, and shows light brown in color. (Fig. 2.13-III)

Group IV: Two pyroxene dacite

This group includes Tateno, Hakusui, Sawatsuno, Nagano lavas and Kusasenrigahama welded pyroclastic rocks. Samples are glassy lavas or pyroclastic

rocks, with 7-17 vol. % crystal content as plagioclase (5-15 vol. %), clinopyroxene (1-2 vol. %) plus minor (< 1 vol. %) orthopyroxene and opaque minerals. Plagioclase (< 0.7 mm) is subhedral to euhedral. Some plagioclase phenocrysts appear undulatory extinction, and include pyroxene, glass and opaque mineral microlite. Both orthopyroxene (< 0.4 mm) and clinopyroxene (< 0.4 mm) are subhedral to euhedral, and usually have weakly corroded rims. Plagioclase, orthopyroxene, clinopyroxene and opaque minerals commonly form glomeroporphyritic aggregates. Groundmass texture is glassy with few microlites or hyaloophytic. (Fig. 2.13-IV)

Group V: Aphyric andesite

Tochinoki lava applies to this group. The samples of Tochinoki lava treated in this study are collected from outcrops and two borehole cores (Fig. 2.14). These borehole cores were obtained by Volcanological laboratory of Kyoto University in 2002. The Tochinoki lava samples are observed in the two borehole cores, AVL1 and AVL4 (Fig. 2.15). The Tochinoki lava shows two compositionally different lava types. One is silicic (SiO_2 63-66 wt. %) and phenocryst-rich (8-16 vol. %), and the other is mafic (SiO_2 60-62 wt. %) and phenocryst-poor (< 7 vol. %). Both the silicic Tochinoki lava (ST) and mafic Tochinoki lava (MT) are commonly observed in the outcrop and borehole core samples (Fig. 2.16). For convenience sake, I call those of the core samples as STC and MTC, and those of the outcrop samples as STO and MTO.

The MTC includes 3–6 vol. % crystal contents as plagioclase (< 5 vol. %; < 1 mm), clinopyroxene (< 1 vol. %; < 0.5 mm), orthopyroxene (< 1 vol. %; < 0.8 mm) plus minor (< 1 vol. %; < 0.5 mm) magnetite. The STC includes 8–15 vol. % crystal contents as plagioclase (5–10 vol. %; < 2 mm), clinopyroxene (1–2 vol. %; < 1 mm), orthopyroxene (< 1 vol. %; < 1 mm) and magnetite (< 2 vol. %; < 0.5 mm). The plagioclase phenocryst content of the STC is higher than that of the MTC. Plagioclase, orthopyroxene, clinopyroxene and magnetite commonly form glomeroporphyritic aggregates in these groups. Groundmasses of the MTC and STC show hyaloophitic or hyalopilitic textures with few microlites of clinopyroxene, plagioclase and magnetite

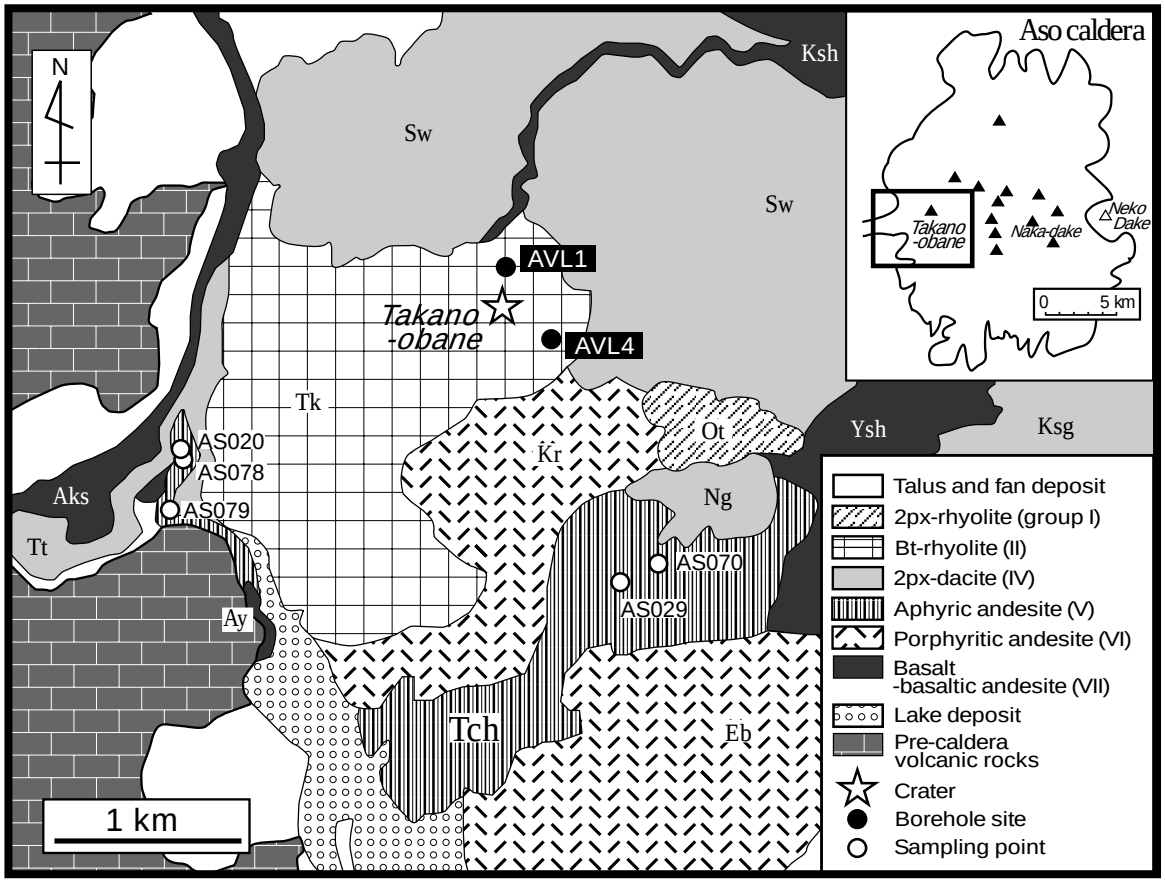

Fig. 2.14

Geologic map of the western part of Aso caldera (Ono and Watanabe, 1985; Masuda et al., 2004; Miyabuchi et al., 2004). Abbreviations: Ot = Otogase; Tk = Takanoobane; Tt = Tateno; Sw = Sawatsuno; Ng = Nagano; Ksg = Kusasenrigahama; Tch = Tochinoki; Eb = Eboshidake; Kr = Karisako; Aks = Akase; Ysh = Yoshioka; Ksh = Kishimadake; Ay = Ayugaerinotaki; 2px = clinopyroxene + orthopyroxene; Bt = biotite.

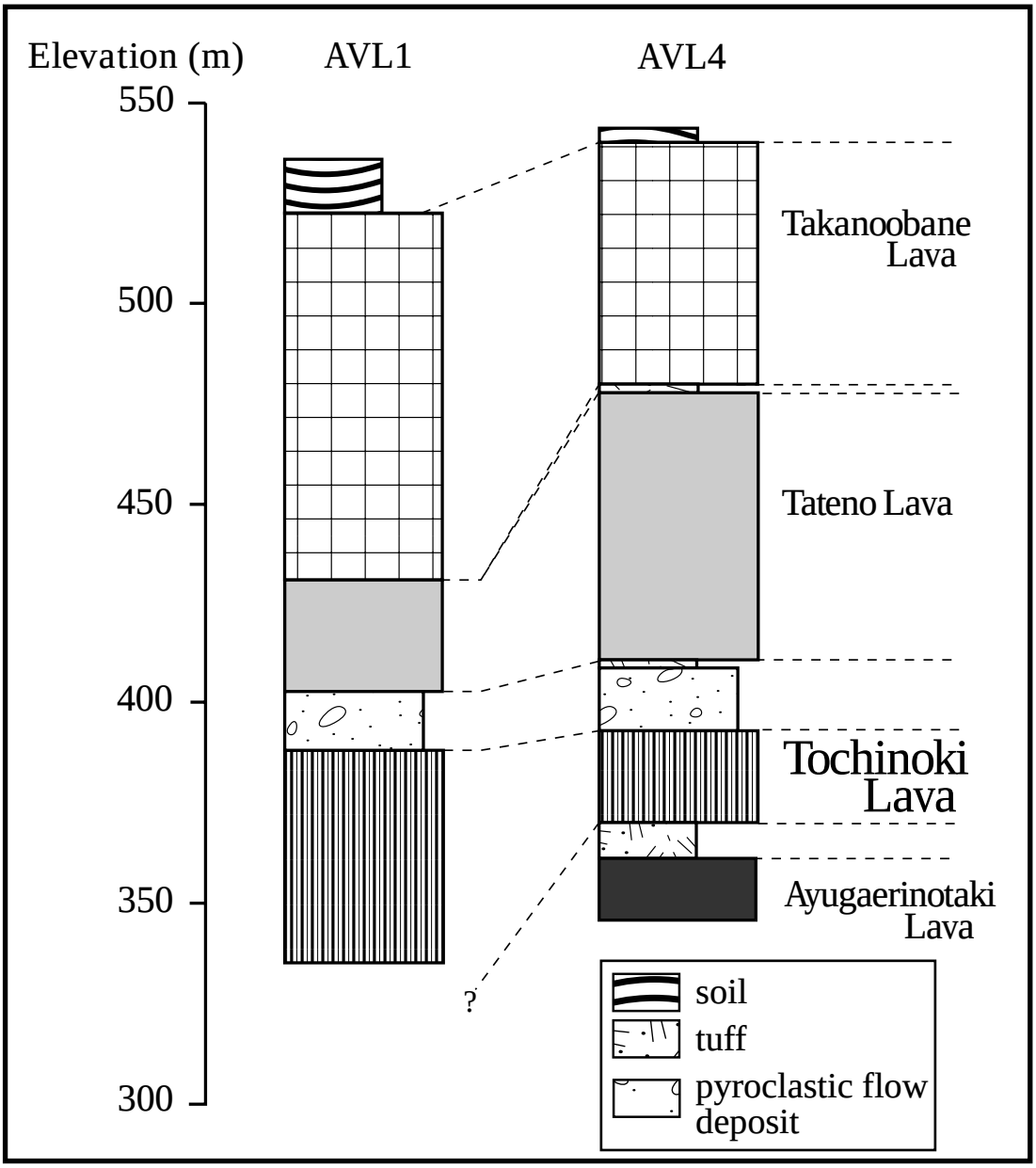

Fig. 2.15

Stratigraphic sections of borehole cores from AVL1 and AVL4 sites.

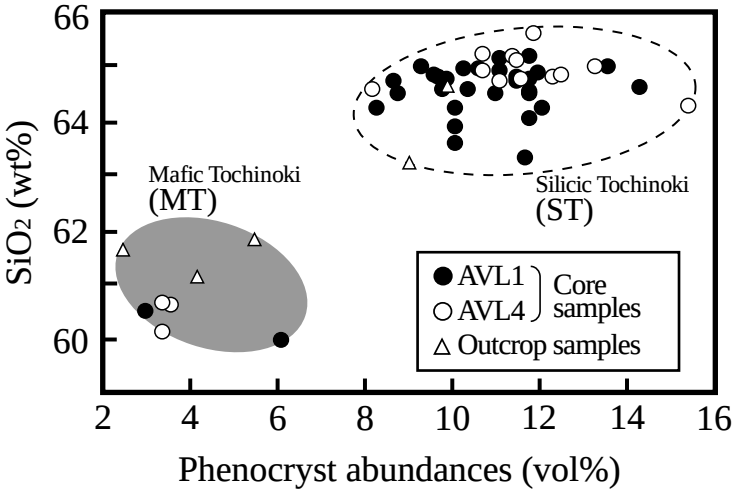

Fig. 2.16

Phenocryst abundances vs. SiO_2 contents of the Tochinoki lava. MT = Mafic Tochinoki group. ST = Silicic Tochinoki group. AVL1 and AVL2 represent borehole sites whose locations are shown in Fig. 2.14.

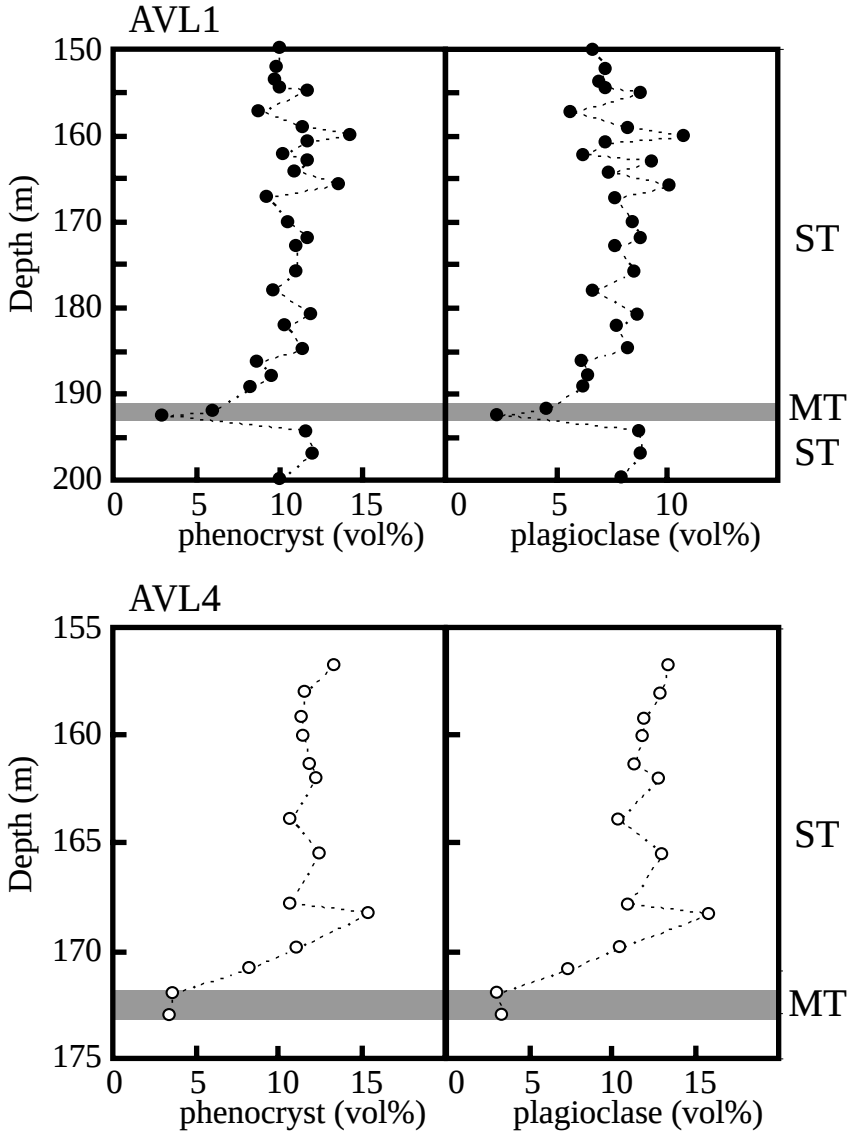

Fig. 2.17

Depth profiles (meters beneath surface) of phenocryst and plagioclase abundances in two Tochinoki core samples. Shaded areas show the occurrence of the mafic Tochinoki lavas (MT) in the borehole cores. ST = silicic Tochinoki lavas.

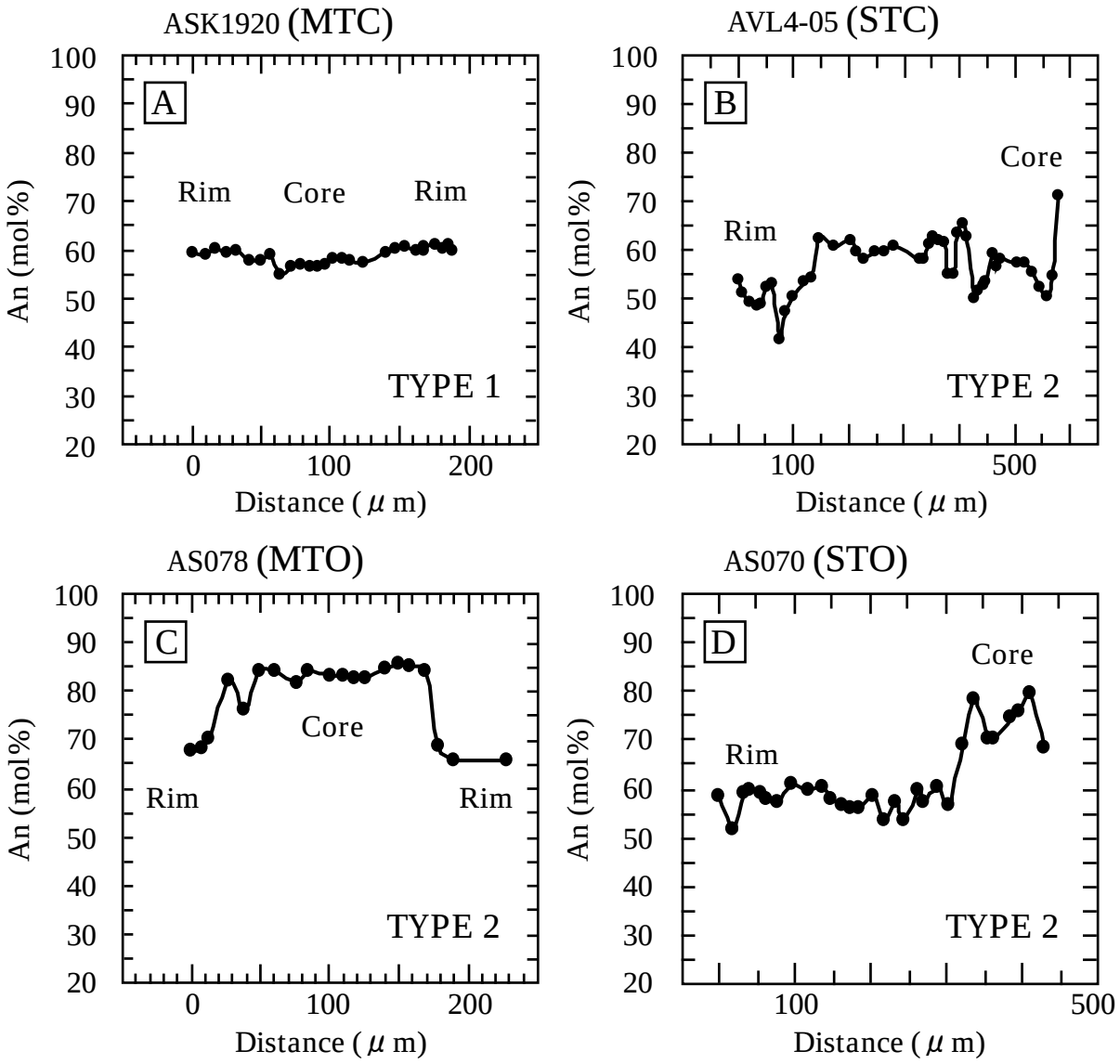

Fig. 2.18

Typical zoning profiles of representative plagioclase phenocrysts in Tochinoki lava. An = 100 x Ca / (Ca + Na + K) (mol %) (A) Discrete phenocryst in one of the mafic Tochinoki core samples ASK1920 (MTC). (B) Phenocryst in the crystal aggregate in one of the silicic Tochinoki core samples AVL4-05 (STC). (C) Discrete phenocryst in one of the mafic Tochinoki outcrop samples AS078 (MTO). (D) Discrete phenocryst in one of the silicic Tochinoki outcrop samples AS070 (STO). The core of TYPE 1 plagioclase is clear, whereas that of TYPE 2 is honey-combed.

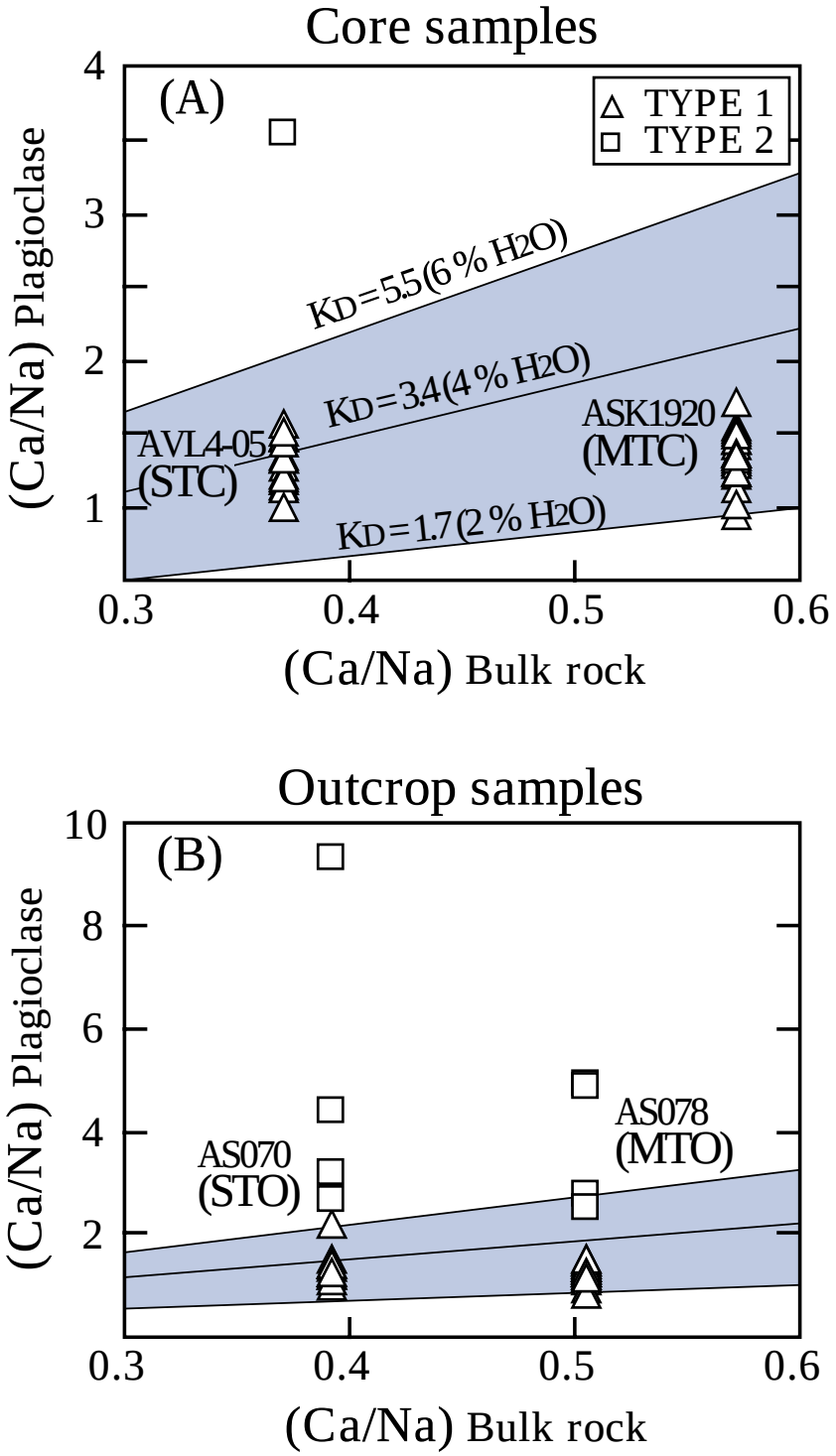

Fig. 2.19

The relationships of the Ca / Na molar ratio in plagioclase and in bulk rock for Tochinoki lavas. (A) Tochinoki core samples (MTC and STC). (B) Tochinoki outcrop samples (MTO and STO). The shaded field shows an experimentally determined compositional range in which a melt equilibrates with plagioclase at variable pressures (1-5 kb) and H_2O contents (2-6 % H_2O). A range of equilibrium KD values (= (Ca/Na) plagioclase / (Ca/Na) bulk rock) are shown for various H_2O contents (Sisson and Grove, 1993). The TYPE 1 plagioclase phenocryst is clear, whereas the TYPE 2 plagioclase phenocryst has honey-combed core mantled by clear rim. TYPE 2 plagioclase phenocrysts in both (A) and (B) are too calcic to be equilibrated with their host rock compositions.

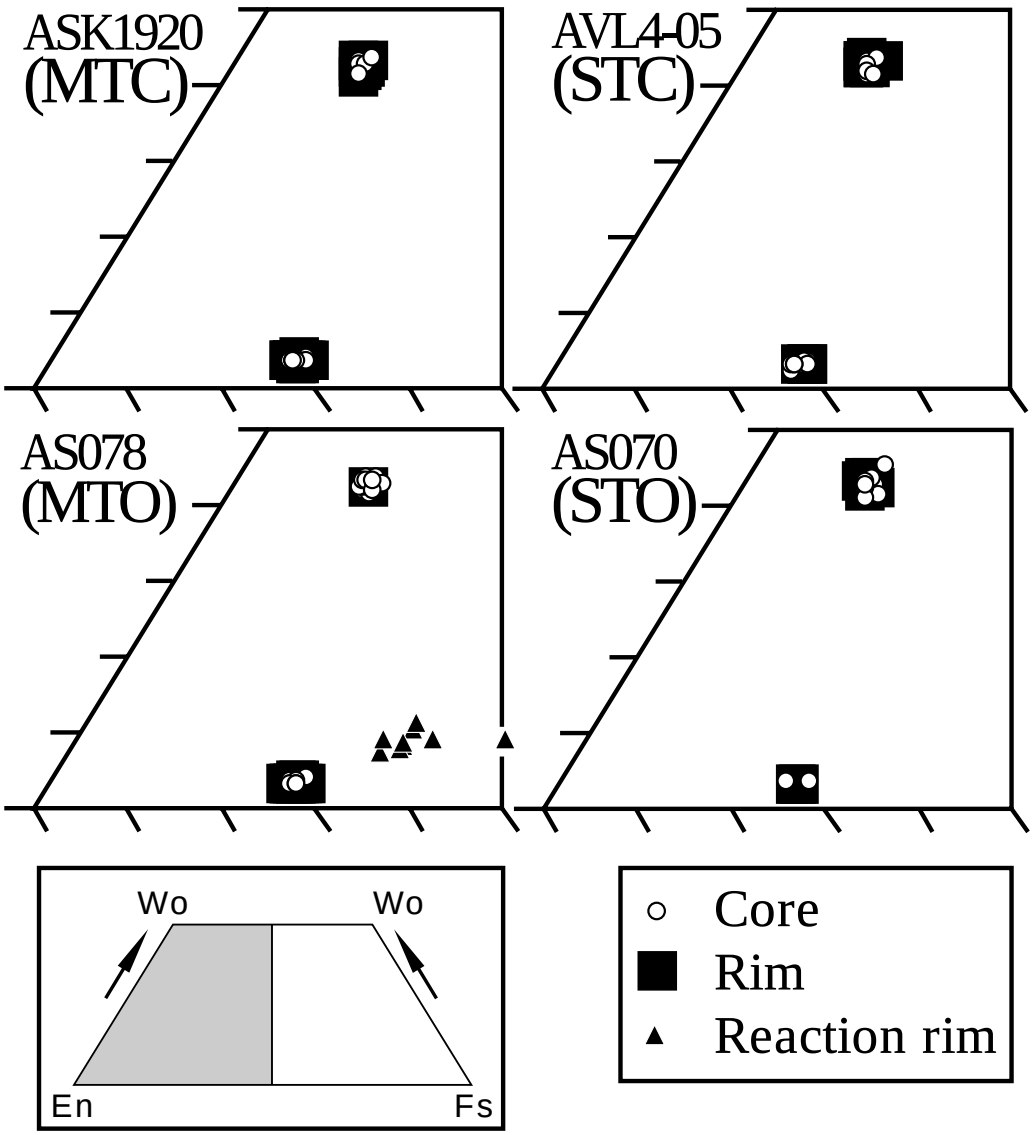

Fig. 2.20

Chemical compositions of ortho- and clinopyroxene phenocrysts in Tochinoki lava. Abbreviations: MTC = mafic Tochinoki core samples; STC = silicic Tochinoki core samples; MTO = mafic Tochinoki outcrop samples; STO = silicic Tochinoki outcrop samples; Wo = 100 x Ca / (Ca + Mg + Fe) (mol %); En = 100x Mg / (Ca + Mg + Fe) (mol %); Fs = 100 x Fe / (Ca + Mg + Fe) (mol %).

or hyaloophytic. The MTC is observed in the bottom of lava flow, and underlies the thick (>20 m) STC (Fig. 2.17).

The MTO includes 3–6 vol. % crystal contents as plagioclase (< 4 vol. %; < 1 mm), clinopyroxene (< 1 vol. %; < 0.5 mm), orthopyroxene (< 1 vol. %; < 0.8 mm) plus minor (< 1 vol. %; < 0.5 mm) magnetite. The STO includes 9–10 vol. % crystal contents as plagioclase (7–8 vol. %; < 2 mm), clinopyroxene (1–2 vol. %; < 1 mm), orthopyroxene (< 1 vol. %; < 1 mm) and magnetite (< 1 vol. %; < 0.5 mm). Plagioclase, orthopyroxene, clinopyroxene and magnetite commonly form glomeroporphyritic aggregates in these groups. Groundmasses of the MTO and STO show hyaloophitic or hyalopilitic textures with few microlites of clinopyroxene, plagioclase and magnetite. (Fig. 2.13-V)

The representative mineral compositions of MTC (ASK1920), STC (AVL4-5), MTO (AS078) and STO (AS070) are shown in Table 2.4.

The following two different types of plagioclase phenocrysts are coexisting in the Tochinoki lava: 1) the euhedral to subhedral phenocryst with clear core and rim; 2) the phenocryst with sieved core and clear rim. More than 90 % of the plagioclase phenocrysts are the type-1. The type-2 plagioclase is observed in the MTO, STO and STC. The MTC does not include the type-2 plagioclase. The modal abundances of type-2 plagioclase are higher in the STO than the STC. The type-2 plagioclase in the STC exists in the glomeroporphyritic clots, whereas the type-2 plagioclase in the STO commonly exists as a discrete phenocryst. The type-1 plagioclase phenocryst does not show significant zoning, and has the core with 54–58 % anorthite (An) and the rim with 40–58 % An (Fig. 2.18 A). The type-2 plagioclase phenocryst has the sieved core with 70–90 % An mantled by the zoned rim with 40–65 % An (Fig. 2.18 B, C and D). Fig. 2.19 shows the relationships between the Ca/Na molar ratios of plagioclase and the Ca/Na ratios of bulk rock compositions. The shaded area shows the experimentally determined plagioclase compositions in equilibrium with melt under various pressures and H_2O contents (Sisson and Grove, 1993). Fig. 2.19 shows the type-1 plagioclase is equilibrium with the host magma, whereas the type-2 plagioclase is not equilibrium with the host magma because it has too Ca-rich core compared with the equilibrium

melt composition.

All data of clino- and orthopyroxene phenocrysts are shown in Fig. 2.20. The clinopyroxene phenocrysts are euhedral to subhedral in the STC, MTC and STO. The clinopyroxene phenocrysts included in the MTO is mantled by the Ca-poor reaction-rim with $Wo_{10}En_{55}Fs_{35}$. The STC and STO include the clinopyroxene phenocrysts which have the core with 73–75 of Mg# (= Mg/ (Mg + Fe) × 100) ($Wo_{40-43}En_{43-46}Fs_{14}$) and the rim with 76 of Mg# ($Wo_{42}En_{44}Fs_{14}$). The MTC and MTO include the clinopyroxene phenocrysts which have the core with 76 of Mg# ($Wo_{42}En_{44}Fs_{14}$) and the rim with 75–76 of Mg# ($Wo_{42}En_{44}Fs_{14}$). The orthopyroxene phenocrysts are euhedral to subhedral in the STC, MTC, STO and MTO. The STC and STO include the orthopyroxene phenocrysts which have the core with 73–75 of Mg# ($Wo_3En_{71-72}Fs_{26}$–$Wo_3En_{72}Fs_{25-26}$) and the rim with 72–74 of Mg# ($Wo_3En_{70-72}Fs_{25-27}$). The MTC and MTO include the orthopyroxene phenocrysts which have the core with 72–73 of Mg# ($Wo_3En_{70-71}Fs_{26-27}$) and the rim with 71–73 of Mg# ($Wo_3En_{69-71}Fs_{26-28}$). The pre-eruptive temperatures of STC, MTC, STO and MTO estimated by using the geothermometer of Wells (1977) are < 1040 °C, 1030–1060 °C, < 1010 °C and 1010–1020 °C, respectively.

The magnetite phenocrysts included in the ST (STC and STO) and MT (MTC and MTO) have 34–40 mol % and 34–36 mol % of ulvöspinel (Usp), respectively.

Group VI: Porphyritic andesite

This group includes Okamadoyama, Eboshidake, Naraodake, Akamizu, Yomineyama, Karisako lavas and the lava forming Kusasenrigahama central cone. All samples are glassy, and are porphyritic lavas, with 40-50 vol. % crystal content as plagioclase (30-40 vol. %), clinopyroxene (3-10 vol. %), orthopyroxene (1-3 vol. %) plus minor (< 1 vol. %) opaque minerals. Plagioclase phenocrysts (< 1.4 mm) are subhedral to euhedral. Some plagioclase phenocrysts show undulatory extinction and corroded rim. Both orthopyroxene (< 0.8 mm) and clinopyroxene (< 1.5 mm) are subhedral to euhedral, and are usually surrounded by weakly corroded rim. Plagioclase,

orthopyroxene, clinopyroxene and opaque minerals commonly form glomeroporphyritic aggregates having diverse sized grain. Groundmass is usually glassy with few microlites, and sometime shows hyaloophytic texture in the devitrificated part. Some sample appears the mingling texture formed by both glassy and microlite-rich parts, or appears swirled texture (Brophy and Dreher, 2000). (Fig. 2.13-VI)

Group VII: Basalt-basaltic andesite

This group includes Ayugaerinotaki, Matsunoki, Yoshioka, Maruyama, Takadake, Kishimadake, Kometsuka, Ojodake, Akase, Nakadake (old and young volcanic edifice) lavas and the volcanic bombs from Nakadake youngest pyroclastic cone. All samples are porphyritic lavas, with 40-55 vol. % crystal content as plagioclase (25-40 vol. %), clinopyroxene (5-10 vol. %), olivine (1-5 vol. %) plus minor (< 1 vol. %) orthopyroxene and opaque minerals. Plagioclase (< 1.6 mm) is euhedral to anhedral. Some plagioclase phenocrysts are clear and unzoned, but others display a wide range of textual features as follows: entirely sieved; sieved cores; corroded rims; dusty zone and overgrown rim; many clinopyroxene inclusions in the phenocryst. Olivine (< 1 mm) is subhedral or corroded form. Clinopyroxene (< 1.2 mm) is subhedral, and sometime is twinned and zoned. Orthopyroxene (< 1.2 mm) is subhedral to anhedral, and is mantled by a reaction rim of clinopyroxene. Hornblende xenocryst surrounded by thick opacite rim is rarely observed. Olivine, Plagioclase, orthopyroxene, clinopyroxene and opaque minerals commonly form glomeroporphyritic aggregates. Groundmass shows hyaloophytic to intergranular or intersertal texture with many pyroxene and plagioclase microlites. Some sample appears the mingling or swirled texture (Brophy and Dreher, 2000). (Fig. 2.13-VII)

Table 2.1.1. Modal analyses of representative rock samples from each group in the pre-caldera stage of Aso volcano.

Sample No.	PAS-BA 03	PAS-BA 04	PAS-BA 05	TTPA45	TTPA46	HYPA35
Group	A	A	A	B	B	C
ol (vol. %)	6	3	6	1	1	-
opx	-	-	-	2	3	2
cpx	tr	tr	5	8	7	6
hb	-	-	-	-	-	-
bt	-	-	-	-	-	-
pl	42	46	35	28	30	31
opq	1	1	-	1	1	1
gm	51	50	54	60	58	60
ph	49	50	46	40	42	40
Sample No.	TTPA47	PRAS 07	PRAS 18	PRAS 22	PRAS 12	KDPA38
Group	C	C	C	C	D	D
ol (vol. %)	-	-	-	-	tr	1
opx	tr	1	1	2	3	3
cpx	2	6	8	6	6	6
hb	-	-	-	-	tr	tr
bt	-	-	-	-	-	-
pl	25	27	22	22	36	29
opq	1	2	1	2	2	1
gm	72	64	68	68	53	61
ph	28	36	32	32	47	39
Sample No.	BCPA41	BCPA42	BCPA43	PRAS 05	PRAS 06	PRAS 13
Group	D	D	D	E	E	E
ol (vol. %)	1	tr	1	-	-	-
opx	2	2	1	tr	tr	2
cpx	5	11	7	4	1	4
hb	1	tr	tr	tr	1	tr
bt	-	-	-	-	-	-
pl	31	33	31	31	27	35
opq	1	1	2	tr	1	1
gm	59	53	58	64	70	58
ph	41	47	42	36	30	42
Sample No.	TTPA44	PRAS 24	PRAS 27	PRAS 30	PRAS 16	PRAS 17
Group	E	F	F	G	H	H
ol (vol. %)	-	-	-	-	-	-
opx	2	-	-	1	-	-
cpx	5	-	-	4	-	-
hb	tr	1	tr	1	tr	tr
bt	-	-	-	-	tr	1
pl	27	19	26	25	5	5
opq	1	2	-	2	1	1
gm	66	78	74	67	94	93
ph	34	22	26	33	6	7

Abbreviations: ol = olivine; cpx = clinopyroxene; opx = orthopyroxene; bt = biotite; pl = plagioclase; opq = opaque minerals; gm = groundmass; ph = phenocryst.

Table 2.1.2. Modal analyses and averaged grain size of plagioclase phenocrysts of representative rock samples from each group in the post-caldera stage of Aso volcano.

Sample	AS2837	ASK217	ASHT01	ASK3463	AS1017	AS025	AS044
Lava name	Otg	Tkn	Hnt	Ttn	Ngn	Swt	Hks
Group	I	II	III	IV	IV	IV	IV
ol (vol. %)	-	-	-	-	-	-	-
opx	< 1	< 1	<1	< 1	< 1	< 1	< 1
cpx	< 1	< 1	<1	< 1	1	< 1	< 1
hb	-	-	<1	-	-	-	-
bt	-	1	-	-	-	-	-
pl	4	9	5	7	7	7	9
opq	1	< 1	<1	< 1	< 1	< 1	< 1
gm	94	89	93	92	91	91	90
ph	6	11	7	8	9	9	10
Grain size of pl (mm)	0.6	0.4	0.5	0.7	0.6	0.6	0.6
1 σ	0.2	0.1	0.2	0.1	0.2	0.2	0.2
Sample	ASKS01	AS083	ASTS60	AS035	AS030	ASKS02	AS060
Lava name	Kss (W)	Tch	Krs	Okm	Ebs	Kss (c)	Nrd
Group	IV	V	VI	VI	VI	VI	VI
ol (vol. %)	-	-	-	-	-	-	<1
opx	<1	< 1	2	2	3	1	<1
cpx	2	2	3	5	5	4	8
hb	-	-	-	-	-	-	-
bt	-	-	-	-	-	-	-
pl	12	8	34	28	38	31	32
opq	1	< 1	< 1	2	2	3	2
gm	84	89	60	63	52	60	57
ph	16	11	40	37	48	40	43
Grain size of pl (mm)	0.5	0.5	1.4	1.0	1.0	1.1	0.9
1 σ	0.1	0.1	0.6	0.2	0.2	0.3	0.3
Sample	AS050	AS040	AS065	AS039	AS1029	AS047	AS046
Lava name	Akm	Ymn	Ayg	Mtn	Ysh	Mry	Tkd
Group	VI	VI	VII	VII	VII	VII	VII
ol (vol. %)	<1	<1	2	3	4	1	3
opx	3	<1	<1	<1	<1	<1	<1
cpx	9	3	7	11	8	7	10
hb	-	-	-	-	-	-	-
bt	-	-	-	-	-	-	-
pl	30	39	39	29	37	42	26
opq	2	1	<1	1	<1	3	1
gm	55	57	52	55	51	46	60
ph	45	43	48	45	49	54	40
Grain size of pl (mm)	1.2	0.9	0.9	0.8	0.8	1.1	1.0
1 σ	0.4	0.3	0.2	0.3	0.2	0.4	0.3
Sample	AS026	AS028	AS051	AS077	AS045	AS043	Vb-01
Lava name	Ksh	Kmt	Ojd	Aks	Nkd (O)	Nkd (Y)	Nkd (Y. P. C)
Group	VII	VII	VII	VII	VII	VII	VII
ol (vol. %)	1	2	1	1	5	2	1
opx	<1	1	<1	<1	1	<1	<1
cpx	9	7	7	9	5	7	9
hb	-	-	-	-	-	-	-
bt	-	-	-	-	-	-	-
pl	32	33	37	28	33	35	39
opq	1	1	<1	2	<1	1	2
gm	56	56	54	60	55	54	49
ph	44	44	46	40	45	46	51
Grain size of pl (mm)	1.2	1.2	1.1	1.6	1.1	1.2	1.0
1 σ	0.3	0.3	0.3	0.6	0.4	0.4	0.2

Abbreviations; Otg = Otogase; Tkn = Takanoobane; Hnt = Hontsuka; Ttn = Tateno; Swt = Sawatsuno; Ngn = Nagano; Hks = Hakusui; Kss = Kusasenrigahama; Tch = Tochinoki; Krs = Karisako; Ebs = Eboshidake; Okm = Okamadoyama; Ymn = Yomineyama; Akm = Akamizu; Nrd = Naraodake; Tkd = Takadake; Mry = Maruyama; Ojd = Ojodake; Kmt = Kometsuka; Kkm = Kamikometsuka; Ksh = Kishimadake; Aks = Akase; Mtn = Matsunoki; Ysh = Yoshioka; Ayg = Ayugaerinotaki; Nkd = Nakadake. (W) = welded pyroclastic rock; (C) = central cone; (O) = old volcanic edifice; (Y) = young volcanic edifice; (YP) = youngest pyroclastic cone; ol = olivine; cpx = clinopyroxene; opx = orthopyroxene; bt = biotite; pl = plagioclase; opq = opaque minerals; gm = groundmass; ph = phenocryst. Names of volcanic products are based on Ono and Watanabe (1985), Watanabe (2001), Masuda et al. (2004), and Miyabuchi et al. (2004). ASK217, ASK3463: Drilling core samples from Takanoobane volcano. They were provided by Aso volcanological laboratory.

Table 2.2.1. Major and trace element data for samples from pre-caldera volcanic stage of Aso

Sample No.	PAS-BA03	PAS-BA04	PAS-BA05	PAS-BA07	PAS-BA07B	PRAS28	TTPA45	TTPA46	HYPA35
Group	A	A	A	A	A	B	B	B	C
SiO_2 (wt. %)	50.09	49.78	48.97	52.82	52.11	54.26	56.23	56.01	55.16
TiO_2	1.12	1.19	1.09	0.80	0.80	0.60	0.95	0.92	0.94
Al_2O_3	19.15	19.75	18.68	19.82	19.53	19.42	16.87	17.05	17.98
Fe_2O_3*	9.77	10.05	10.02	8.91	8.90	7.64	8.20	8.14	7.85
MnO	0.17	0.18	0.17	0.17	0.17	0.14	0.14	0.14	0.14
MgO	5.04	4.50	6.64	4.07	4.05	5.24	4.14	4.11	3.54
CaO	9.55	9.81	10.69	9.33	9.40	9.08	7.14	6.93	7.41
Na_2O	3.71	3.81	3.18	3.37	3.33	3.03	3.19	3.17	3.28
K_2O	1.46	0.95	0.88	0.76	0.74	1.12	1.97	1.97	1.67
P_2O_5	0.31	0.19	0.16	0.15	0.15	0.13	0.22	0.21	0.19
Total	100.35	100.21	100.48	100.19	99.18	100.67	99.04	98.65	98.17
V (ppm)	279	304	336	189	187	177	216	214	203
Cr	11	10	60	7	9	24	31	30	12
Ni	6	6	17	2	3	8	4	4	1
Rb	37	16	13	17	16	28	60	56	48
Zr	104	83	62	70	71	89	149	150	131
Sr	686	586	631	498	502	538	573	576	525
Y	22	22	18	18	18	17	25	27	22
Nb	5	5	4	5	5	5	8	8	8
Ba	331	249	288	225	212	264	378	392	355
Sample No.	TTPA47	TTPA48	PRAS07	PRAS15	PRAS18	PRAS22	PRAS26	AS062	KDPA38
Group	C	C	C	C	C	C	C	C	D
SiO_2 (wt. %)	61.92	58.12	58.72	55.72	56.44	53.99	56.22	59.42	56.19
TiO_2	0.69	0.91	0.82	1.08	1.02	0.99	1.01	0.67	0.81
Al_2O_3	18.64	17.43	18.03	17.99	17.80	17.08	17.99	17.85	17.72
Fe_2O_3*	4.02	7.70	6.44	8.42	7.88	7.82	7.77	6.94	7.31
MnO	0.09	0.13	0.12	0.15	0.14	0.14	0.14	0.13	0.13
MgO	0.98	3.41	2.76	4.06	3.63	3.80	3.67	3.43	4.02
CaO	4.64	6.84	6.69	7.95	7.19	7.23	6.85	6.75	7.58
Na_2O	4.14	3.52	3.57	3.34	3.39	3.36	3.49	3.78	3.35
K_2O	2.81	2.31	2.16	1.42	1.80	1.77	1.93	1.48	1.60
P_2O_5	0.25	0.21	0.22	0.21	0.23	0.23	0.23	0.17	0.17
Total	98.17	100.57	99.52	100.33	99.51	96.42	99.31	100.61	98.88
V (ppm)	64	195	148	230	197	196	194	133	185
Cr	9	22	17	18	20	17	19	21	33
Ni	-1	7	6	7	0	2	3	8	4
Rb	88	70	65	37	49	50	54	41	47
Zr	188	157	152	108	146	140	148	117	124
Sr	511	485	502	488	513	511	525	387	439
Y	32	28	25	23	26	26	29	20	24
Nb	11	9	10	9	9	9	10	7	7
Ba	500	399	396	298	352	349	371	279	324

Table 2.2.1. (Continued 1)

Sample No.	BCPA40	BCPA41	BCPA42	BCPA43	PRAS11	PRAS12	TTPA44	TTPA44U	PRAS05
Group	D	D	D	D	D	D	E	E	E
SiO_2 (wt. %)	58.35	58.76	57.01	58.63	58.90	56.87	58.23	58.09	55.16
TiO_2	0.68	0.66	0.95	0.72	0.63	0.65	0.72	1.08	0.48
Al_2O_3	17.63	17.46	16.99	17.50	18.13	18.64	17.69	16.87	20.49
Fe_2O_3*	7.02	6.62	7.52	7.06	6.40	6.76	6.80	7.92	6.79
MnO	0.12	0.12	0.13	0.12	0.12	0.13	0.13	0.13	0.14
MgO	4.25	3.69	3.63	3.86	3.26	3.75	3.35	3.80	3.23
CaO	7.86	6.39	6.93	6.60	5.23	7.60	6.95	7.22	8.12
Na_2O	3.28	3.06	3.54	3.04	3.15	3.25	3.58	3.39	3.32
K_2O	1.97	2.04	1.87	1.98	2.11	1.75	1.61	2.25	1.29
P_2O_5	0.15	0.14	0.21	0.15	0.15	0.15	0.21	0.25	0.17
Total	101.31	98.93	98.78	99.65	98.09	99.53	99.27	101.01	99.17
V (ppm)	182	167	193	179	149	162	138	210	137
Cr	21	20	24	20	12	13	18	27	13
Ni	5	4	6	4	1	2	3	4	0
Rb	54	63	57	61	64	44	47	62	32
Zr	123	133	154	131	132	123	153	173	87
Sr	483	438	428	441	416	528	472	531	666
Y	20	21	29	20	22	20	22	27	16
Nb	7	7	9	7	8	7	8	11	4
Ba	365	393	354	401	401	371	334	430	337
Sample No.	PRAS06	PRAS13	PRAS25	PRAS24	PRAS27	HB-AN	PRAS29	PRAS30	PRAS30-2
Group	E	E	E	F	F	F	G	G	G
SiO_2 (wt. %)	58.72	58.65	55.30	57.03	54.18	53.34	65.09	65.12	64.61
TiO_2	0.32	0.58	0.56	0.56	0.60	0.84	0.79	0.73	0.70
Al_2O_3	19.46	17.88	18.85	18.86	20.00	19.29	17.56	16.87	16.78
Fe_2O_3*	5.76	6.16	7.28	6.62	7.89	8.75	6.05	5.66	5.35
MnO	0.15	0.12	0.15	0.15	0.15	0.16	0.12	0.12	0.11
MgO	1.77	3.21	4.48	2.43	4.91	3.68	1.88	2.10	1.88
CaO	7.25	6.66	8.81	6.55	7.53	9.01	2.21	3.04	2.98
Na_2O	3.60	3.26	3.21	3.27	2.80	3.18	2.76	3.41	3.48
K_2O	1.54	2.01	1.21	1.44	1.08	0.86	3.54	3.39	3.40
P_2O_5	0.22	0.14	0.14	0.21	0.14	0.17	0.16	0.17	0.17
Total	98.76	98.68	99.99	97.11	99.27	99.27	100.15	100.62	99.46
V (ppm)	80	136	156	112	163	186	116	112	114
Cr	9	12	25	10	32	27	15	18	14
Ni	-3	-3	10	2	8	7	2	4	4
Rb	40	63	30	40	26	17	116	113	115
Zr	106	120	88	145	83	80	244	233	224
Sr	696	465	560	520	477	529	256	367	348
Y	16	19	16	19	17	20	37	37	32
Nb	4	7	5	8	5	5	13	12	12
Ba	406	373	271	362	274	229	616	556	561

Table 2.2.1. (Continued 2)

Sample No.	PRAS16	PRAS17	BT-RH	PRAS19	PRAS20	PRAS21	HD-MI
Group	H	H	H	HMA	HMA	HMA	HMA
SiO_2 (wt. %)	73.00	72.19	72.30	55.16	56.46	55.04	54.61
TiO_2	0.32	0.31	0.30	0.63	0.75	0.76	0.82
Al_2O_3	15.49	14.84	14.85	14.70	16.41	16.16	15.99
Fe_2O_3*	2.06	1.75	2.07	6.53	6.63	7.19	7.17
MnO	0.10	0.07	0.09	0.10	0.11	0.12	0.12
MgO	0.13	0.22	0.50	9.25	6.79	7.89	7.91
CaO	1.54	1.55	1.68	7.37	7.11	7.62	7.39
Na_2O	4.43	4.57	4.67	3.28	3.28	3.06	3.10
K_2O	3.75	3.73	3.78	0.75	0.94	0.90	0.97
P_2O_5	0.07	0.08	0.09	0.14	0.19	0.17	0.18
Total	100.88	99.30	100.33	97.91	98.64	98.91	98.25
V (ppm)	18	9	14	129	112	131	141
Cr	8	8	8	488	258	321	315
Ni	0	0	0	256	158	176	152
Rb	119	115	124	14	21	20	21
Zr	233	227	226	80	99	93	99
Sr	255	247	255	395	450	434	413
Y	26	23	19	49	26	29	31
Nb	12	11	11	8	11	11	12
Ba	667	636	621	226	272	252	293

PRAS19, PRAS20, PRAS21 and HD-MI are high-Mg andesite lavas from Haidoko area, the western part of Aso caldera.

Table 2.2.2. Major and trace element data for samples from post-caldera volcanic stage of Aso

Sample	AS2837	AS28372	ASK217	ASK494	ASK630	ASTS251	AS063	AS064	AS076	ASHT01
Lava name	Otg	Otg	Tkn	Tkn	Tkn	Tkn	Tkn	Tkn	Tkn	Hnt
Group No.	I	I	II	II	II	II	II	II	II	III
SiO_2 (wt. %)	71.29	71.36	70.77	71.00	71.09	70.23	69.77	69.76	69.77	68.63
TiO_2	0.39	0.39	0.42	0.43	0.43	0.44	0.44	0.44	0.44	0.59
Al_2O_3	13.92	13.93	14.73	14.98	14.98	14.76	14.72	14.75	14.83	15.35
Fe_2O_3	2.75	2.58	2.80	2.36	2.16	2.44	2.83	2.90	2.85	2.57
MnO	0.04	0.04	0.08	0.07	0.07	0.08	0.08	0.08	0.08	0.10
MgO	0.59	0.57	0.54	0.54	0.53	0.57	0.55	0.54	0.57	0.61
CaO	1.36	1.30	1.03	1.11	1.09	1.13	1.11	1.12	1.15	1.70
Na_2O	3.47	3.45	4.76	4.81	4.80	4.81	4.84	4.78	4.79	4.78
K_2O	5.54	5.57	4.87	4.81	4.83	4.80	4.69	4.77	4.75	4.24
P_2O_5	0.06	0.05	0.05	0.06	0.06	0.06	0.06	0.06	0.06	0.10
Total	99.42	99.23	100.06	100.17	100.04	99.31	99.08	99.18	99.27	98.67
Ba (ppm)	627	621	755	755	781	769	807	787	764	758
Cr	8	8	8	8	5	6	7	7	7	-
Nb	16	15	16	15	15	15	15	15	15	16
Ni	9	9	10	10	9	10	10	10	12	12
Rb	203	205	165	161	163	165	161	162	161	139
Sr	143	139	118	139	136	138	133	139	138	246
V	25	30	16	15		20	13	14	21	41
Y	27	27	35	34	37	36	37	36	35	38
Zr	300	308	353	348	356	357	355	356	345	263

Sample	ASHT02	ASK1109	ASK1127	ASK3112	ASK3118	ASK3124	ASK3463	AST8257	AS023	AS025
Lava name	Hnt	Ttn	Ttn	Ttn	Ttn	Ttn	Ttn	Ttn	Ttn	Swt
Group No.	III	IV	IV	IV	IV	IV	IV	IV	IV	IV
SiO_2 (wt. %)	68.74	65.94	66.55	66.14	66.44	66.38	66.04	66.19	65.48	65.27
TiO_2	0.58	0.68	0.67	0.69	0.70	0.69	0.70	0.68	0.68	0.78
Al_2O_3	15.45	16.27	16.17	16.07	16.14	15.95	16.08	15.93	15.93	15.62
Fe_2O_3	2.59	4.25	3.76	4.49	4.08	4.43	4.22	4.59	4.77	4.66
MnO	0.10	0.10	0.10	0.08	0.08	0.08	0.10	0.10	0.10	0.13
MgO	0.61	1.02	0.97	0.99	1.00	0.96	1.05	0.98	1.05	1.18
CaO	1.72	2.73	2.59	2.61	2.59	2.49	2.70	2.52	2.74	2.66
Na_2O	4.79	4.58	4.57	4.56	4.56	4.58	4.58	4.57	4.54	4.83
K_2O	4.24	3.96	4.06	4.01	4.03	4.08	3.98	4.06	3.96	3.79
P_2O_5	0.10	0.13	0.12	0.13	0.12	0.12	0.13	0.13	0.13	0.16
Total	98.92	99.65	99.56	99.77	99.74	99.76	99.57	99.75	99.37	99.08
Ba (ppm)	788	697	688	720	713	673	687	703	681	727
Cr	-	8	6	10	8	8	8	9	8	7
Nb	16	14	13	14	14	14	14	14	14	15
Ni	11	7	6	7	4	7	9	9	7	5
Rb	136	137	139	136	138	137	137	139	135	126
Sr	249	352	326	329	330	313	337	319	331	347
V	46	53	50	60	56	47	53	51	48	47
Y	37	28	29	30	30	30	30	29	27	33
Zr	265	291	288	288	292	292	294	291	283	278

Sample	AS1017	AS044	ASKS01	AS031	AS070	AST1176	AS078	AS083	ASK1545	ASK1630
Lava name	Ngn	Hks	Kss (W)	Tch	Tch	Tch	Tch	Tch	Tch	Tch
Group No.	IV	IV	IV	V	V	V	V	V	V	V
SiO_2 (wt. %)	64.82	66.26	66.12	63.71	63.22	60.22	61.84	63.71	63.59	64.02
TiO_2	0.79	0.74	0.79	0.81	0.79	0.90	0.90	0.76	0.75	0.75
Al_2O_3	15.90	15.72	16.09	16.73	16.57	16.17	16.51	16.00	15.98	15.98
Fe_2O_3	4.99	4.39	3.78	5.18	5.01	7.76	6.82	5.58	5.94	5.95
MnO	0.13	0.11	0.13	0.16	0.17	0.15	0.12	0.13	0.15	0.19
MgO	1.16	1.00	1.12	1.35	1.51	1.97	1.64	1.36	1.44	1.20
CaO	2.63	2.35	2.74	3.27	3.34	4.41	4.05	3.14	3.22	2.95
Na_2O	4.77	4.81	4.41	4.48	4.71	4.24	4.43	4.47	4.43	4.42
K_2O	3.74	4.03	3.99	3.59	3.6	3.37	3.59	4.04	4.01	4.09
P_2O_5	0.15	0.13	0.20	0.32	0.28	0.44	0.41	0.24	0.24	0.24
Total	99.08	99.55	99.37	99.60	99.20	99.62	100.28	99.42	99.76	99.80
Ba (ppm)	691	708	646	643	694	600	638	681	715	660
Cr	8	7	-	7	3	9	9	8	10	8
Nb	14	15	15	11	10	10	11	12	12	11
Ni	7	8	5	5	2	0	2	3	6	5
Rb	125	134	115	125	123	114	122	139	138	139
Sr	346	306	359	526	509	546	542	462	457	434
V	51	41	59	53	39	87	71	50	43	41
Y	31	32	34	46	30	28	29	29	29	29
Zr	279	294	229	244	258	229	246	281	277	275

Table 2.2.2. (Continued 1)

Sample	ASK1920	ASK1971	ASK1999	ASKS02	ASTS60	AS004	AS030	AS035	AS037	AS038
Lava name	Tch	Tch	Tch	Kss (C)	Krs	Krs	Ebs	Okm	Okm	Okm
Group	V	V	V	VI	VI	VI	VI	VI	VI	VI
SiO_2 (wt. %)	59.97	64.23	63.88	62.60	58.40	57.57	57.45	60.65	60.07	60.59
TiO_2	0.91	0.75	0.76	0.68	0.91	0.96	0.94	0.80	0.84	0.82
Al_2O_3	16.10	16.13	16.02	16.57	16.49	16.52	17.93	17.67	17.2	17.17
Fe_2O_3	8.28	5.57	5.92	4.89	8.33	8.49	7.65	6.08	6.19	6.12
MnO	0.15	0.11	0.11	0.11	0.14	0.14	0.14	0.15	0.14	0.14
MgO	1.89	1.21	1.25	1.89	2.93	3.09	3.17	2.11	2.29	2.2
CaO	4.35	2.98	3.04	4.36	5.87	6.27	6.63	5.16	4.94	5.07
Na_2O	4.20	4.42	4.43	3.62	3.30	3.35	3.74	4.22	4.18	4.22
K_2O	3.36	4.11	4.07	3.42	2.98	2.80	2.29	2.79	2.84	2.86
P_2O_5	0.45	0.24	0.25	0.20	0.20	0.21	0.22	0.25	0.24	0.25
Total	99.64	99.76	99.74	98.34	99.53	99.41	100.16	99.88	98.93	99.44
Ba (ppm)	609	739	712	551	453	494	400	525	535	536
Cr	10	7	8	6	20	19	17	10	11	10
Nb	9	12	16	11	11	10	9	9	10	10
Ni	3	2	4	7	5	3	1	3	1	2
Rb	114	139	139	115	105	90	68	92	89	93
Sr	531	437	442	420	412	436	481	526	486	497
V	86	44	46	121	177	191	198	113	132	128
Y	26	27	29	30	22	25	24	26	23	24
Zr	224	274	275	197	204	196	168	197	206	205
Sample	AS041	AS040	AS027	AS050	AS060	AS046	AS047	AS051	AS028	AS048
Lava name	Okm	Ymn	Akm	Akm	Nrd	Tkd	Mry	Ojd	Kmt	Kmt
Group	VI	VI	VI	VI	VI	VII	VII	VII	VII	VII
SiO_2 (wt. %)	58.6	54.38	55.46	54.43	58.12	51.16	53.52	51.13	50.98	52.16
TiO_2	0.84	0.81	1.01	0.98	0.91	0.90	1.15	0.93	0.93	1.02
Al_2O_3	17.64	19.45	16.39	17.37	17.83	16.83	18.13	17.75	17.24	17.38
Fe_2O_3	6.45	7.81	9.86	9.26	6.83	10.83	8.98	10.89	11.06	11.30
MnO	0.15	0.15	0.16	0.15	0.17	0.18	0.17	0.17	0.17	0.17
MgO	2.53	2.49	3.69	3.82	2.97	5.38	4.33	4.80	5.20	4.24
CaO	5.74	7.87	7.10	7.82	5.68	9.74	8.38	9.41	9.43	8.18
Na_2O	4.1	3.31	3.09	3.11	4.02	2.70	3.16	2.82	2.72	3.05
K_2O	2.51	2.24	2.56	2.22	2.32	1.42	1.25	1.51	1.44	1.88
P_2O_5	0.26	0.34	0.23	0.27	0.25	0.22	0.20	0.19	0.19	0.23
Total	98.82	98.85	99.56	99.43	99.10	99.36	99.27	99.60	99.36	99.60
Ba (ppm)	538	412	434	387	499	333	290	303	325	366
Cr	10	10	21	21	14	39	18	24	26	22
Nb	8	7	10	9	8	5	8	7	7	7
Ni	3	0	4	2	5	12	2	9	11	9
Rb	83	66	81	68	61	37	35	42	40	54
Sr	550	709	479	525	479	620	481	593	568	597
V	138	162	235	225	158	283	241	294	303	300
Y	25	21	23	23	35	19	22	18	20	21
Zr	189	157	188	163	172	105	114	116	112	139
Sample	AS058	AS057	AS026	AS049	AS056	ASKS	AST5695	AS077	AS-1105	AS034
Lava name	Kmt	Kkm	Ksh	Ksh	Ksh	Ksh	Aks	Aks	Aks	Mtn
Group	VII	VII	VII	VII	VII	VII	VII	VII	VII	VII
SiO_2 (wt. %)	50.73	49.94	50.66	52.02	51.47	50.83	53.22	53.33	53.424	48.18
TiO_2	0.94	0.91	0.93	1.02	1.01	0.90	1.00	0.99	0.984	0.87
Al_2O_3	16.98	17.38	16.85	17.44	17.54	18.15	17.83	17.50	17.664	17.63
Fe_2O_3	11.41	11.24	10.97	11.36	11.32	9.46	9.85	10.06	9.594	11.52
MnO	0.17	0.17	0.17	0.17	0.17	0.17	0.16	0.16	0.161	0.16
MgO	5.36	5.44	5.32	4.27	4.26	4.88	4.08	4.00	4.071	6.06
CaO	9.68	9.96	9.58	8.18	8.58	9.72	8.12	8.09	8.132	11.78
Na_2O	2.66	2.63	2.65	3.04	2.99	2.72	3.23	3.30	3.212	2.17
K_2O	1.37	1.18	1.41	1.86	1.69	1.27	1.70	1.77	1.8	0.86
P_2O_5	0.18	0.18	0.19	0.23	0.22	0.21	0.20	0.20	0.194	0.18
Total	99.49	99.01	98.73	99.58	99.26	98.30	99.39	99.41	99.24	99.41
Ba (ppm)	286	292	292	351	354	294	333	358	359	158
Cr	32	28	29	23	19	21	24	23	21	35
Nb	5	5	6	6	6	4	7	7	7	4
Ni	14	13	12	10	6	15	2	3	3	16
Rb	38	31	39	52	46	35	47	48	49	25
Sr	555	583	561	600	623	588	543	543	546	545
V	307	301	299	283	306	294	253	257	243	327
Y	20	19	19	22	20	18	22	23	21	16
Zr	107	97	112	137	127	99	136	135	135	71

Table 2.2.2. (Continued 2)

Sample	AS039	AS1029	AS021	AS065	AS082	AS082B	AS-091	Vb-01
Lava name	Mtn	Ysh	Ayg	Ayg	Ayg	Ayg	Ayg	Nkd (YP)
Group	Ⅶ	Ⅶ	Ⅶ	Ⅶ	Ⅶ	Ⅶ	Ⅶ	Ⅶ
SiO_2 (wt. %)	47.64	52.04	50.80	50.91	51.50	52.69	52.18	53.17
TiO_2	0.93	0.81	0.96	0.85	0.86	0.90	0.86	0.94
Al_2O_3	18.39	18.02	19.78	18.60	18.97	19.93	19.08	17.65
Fe_2O_3	11.25	9.82	10.24	9.65	9.34	7.36	8.65	9.49
MnO	0.17	0.15	0.23	0.17	0.16	0.11	0.12	0.15
MgO	5.71	4.23	2.93	3.66	3.59	2.70	3.13	4.55
CaO	11.62	9.30	9.09	10.28	9.93	10.16	10.17	8.57
Na_2O	2.19	2.97	3.70	2.92	2.99	3.00	2.81	2.97
K_2O	0.75	1.60	1.04	1.49	1.56	1.62	1.63	2.05
P_2O_5	0.22	0.21	0.17	0.20	0.22	0.22	0.20	0.26
Total	98.87	99.16	98.93	98.70	99.11	98.69	98.82	99.80
Ba (ppm)	193	353	261	288	323	341	315	364
Cr	36	24	16	30	27	27	31	112
Nb	4	5	5	5	5	6	5	7
Ni	13	8	-	11	8	1	9	31
Rb	20	45	25	42	45	49	47	63
Sr	621	662	552	628	647	688	666	531
V	341	255	205	269	258	261	281	232
Y	16	19	22	18	20	21	20	21
Zr	84	116	128	112	119	126	115	150
Sample	VB02	AG01	AS036	AS043	AS055	AS061	AS054	AS045
Lava name	Nkd (YP)	Nkd (YP)	Nkd (Y)	Nkd (Y)	Nkd (Y)	Nkd (Y)	Nkd (O)	Nkd (O)
Group	Ⅶ	Ⅶ	Ⅶ	Ⅶ	Ⅶ	Ⅶ	Ⅶ	Ⅶ
SiO_2 (wt. %)	53.28	52.64	52.18	52.21	51.53	53.97	51.46	50.53
TiO_2	0.93	0.94	0.93	0.97	0.99	1	0.99	0.93
Al_2O_3	17.82	17.87	16.97	17.48	16.89	17.93	16.74	17.74
Fe_2O_3	9.15	9.84	10.39	10.31	10.63	8.7	10.65	11.19
MnO	0.15	0.16	0.18	0.16	0.17	0.16	0.17	0.18
MgO	4.43	4.27	5.12	4.51	5.36	4.28	5.72	5.21
CaO	8.64	9.10	9.34	8.98	9.31	7.8	9.34	9.71
Na_2O	3.00	2.89	2.81	2.86	2.69	3.34	2.62	2.96
K_2O	2.05	1.71	1.55	1.76	1.51	1.73	1.49	0.99
P_2O_5	0.26	0.24	0.24	0.24	0.22	0.2	0.22	0.19
Total	99.71	99.66	99.71	99.48	99.30	99.11	99.40	99.61
Ba (ppm)	378	362	336	314	309	391	326	283
Cr	112	22	38	21	43	21	44	34
Nb	6	6	6	8	6	8	6	5
Ni	28	3	8	5	7	2	10	9
Rb	66	50	41	51	42	46	43	21
Sr	543	601	548	575	525	534	517	643
V	223	273	272	273	290	236	291	304
Y	22	20	22	21	22	23	20	18
Zr	151	132	117	130	118	129	113	88

Abbreviations are the same as Table 2.1.2. ASK217, ASK494, ASK630, ASK1109, ASK1127, ASK3112, ASK3118, ASK3124, ASK3463, ASK1545, ASK1630, ASK1920, ASK1971, ASK1999: Drilling core samples from Takanoobane volcano. They were provided by Aso volcanological laboratory.

Table 2.2.3. Boron and other selected trace element contents of the basaltic and andesitic volcanic products from Aso area.

Sample No.	PAS-BA03	PAS-BA04	PAS-BA05	PAS-BA07	PAS-BA07B	PRAS28	TTPA46	HYPA35	TTPA47
Stage	Pre-caldera	Pre-caldera	Pre-caldera	Pre-caldera	Pre-caldera	Pre-caldera	Pre-caldera	Pre-caldera	Pre-caldera
Group	A	A	A	A	A	B	B	C	C
B (ppm)	15.35	9.06	7.87	9.32	9.97	8.98	16.65	12.01	24.71
error	0.44	0.24	0.20	0.23	0.27	0.38	0.62	0.49	0.87
Gd	5.24	4.10	3.80	3.24	3.29	3.18	5.16	4.37	6.41
error	0.17	0.12	0.10	0.09	0.11	0.15	0.22	0.19	0.27
Sm	5.04	3.93	3.80	3.17	3.09	3.26	5.64	4.27	6.88
error	0.23	7.12	0.15	0.14	0.15	0.24	0.35	0.29	0.41
Sample No.	PRAS18	TTPA44U	TTPA48	PRAS15	KDPA38	BCPA42	BCPA40	PRAS05	PRAS25
Stage	Pre-caldera	Pre-caldera	Pre-caldera	Pre-caldera	Pre-caldera	Pre-caldera	Pre-caldera	Pre-caldera	Pre-caldera
Group	C	C	C	C	D	D	D	E	E
B (ppm)	14.48	14.99	18.87	14.49	12.98	13.17	14.25	9.59	6.69
error	0.57	0.57	0.68	0.56	0.50	0.49	0.56	0.36	0.27
Gd	5.14	5.40	5.30	4.37	3.80	5.38	3.84	3.23	2.98
error	0.22	0.22	0.22	0.19	0.17	0.21	0.18	0.14	0.12
Sm	5.24	5.28	4.96	4.56	3.70	5.32	3.67	3.31	3.34
error	0.34	0.33	0.32	0.30	0.26	0.32	0.27	0.22	0.20
Sample No.	PRAS06	PRAS13	PRAS24	PRAS27	PRAS19	PRAS20	PRAS21	HD-MI	AS079
Stage	Pre-caldera	Pre-caldera	Pre-caldera	Pre-caldera	Pre-caldera	Pre-caldera	Pre-caldera	Pre-caldera	Post-caldera
Group	E	E	F	F	(HMA)	(HMA)	(HMA)	(HMA)	V
B (ppm)	11.39	16.81	8.72	5.70	0.87	1.67	1.83	1.46	24.46
error	0.42	0.58	0.34	0.29	0.06	0.10	0.11	0.11	1.03
Gd	2.83	3.54	3.40	3.12	2.03	1.53	2.08	3.02	7.04
error	0.13	0.16	0.14	0.14	0.10	0.08	0.11	0.15	0.35
Sm	3.25	3.77	3.53	3.06	1.50	1.52	1.98	3.76	7.70
error	0.23	0.25	0.22	0.23	0.10	0.11	0.14	0.25	0.53
Sample No.	AS-004	AS030	AS035	AS067	AS046	AS047	AS054	AS-051-U	AS-028
Stage	Post-caldera	Post-caldera	Post-caldera	Post-caldera	Post-caldera	Post-caldera	Post-caldera	Post-caldera	Post-caldera
Group	VI	VI	VI	VI	VII	VII	VII	VII	VII
B (ppm)	29.57	20.55	18.87	34.74	14.54	14.00	15.64	13.78	17.17
error	0.89	0.70	0.64	1.46	0.42	0.45	0.48	0.40	0.66
Gd	5.45	5.70	6.33	5.76	3.99	4.63	4.09	4.37	4.03
error	0.33	0.35	0.37	0.30	0.16	0.17	0.18	0.15	0.19
Sm	5.65	5.58	6.61	5.77	4.29	4.68	4.44	4.54	4.11
error	0.30	0.31	0.35	0.41	0.20	0.27	0.22	0.24	0.27
Sample No.	AS-057	AS-049	AS-077	AS034	AS039	AS-1029-46	AS-021	AS-065B	AS-082B
Stage	Post-caldera	Post-caldera	Post-caldera	Post-caldera	Post-caldera	Post-caldera	Post-caldera	Post-caldera	Post-caldera
Group	VII	VII	VII	VII	VII	VII	VII	VII	VII
B (ppm)	13.63	22.64	14.95	5.59	6.17	15.68	7.06	12.10	17.11
error	0.40	0.98	0.43	0.24	0.22	0.69	0.26	0.56	0.50
Gd	3.54	4.80	4.61	2.86	3.18	4.06	3.59	3.92	4.45
error	0.13	0.25	0.15	0.11	0.13	0.22	0.12	0.21	0.15
Sm	4.04	5.24	5.09	2.92	3.23	4.38	4.45	3.94	5.25
error	0.22	0.38	0.27	0.19	0.15	0.32	0.23	0.29	0.27

B, Sm and Gd contents are determined by the PGA. Error shows the standard deviation (one sigma). PRAS19, PRAS20, PRAS21 and HD-MI are high-magnesian andesite (HMA) lavas from Haidoko area, the western part of Aso caldera.

Table 2.3. Modal and bulk rock compositions for Tochinoki lavas

Sample No.	AVL1-01	AVL1-02	AVL1-03	*ASK1545	AVL1-04	AVL1-05	AVL1-06	AVL1-07	AVL1-08	AVL1-08b
Depth (m)	150.07	152.25	153.70	154.51	155.05	157.30	159.20	160.15	160.90	160.90
Group	ST	ST	ST	ST	ST	ST	ST	ST	ST	ST
pl (vol%)	7	7	7	7	9	6	8	11	7	7
ph	10	10	10	10	12	9	12	14	12	12
SiO_2 (wt%)	64.22	64.74	64.55	63.59	64.74	64.47	64.72	64.60	65.16	64.50
TiO_2	0.73	0.73	0.73	0.75	0.72	0.72	0.73	0.72	0.72	0.73
Al_2O_3	15.87	15.89	15.78	15.98	15.84	15.68	15.86	15.82	15.87	15.86
Fe_2O_3*	5.08	4.92	4.78	5.94	5.05	4.85	4.75	4.85	4.83	5.11
MnO	0.14	0.14	0.13	0.15	0.14	0.14	0.13	0.14	0.11	0.13
MgO	1.21	1.22	1.19	1.44	1.21	1.27	1.16	1.23	1.08	1.17
CaO	3.14	3.11	3.10	3.22	3.15	3.12	3.08	3.14	2.90	3.07
Na_2O	4.49	4.44	4.54	4.43	4.52	4.44	4.43	4.51	4.44	4.46
K_2O	3.82	3.93	3.96	4.01	3.89	3.88	3.97	3.88	4.05	3.88
P_2O_5	0.30	0.30	0.30	0.24	0.30	0.30	0.30	0.30	0.30	0.30
Total	98.98	99.42	99.05	99.76	99.56	98.86	99.13	99.19	99.44	99.22
Rb (ppm)	138	146	143	138	143	143	144	138	144	138
Sr	416	412	409	457	411	408	408	411	400	411
Y	34	35	35	29	34	35	35	35	31	34
Zr	243	244	245	277	241	246	244	242	240	244
Nb	12	12	12	12	12	12	12	12	12	12
Ba	694	698	700	715	691	694	699	688	698	700
Sample No.	AVL1-09	*ASK1630	AVL1-10	AVL1-11	AVL1-12	AVL1-13	AVL1-14	AVL1-15	AVL1-16	AVL1-17
Depth (m)	162.24	163.00	164.32	165.80	167.35	170.23	172.00	173.00	176.00	178.08
Group	ST	ST	ST	ST	ST	ST	ST	ST	ST	ST
pl (vol%)	6	9	7	10	8	9	9	8	9	7
ph	10	12	11	14	9	11	12	11	11	10
SiO_2 (wt%)	64.94	64.02	64.48	64.99	64.99	64.93	64.52	64.91	65.12	64.77
TiO_2	0.73	0.75	0.72	0.72	0.73	0.73	0.73	0.72	0.73	0.73
Al_2O_3	15.89	15.98	15.88	15.90	15.93	16.02	15.79	15.82	15.86	15.82
Fe_2O_3*	4.70	5.95	5.14	4.85	4.87	5.09	4.95	4.82	4.88	4.88
MnO	0.15	0.19	0.16	0.10	0.10	0.19	0.17	0.15	0.10	0.10
MgO	1.06	1.20	1.14	0.88	0.91	1.08	1.07	1.14	1.02	1.05
CaO	2.97	2.95	3.11	2.90	2.95	3.15	3.11	3.07	2.95	2.99
Na_2O	4.50	4.42	4.48	4.52	4.53	4.51	4.43	4.53	4.52	4.49
K_2O	3.94	4.09	3.88	3.93	3.92	4.01	3.89	3.95	4.03	3.98
P_2O_5	0.30	0.24	0.30	0.30	0.30	0.30	0.30	0.30	0.30	0.30
Total	99.17	99.80	99.30	99.07	99.24	100.01	98.95	99.41	99.50	99.13
Rb (ppm)	138	139	136	137	138	138	137	137	142	137
Sr	406	434	417	407	412	420	415	408	405	405
Y	35	29	35	37	39	36	36	35	35	34
Zr	245	275	240	245	245	244	242	245	244	243
Nb	12	11	12	12	12	12	12	12	12	12
Ba	700	660	688	696	691	696	693	695	704	701

Table 2.3. (Continued 1)

Sample No.	AVL1-18	AVL1-19	AVL1-20	AVL1-21	AVL1-22	AVL1-23	*ASK1920	AVL1-24	AVL1-25	*ASK1971
Depth (m)	180.90	182.20	184.87	186.35	188.13	189.30	192.04	192.70	194.55	197.15
Group	ST	ST	ST	ST	ST	ST	MT	MT	ST	ST
pl (vol%)	9	8	8	6	7	6	5	2	9	9
ph	12	10	12	9	10	8	6	3	12	12
SiO_2 (wt%)	64.88	64.55	64.78	64.70	64.82	64.22	59.97	60.53	63.31	64.23
TiO_2	0.73	0.73	0.72	0.72	0.72	0.73	0.91	0.87	0.73	0.75
Al_2O_3	15.84	15.82	15.86	15.84	15.83	15.86	16.10	15.99	15.65	16.13
Fe_2O_3*	4.95	5.33	5.18	5.13	4.92	5.41	8.28	7.70	5.78	5.57
MnO	0.10	0.11	0.10	0.11	0.11	0.11	0.15	0.15	0.14	0.11
MgO	1.07	1.10	1.02	1.05	1.06	1.18	1.89	1.81	1.33	1.21
CaO	2.99	3.05	3.04	3.03	2.99	3.16	4.35	4.45	3.29	2.98
Na_2O	4.52	4.51	4.54	4.52	4.53	4.46	4.20	4.29	4.37	4.42
K_2O	4.04	3.87	3.92	3.95	3.97	3.86	3.36	3.23	3.89	4.11
P_2O_5	0.30	0.29	0.30	0.30	0.30	0.30	0.45	0.56	0.32	0.24
Total	99.42	99.35	99.46	99.35	99.25	99.29	99.64	99.58	98.81	99.76
Rb (ppm)	139	137	138	138	139	135	114	112	143	139
Sr	406	413	408	409	403	417	531	517	420	437
Y	36	34	34	34	34	34	26	33	34	27
Zr	244	242	241	244	244	240	224	204	237	274
Nb	12	12	12	12	12	12	9	10	12	12
Ba	698	691	700	695	706	689	609	609	674	739
Sample No.	*ASK1999	AVL4-01	AVL4-02	AVL4-03	AVL4-04	AVL4-05	AVL4-06	AVL4-07	AVL4-08	AVL4-09
Depth (m)	199.91	156.72	158.00	159.18	160.00	161.32	162.00	163.90	165.50	167.87
Group	ST	ST	ST	ST	ST	ST	ST	ST	ST	ST
pl (vol%)	8	10	10	9	9	9	10	8	10	8
ph	10	13	12	11	12	12	12	11	13	11
SiO_2 (wt%)	63.88	64.99	64.75	65.16	65.08	65.60	64.80	64.89	64.84	65.19
TiO_2	0.76	0.73	0.73	0.74	0.73	0.72	0.73	0.73	0.73	0.73
Al_2O_3	16.02	15.83	15.77	15.91	15.84	15.83	15.87	15.88	15.96	15.78
Fe_2O_3*	5.92	5.11	5.42	5.14	5.14	4.91	5.28	5.38	5.24	5.18
MnO	0.11	0.14	0.13	0.16	0.12	0.12	0.13	0.11	0.11	0.12
MgO	1.25	1.12	1.18	1.04	1.15	1.11	1.10	1.10	1.05	1.16
CaO	3.04	3.13	3.13	3.03	3.07	2.98	3.15	3.05	3.13	3.06
Na_2O	4.43	4.38	4.38	4.43	4.43	4.44	4.41	4.43	4.40	4.44
K_2O	4.07	3.87	3.87	3.90	3.88	3.98	3.85	3.91	3.87	3.91
P_2O_5	0.25	0.30	0.31	0.31	0.31	0.29	0.31	0.30	0.31	0.30
Total	99.74	99.61	99.67	99.81	99.75	99.99	99.62	99.76	99.66	99.86
Rb (ppm)	139	137	135	143	135	140	132	135	134	137
Sr	442	414	414	412	410	404	418	408	416	407
Y	29	32	35	34	35	37	35	34	34	36
Zr	275	239	239	245	242	245	240	242	242	245
Nb	16	11	12	12	12	13	12	12	12	13
Ba	712	676	665	677	673	687	672	673	668	676

Table 2.3. (Continued 2)

Sample No.	AVL4-10	AVL4-11	AVL4-12	AVL4-13	AVL4-14	AVL4-14b	AS020	AS0029	*AS070	*AS078	AS079
Depth (m)	168.31	169.87	170.85	172.00	173.00	173.00	240 (Elv.)	440 (Elv.)	460 (Elv.)	240 (Elv.)	250 (Elv.)
Group	ST	ST	ST	MT	MT	MT	MT	ST	ST	MT	MT
pl (vol%)	12	8	6	2	3	3	2	8	7	4	3
ph	15	11	8	4	3	3	3	10	9	6	4
SiO_2 (wt%)	64.28	64.70	64.57	60.63	60.15	60.67	61.64	64.65	63.22	61.84	61.15
TiO_2	0.73	0.72	0.73	0.85	0.86	0.87	0.87	0.75	0.79	0.90	0.88
Al_2O_3	15.80	15.83	15.82	15.88	15.87	16.02	16.27	16.32	16.57	16.51	16.06
Fe_2O_3*	5.20	5.06	5.15	7.60	7.90	7.43	7.15	5.02	5.01	6.82	7.56
MnO	0.12	0.12	0.12	0.15	0.16	0.16	0.13	0.16	0.17	0.12	0.14
MgO	1.11	1.13	1.10	1.73	1.89	1.85	1.56	1.38	1.51	1.64	1.66
CaO	3.13	3.01	3.06	4.34	4.43	4.46	4.32	3.32	3.34	4.05	4.58
Na_2O	4.50	4.53	4.50	4.29	4.22	4.26	4.35	4.69	4.71	4.43	4.29
K_2O	3.88	3.93	3.88	3.26	3.23	3.23	3.28	3.49	3.60	3.59	3.21
P_2O_5	0.30	0.30	0.30	0.53	0.56	0.56	0.53	0.30	0.28	0.41	0.58
Total	99.04	99.33	99.22	99.27	99.27	99.48	100.09	100.07	99.20	100.28	100.09
Rb (ppm)	136	138	136	114	114	111	114	119	123	122	111
Sr	414	406	409	506	512	514	515	461	509	542	526
Y	34	35	35	35	34	34	36	35	30	29	35
Zr	240	245	242	209	204	206	211	225	258	246	203
Nb	12	12	12	11	10	11	10	11	10	11	10
Ba	695	697	694	616	613	611	605	664	694	638	590

AS020, AS029, AS070, AS078 and AS079 are the samples from outcrops. Others are from borehole cores. The depth (m) is given for the core samples, whereas the elevation (m) is given for outcrop samples. Abbreviations: pl = plagioclase; ph = phenocryst; ST = Silicic Tochinoki lava; MT = Mafic Tochinoki lava; Elv. = elevation. Data of *ASK1545, *ASK1630, *ASK1920, *ASK1971, *ASK1999, *AS070 and *AS078 are the same as Table 2.2.

Table 2.4. Representative chemical compositions of phenocrysts in Tochinoki lavas

plagioclase								
Group	MTC		MTO		STC		STO	
Sample No.	ASK1920		AS078		AVL4-05		AS070	
	TYPE 1-c	TYPE 1-r	TYPE 1-c	TYPE 2-c	TYPE 1-c	TYPE 2-c	TYPE 1-c	TYPE 2-c
SiO_2	53.18	52.62	53.40	47.22	53.04	48.58	53.02	44.87
Al_2O_3	28.14	28.74	27.90	32.60	28.06	31.89	28.76	33.42
FeO	0.56	0.66	0.58	0.79	0.55	0.67	0.56	0.52
CaO	11.45	11.96	11.56	16.58	11.62	15.68	11.90	17.98
Na_2O	4.35	4.57	4.87	1.88	4.46	2.45	4.58	1.07
K_2O	0.41	0.38	0.37	0.10	0.40	0.16	0.34	0.03
Total	98.09	98.92	98.68	99.16	98.13	99.43	99.15	97.89
An	57.8	57.8	55.5	82.5	57.7	77.3	57.8	90.1
Ab	39.7	40.0	42.3	16.9	40.0	21.8	40.2	9.7
Or	2.5	2.2	2.1	0.6	2.4	0.9	2.0	0.2

pyroxene									
Group	MTC		MTO			STC		STO	
Sample No.	ASK1920		AS078			AVL4-05		AS070	
	cpx-c	opx-c	cpx-c	opx-c	rr	cpx-c	opx-c	cpx-c	opx-c
SiO_2	50.98	53.33	50.94	54.11	52.05	51.12	53.53	51.21	53.33
TiO_2	0.83	0.29	0.76	0.24	0.42	0.67	0.24	0.33	0.26
Al_2O_3	2.02	0.93	2.12	0.68	0.71	2.39	0.84	3.31	0.90
FeO	8.66	16.80	8.76	17.28	21.66	8.89	16.63	8.59	15.44
MnO	0.00	0.00	0.00	0.00	0.00	0.00	0.07	0.00	0.00
MgO	15.36	25.64	15.19	25.56	18.83	14.63	25.23	15.58	25.79
CaO	20.39	1.67	20.27	1.57	4.97	20.47	1.49	19.30	1.60
Total	98.23	98.66	98.04	99.44	98.63	98.17	98.04	98.31	97.32
Wo	41.8	3.3	42.0	3.1	10.3	42.9	3.0	40.5	3.2
En	44.3	70.7	43.8	70.3	54.5	42.6	70.8	45.5	72.4
Fs	13.9	26.0	14.2	26.6	35.2	14.5	26.2	14.1	24.3
Mg#	76.0	73.1	75.6	72.5	61.0	74.6	73.0	76.4	74.9

magnetite								
Group	MTC		MTO		STC		STO	
Sample No.	ASK1920		AS078		AVL4-05		AS070	
	c	c	c	c	c	c	c	c
SiO_2	0.10	0.09	0.17	0.12	0.05	0.14	0.07	0.08
TiO_2	10.99	10.84	11.29	11.58	11.70	12.66	12.34	11.56
Al_2O_3	3.41	2.67	3.42	3.29	3.11	2.46	2.87	3.37
FeO	77.26	79.30	77.16	77.34	78.50	78.32	77.28	76.55
MnO	0.00	0.00	0.00	0.00	0.00	0.00	0.00	0.00
MgO	2.03	0.86	2.03	2.03	0.93	0.77	1.81	2.94
CaO	0.00	0.00	0.00	0.00	0.09	0.00	0.00	0.19
Total	93.79	93.76	94.07	94.35	94.38	94.34	94.37	94.68
Fe_2O_3	43.33	43.91	42.72	42.62	42.17	40.64	41.59	43.47
FeO	38.28	39.79	38.71	38.98	40.56	41.75	39.86	37.43
Total	98.13	98.15	98.35	98.62	98.60	98.41	98.53	99.03
Usp mol %	34.21	34.21	35.21	35.77	37.21	39.76	37.80	34.21

Ferric iron is calculated on the basis of stoichiometry (Carmichael, 1967). Abbreviations: MTC = mafic Tochinoki core samples; STC = silicic Tochinoki core samples; MTO = mafic Tochinoki outcrop samples; STO = silicic Tochinoki outcrop samples; dsph = discrete phenocryst; agph = aggregated phenocryst; c = core; r = rim; cpx = clinopyroxene; opx = orthopyroxene; c = core; r = rim; rr = reaction rim; An = 100 x Ca / (Ca + Na + K) (mol %); Ab = 100 x Na / (Ca + Na + K) (mol %); Or = 100 x K / (Ca + Na + K) (mol %); Wo = 100 x Ca / (Ca + Mg + Fe) (mol %); En = 100 x Mg / (Ca + Mg + Fe) (mol %); Fs = 100 x Fe / (Ca + Mg + Fe) (mol %); Mg# = 100 x Mg / (Mg + Fe) (mol %); Usp = ulvo spinel.

Table 2.5. Criteria for classifying the post-caldera volcanic products into seven groups.

Group No.	I	II	III	IV	V	VI	VII
Group Name	2px-rhyolite	bt-rhyolite	hb-dacite	2px-dacite	aphyric andesite	porphyritic andesite	basalt -basaltic andesite
Phenocryst abundances (vol. %)	< 20	< 20	< 20	< 20	< 20	35-55	35-55
Grain size range of Plagioclase phenocryst (mm)	< 0.6	< 0.5	< 0.5	< 0.7	< 0.5	0.8-1.4	0.8-1.6
Phenocryst assemblage	opx, cpx, pl, opq	opx, cpx, bt, pl, opq	hb (tr), opx, cpx, pl, opq	opx, cpx, pl, opq	opx, cpx, pl, opq	ol (tr), opx, cpx, pl, opq	ol, opx, cpx, pl, opq
SiO_2 wt. %	69 <	69 <	68-69	65-67	59-64	55-62	< 54
Names of volcanic products	Otogase	Takanoobane	Hon-tsuka	Tateno Nagano Sawatsuno Hakusui Kusasenri (w)	Tochinoki	Karisako Okamadoyama Eboshidake Kusasenri (c) Naraodake Akamizu Yomineyama	Ayugaerinotaki Matsunoki Yoshioka Maruyama Takadake Kishimadake Kometsuka Ojodake Akase Nakadake (O) Nakadake (Y) Nakadake (Y. P. C)

Wavy lines show boundaries. Names of volcanic products are based on Ono and Watanabe (1985), Watanabe (2001), Masuda et al. (2004) and Miyabuchi et al. (2004). Abbreviations: (w) = welded pyroclastic rock; (c) = central cone; (O) = old volcanic edifice; (Y) = young volcanic edifice; (Y. P. C.) = youngest pyroclastic cone; ol = olivine; cpx = clinopyroxene; opx = orthopyroxene; bt = biotite; hb = hornblende; pl = plagioclase; opq = opaque minerals.

2.5.2 Major and trace element compositions

Geochemical characteristics of the post-caldera lavas

On a total alkali vs. silica diagram (Fig. 2.21) the post-caldera lava samples are plotted in the range from basalt to rhyolite. The basaltic products are plotted around the boundary between alkalic and sub-alkalic rock series. On the other hand, the andesitic, dacitic and rhyolitic products are plotted in the field of alkaline rock series. The contents of total alkali of the post-caldera silicic products are higher than those of the pre-caldera silicic products (Fig. 2.21).

The geochemical trends of the post-caldera lavas are depicted through the use of the Harker diagrams (Fig. 2.22, 2.23). With the exception of TiO_2, Na_2O, MnO, P_2O_5, Sr, Ni and Cr which show no linear trend, Al_2O_3, FeO*, MgO, CaO and V display well defined negative, whereas K_2O, Ba, Rb, Zr, Nb and Y display positive correlation with SiO_2. The samples of group VII are plotted in the field of medium-K and high-K series rocks. The samples of andesite to rhyolite are plotted in the field of high-K series rocks (Fig. 2.22). The post-caldera silicic products have higher Na_2O, K_2O, MnO, P_2O_5, Ba, Rb, Zr and Nb contents than those of the pre-caldera lavas (Fig. 2.22, 2.23). The boundaries between the group VII and VI, VI and V, V and IV are approximately 54 wt. %, 62–64 wt. % and 64–65 wt. % of SiO_2, respectively. The boundaries between the group IV and III, III and II are 64–65 wt. % and 69 wt. % of SiO_2. The group I has the highest silica content in the post-caldera volcanic products (Fig. 2.22, 2.23).

In MgO vs. Al_2O_3 diagram (Fig. 2.24), the basalt samples in group VII are plotted in the field of low-magnesium high-alumina basalt which is suggested by Kuno (1960) and Sisson and Grove (1993b). The major element compositions of these post-caldera basaltic products are very similar to those of the pre-caldera basaltic products (group A). In Y vs. S/Y diagram (Fig. 2.25), the post-caldera andesitic, dacitic and rhyolitic products are plotted in the field of the Island-arc type andesite, dacite and rhyolite composition.

The trace element characteristics of the basalts and andesites from the post-caldera

stage are simply illustrated by normalizing their trace element contents to those of the normal-MORB (Fig. 2.26; Sun and McDonough, 1989). The incompatible elements of the basalts (group VII) represent the IAB-like patterns which are characterized by their positive B and negative Nb. These basalts have lower B and higher Rb, K, Nb, Sr, Sm and Zr than those of the typical IAB (JB-2: basalt from Izu-Bonin arc). The andesites (group VI and V) represent the patterns which are similar to the typical Island-arc andesites (JA-1: Hakone volcano; JA-3: Asama volcano). The andesites have higher Rb, K, Nb, Sr, Sm and Zr and lower B contents than those of the typical arc-type andesite. The incompatible element patterns of basaltic and andesitic products from the caldera-forming stage are similar to those of the post-caldera stage basalts and andesites, respectively.

The compositional zonation observed in the Tochinoki lava

Fig. 2.27 indicates the depth profiles of the selected major and trace element contents in the borehole core samples. The silicic Tochinoki lava (ST) has higher SiO_2, K_2O, Rb and Zr contents and lower Fe_2O_3 and Sr contents than those of the mafic Tochinoki lava (MT).

Harker diagrams (Fig. 2.28) indicate that the boundary between MT and ST is 62–63 wt. % SiO_2. The MT borehole core samples (MTC) have higher Fe_2O_3 contents and lower SiO_2 and Na_2O contents than those of the outcrop samples (MTO). The ST borehole core samples (STC) have higher K_2O and Rb contents and lower Na_2O and Sr contents than the outcrop samples (STO). These Harker diagrams generally show the linear trends (Fig. 2.28).

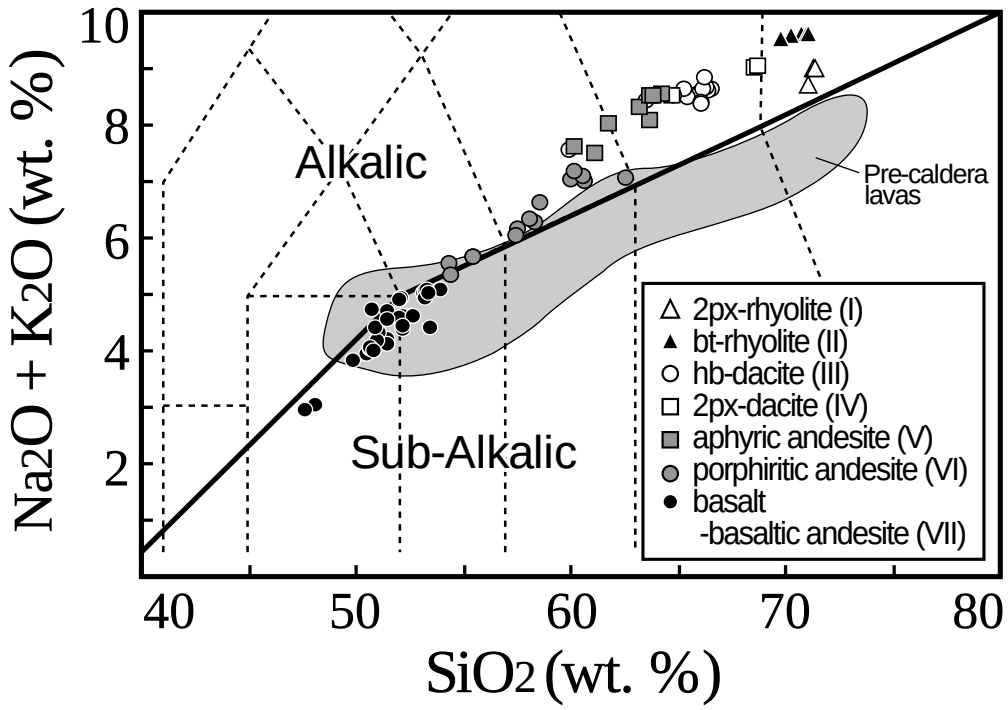

Fig. 2.21

Total alkali versus silica plots for the post-caldera volcanic products. Thick lines indicate alkali-tholeiitic rocks suite boundary (LeMaitre et al., 1989; MacDonald and Katsura, 1964). The shaded area shows the composition of pre-caldera lavas.

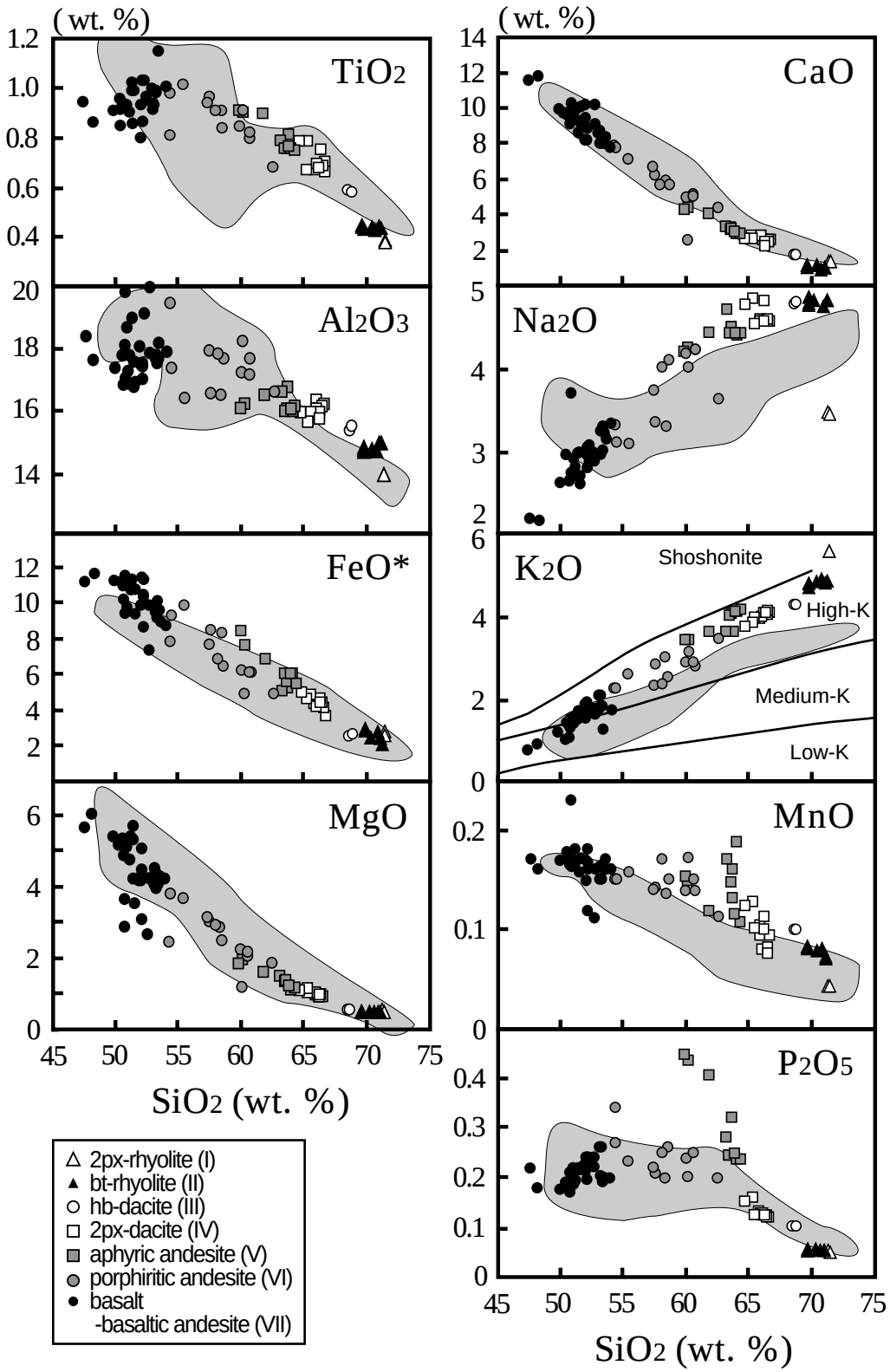

Fig. 2.22

Major elements (TiO_2, Al_2O_3, Fe_2O_3, MgO, CaO, Na_2O, K_2O and P_2O_5) vs. SiO_2 for the post-caldera volcanic rocks. Thick lines indicate Low-K, Medium-K, High-K and Shoshonite rock series boundary (LeMaitre et al., 1989; Rickwood, 1989). The shaded area shows the composition of pre-caldera lavas.

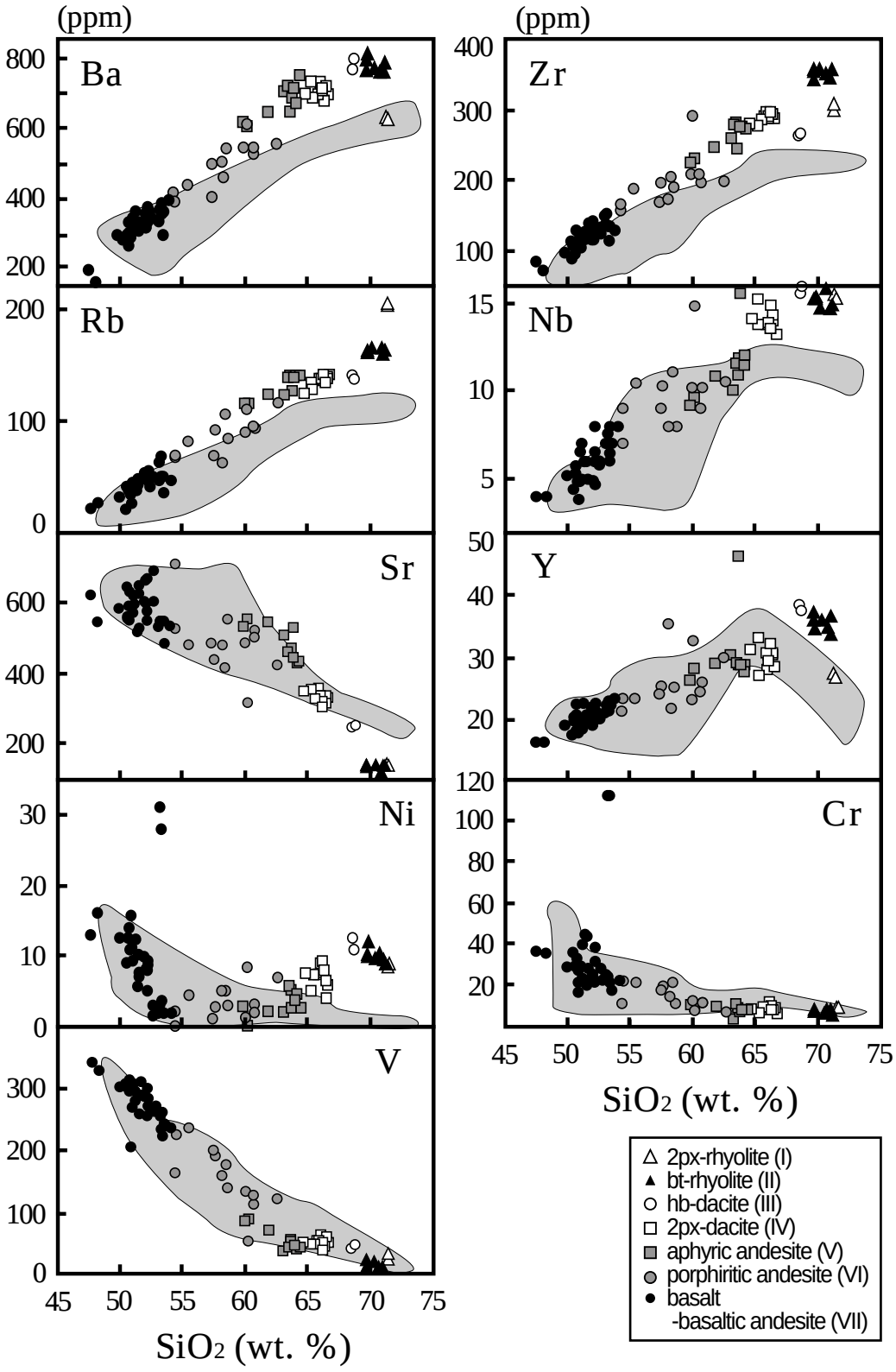

Fig. 2.23

Trace elements (Ba, Rb, Sr, Ni, V, Zr, Nb, Y, Cr) vs. SiO_2 for the post-caldera volcanic rocks. The shaded area shows the composition of pre-caldera lavas.

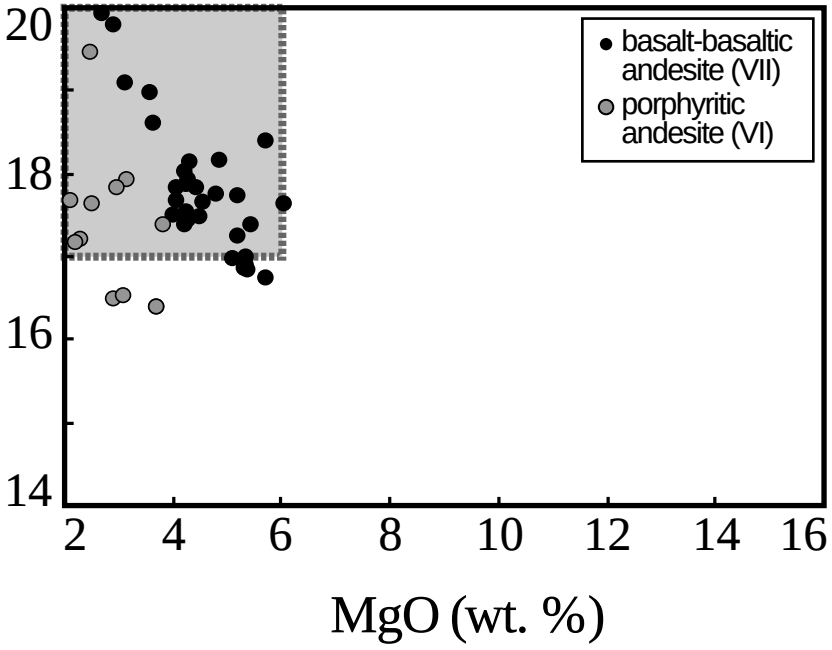

Fig. 2.24

MgO vs. Al_2O_3 diagram for the post-caldera basaltic rocks. Shaded area shows the compositional range of low-MgO high-Alumina basalt (Kuno, 1960; Sisson and Grove, 1993b).

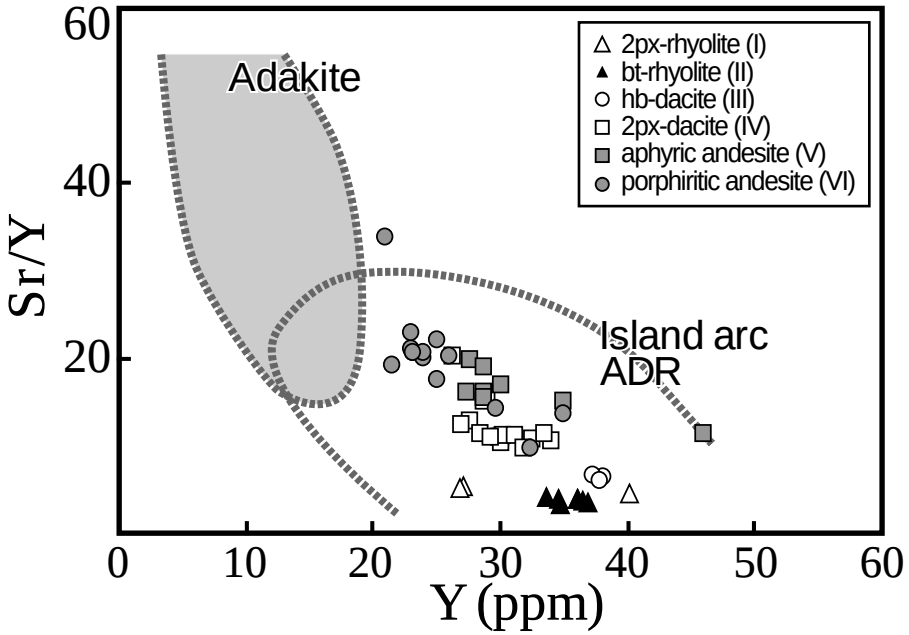

Fig. 2.25

Y vs. Sr/Y diagram for the post-caldera volcanic rocks. The adakite and island arc ADR (andesite, dacite and rhyolites) fields are given by Defant and Drummond (1993).

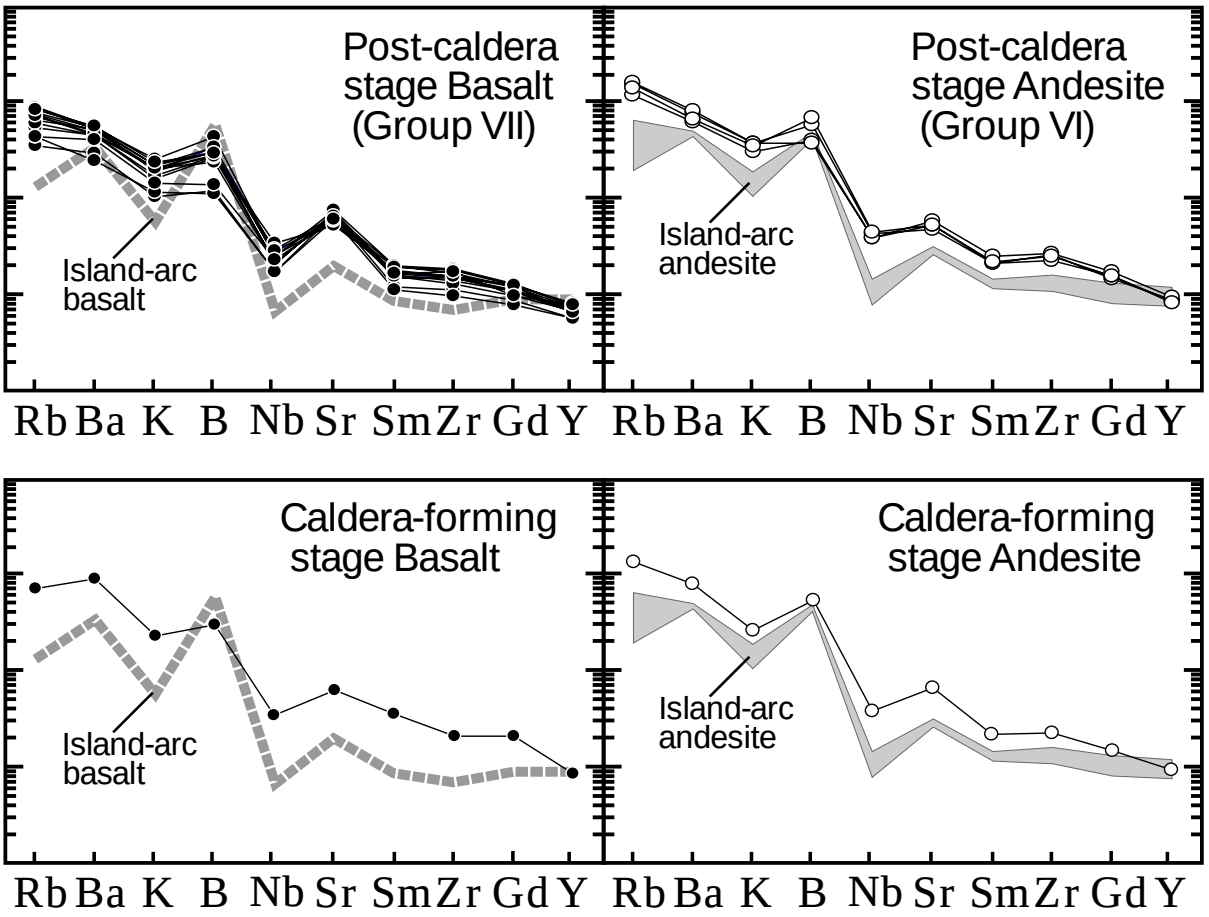

Fig. 2.26

Spider diagrams of incompatible elements for mafic rocks from the post-caldera and caldera-forming stages. Data for Island-arc basalt and andesite are from the database of GSJ standard samples (JB-2, JA-1 and JA-3). Abundances are normalized by n-MORB values: Rb (0.56), Ba (6.3), K (600), B (0.5), Nb (2.33), Sr (90), Sm (2.63), Zr (74), Gd (3.68), Y (28) (Sun and McDonough, 1989).

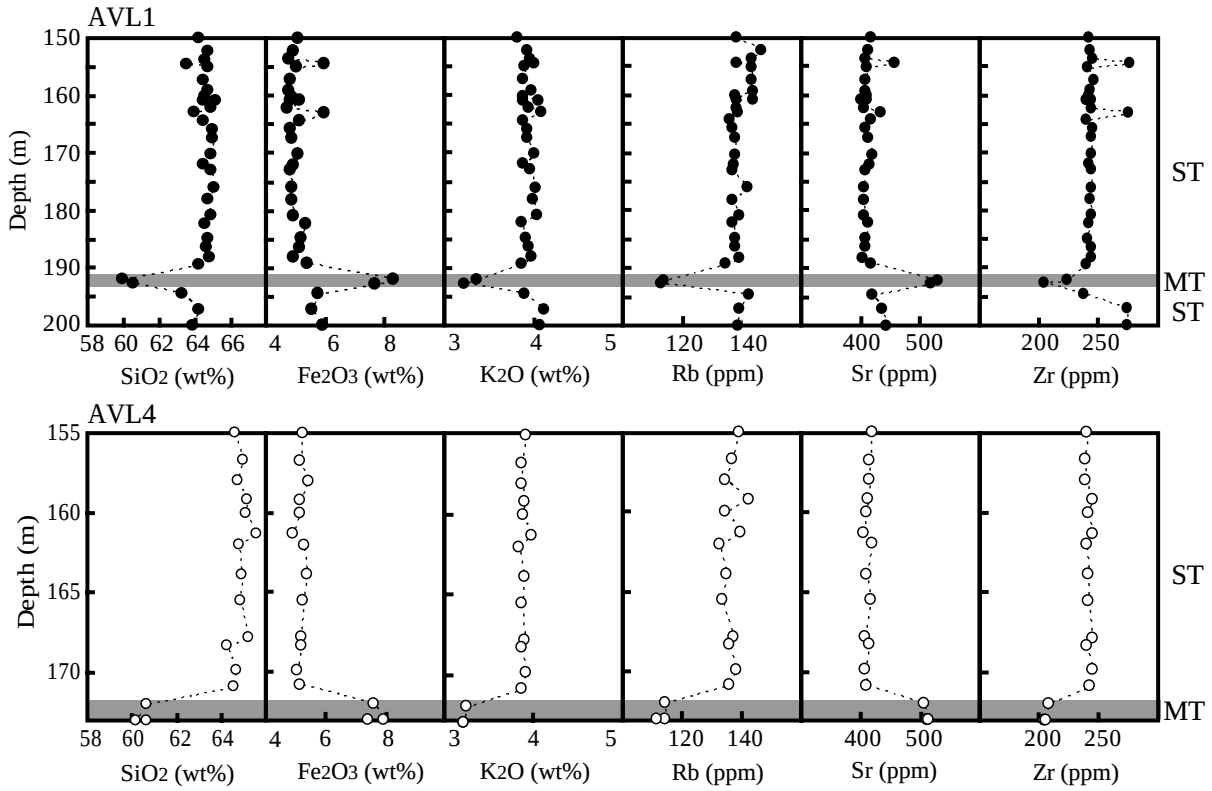

Fig. 2.27

Depth profile (meters beneath surface) of major and trace element compositions of Tochinoki core samples. The shaded field shows the depth of the mafic Tochinoki lava (MT).

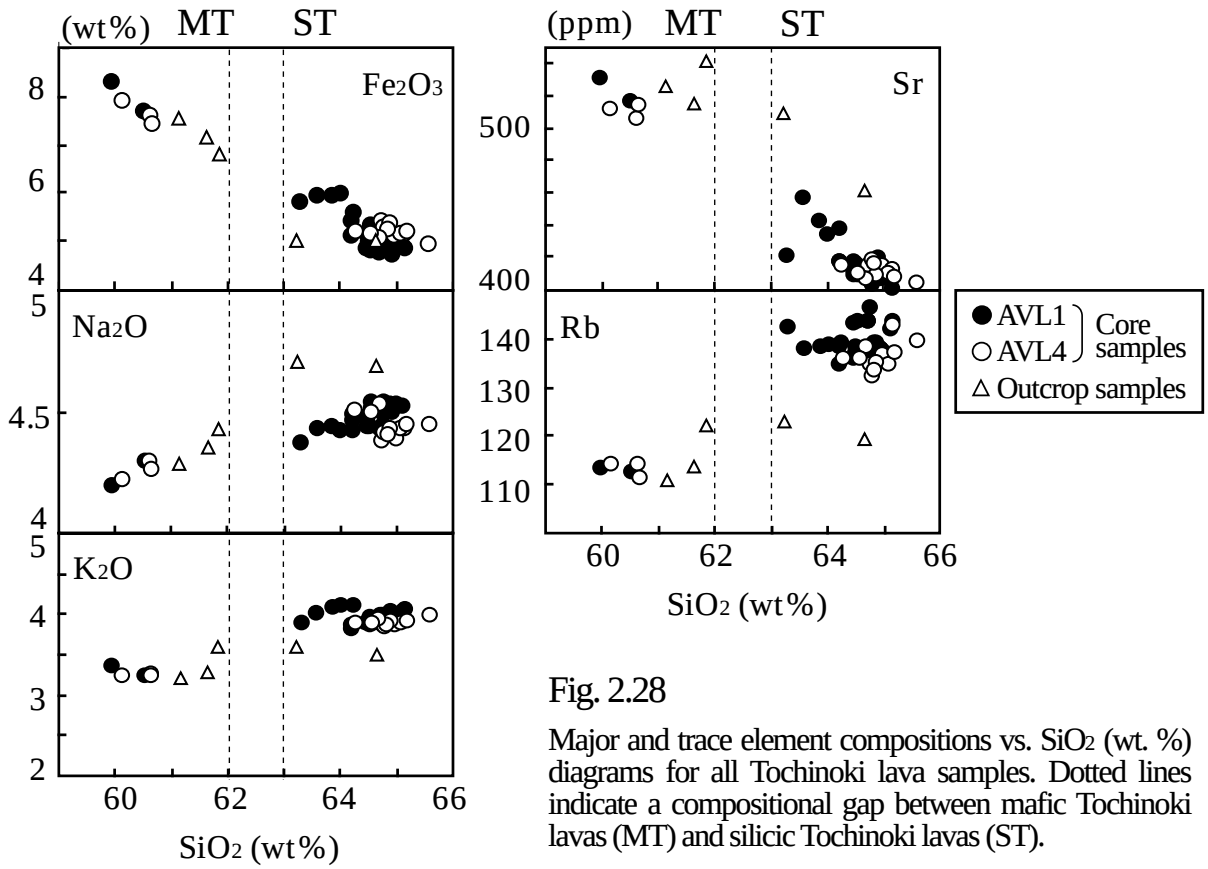

Fig. 2.28

Major and trace element compositions vs. SiO_2 (wt. %) diagrams for all Tochinoki lava samples. Dotted lines indicate a compositional gap between mafic Tochinoki lavas (MT) and silicic Tochinoki lavas (ST).

2.6 Discussions

2.6.1 Origin of the compositionally diverse magmas from the products of Aso post-caldera volcanism

2.6.1-1 Genetic relationship between the seven distinct magma groups

An examination of the parent-daughter relationships among seven distinct magma groups

The genetic relationships among seven distinct magma groups in the post-caldera lavas are examined by using the Rayleigh fractionation equation:
$C_L/C_0=F^{(D-1)}$, where C_L is concentration of some element in the residual liquid (melt), C_0 is the concentration of some element in the initial liquid, F is the amount of liquid remaining and D is bulk distribution coefficient in the fractional crystallization process in the magma chamber. The bulk distribution coefficients (D) of Rb, Nb and Zr are between 0 and 0.1 on the basis of their mineral-melt partition coefficients (Green, 1994; Rollinson, 1993). The compositional ranges formed by simple fractional crystallization are shown in the shaded areas in the Fig. 2.29. The sample which has the lowest incompatible element contents is assumed as the parental magma in each group (Fig. 2.29).

Fig. 2.29a and 2.29b indicate that the simple fractional crystallization of the parental magma of group VII does not produce the other magma groups. In addition, the compositional range observed in the group VII is not produced by the fractionation of the parental magma. Fig. 2.29c and 2.29d indicate that the group II and IV can be produced by the fractional crystallization of parental magma of group VI. The compositional range observed in the group VI also can be explained by the simple fractionation of the parental magma. The group I and V are not produced by the simple fractional crystallization of the parental magma of group VI. The group III is plotted close to the compositional range of the fractionation of the group VI, however the

genetic relationship between group III and VI is unclear. Fig. 2.29e and 2.29f indicate that the compositional range observed in group V can be produced by the simple fractional crystallization of the parental magma. In Fig. 2.29e, the group III and IV are not plotted within the compositional range of the fractionation of the group V. In Fig. 2.29f, the group I and II are not plotted within the compositional range of the fractionation of the group V. These observations indicate that the group I, II, III and IV are not produced by the simple fractional crystallization of the parental magma of group V. Similarly, Fig. 2.29g and 2.29h indicate the genetic relationship between group IV and III is unclear. In addition, the group II and I are not produced by the simple fractional crystallization of the parental magma of group IV. Fig. 2.29i and 2.29j indicate that the group I and II are not produced by the simple fractional crystallization of the parental magma of group III. Moreover, the group I is not produced by the simple fractional crystallization of the parental magma of group II.

As indicated above, the compositional diversity observed in the distinct seven magma groups of the post-caldera lavas are not completely explained by the simple fractional crystallization model. The genetic relationships observed in these seven groups (Fig. 2.30) indicate that at least four distinct end-member magmas, the group VII, VI (=II and IV), V and I, are coexisted in the post-caldera stage. Group II, III, IV and VI are distributed in the wide region in the caldera, and were simultaneously active, hence the temporal and spatial variations among these groups are not recognized. The disequilibrium textures commonly observed in the post-caldera lavas also indicate the compositional diversity observed among seven groups is not occurred by the simple fractional crystallization. The coexistence of the distinct magma groups possibly causes the mixing among different magmas. The increase of the activity of basaltic magma (group VII) observed in the later stage of the post-caldera volcanism (Fig. 2.1) may indicate the decrease or extinction of the silicic end-members which are possibly mixed with the supplied basaltic magma beneath the caldera.

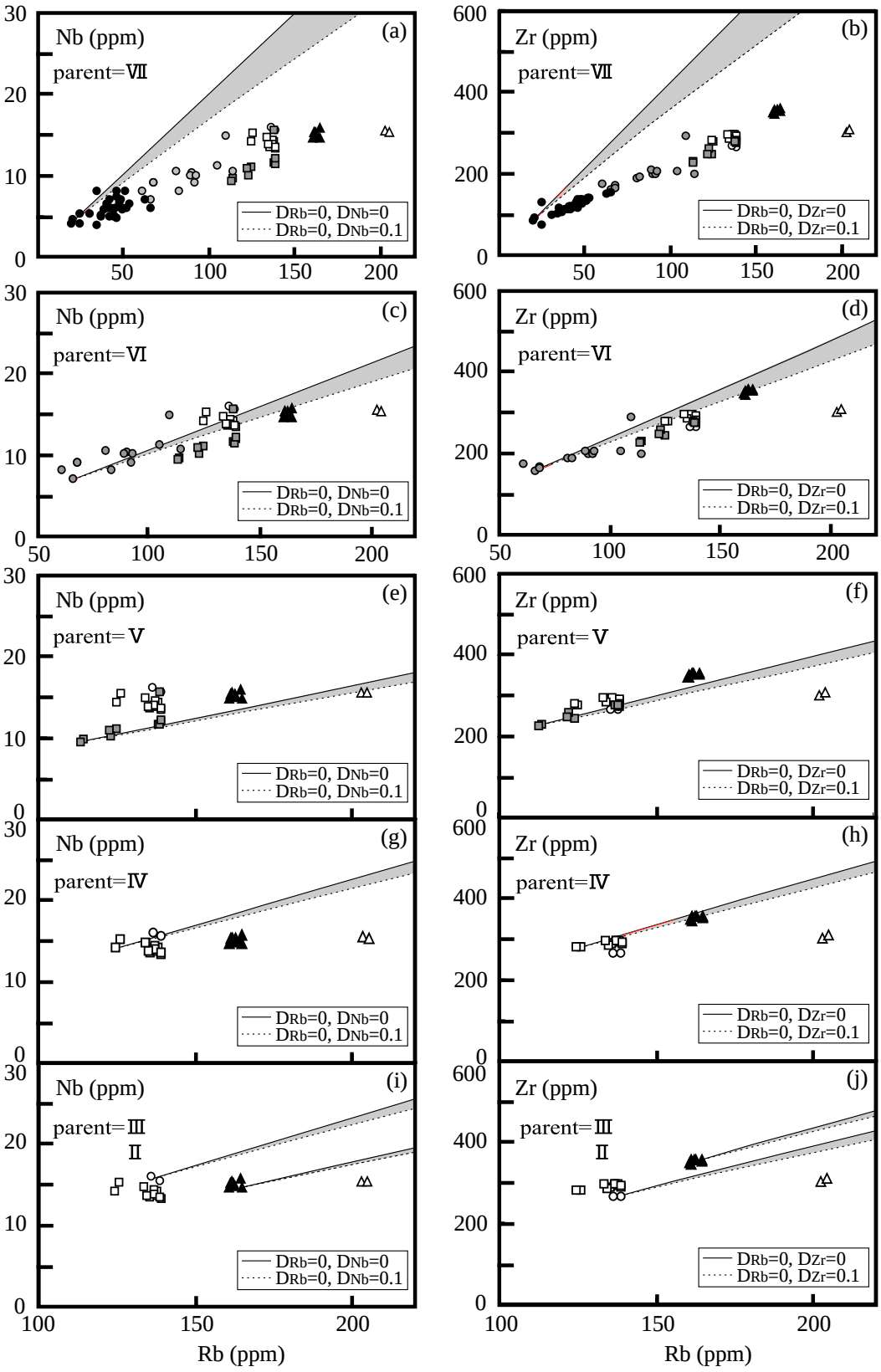

Fig. 2.29

Rb-Nb and Rb-Zr diagrams for the seven groups from Aso post-caldera stage. Shaded areas show the compositional ranges formed by simple fractional crystallization. Symbols are the same as Fig. 2.21.

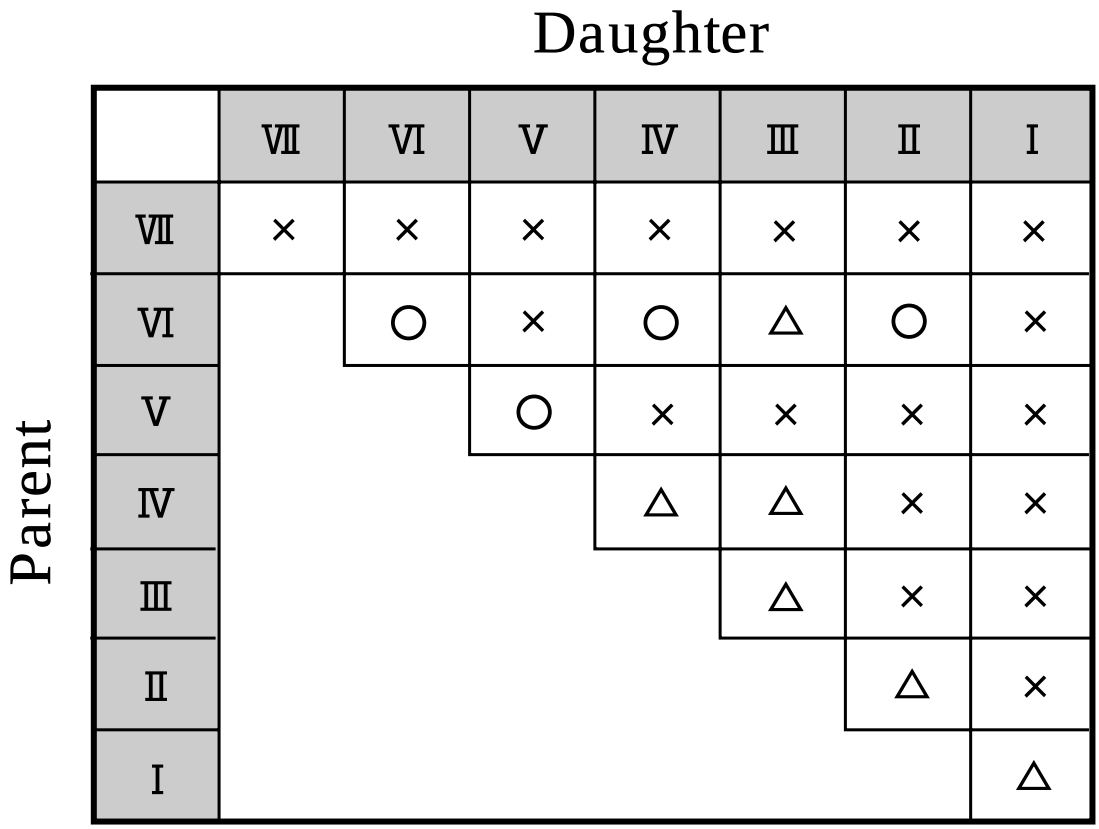

Fig. 2.30

Parent-daughter relationships among the seven groups of post-caldera volcanic products. Open circle = parent-daughter relationship; Cross = not in parent-daughter relationship; Open triangle = unclear.

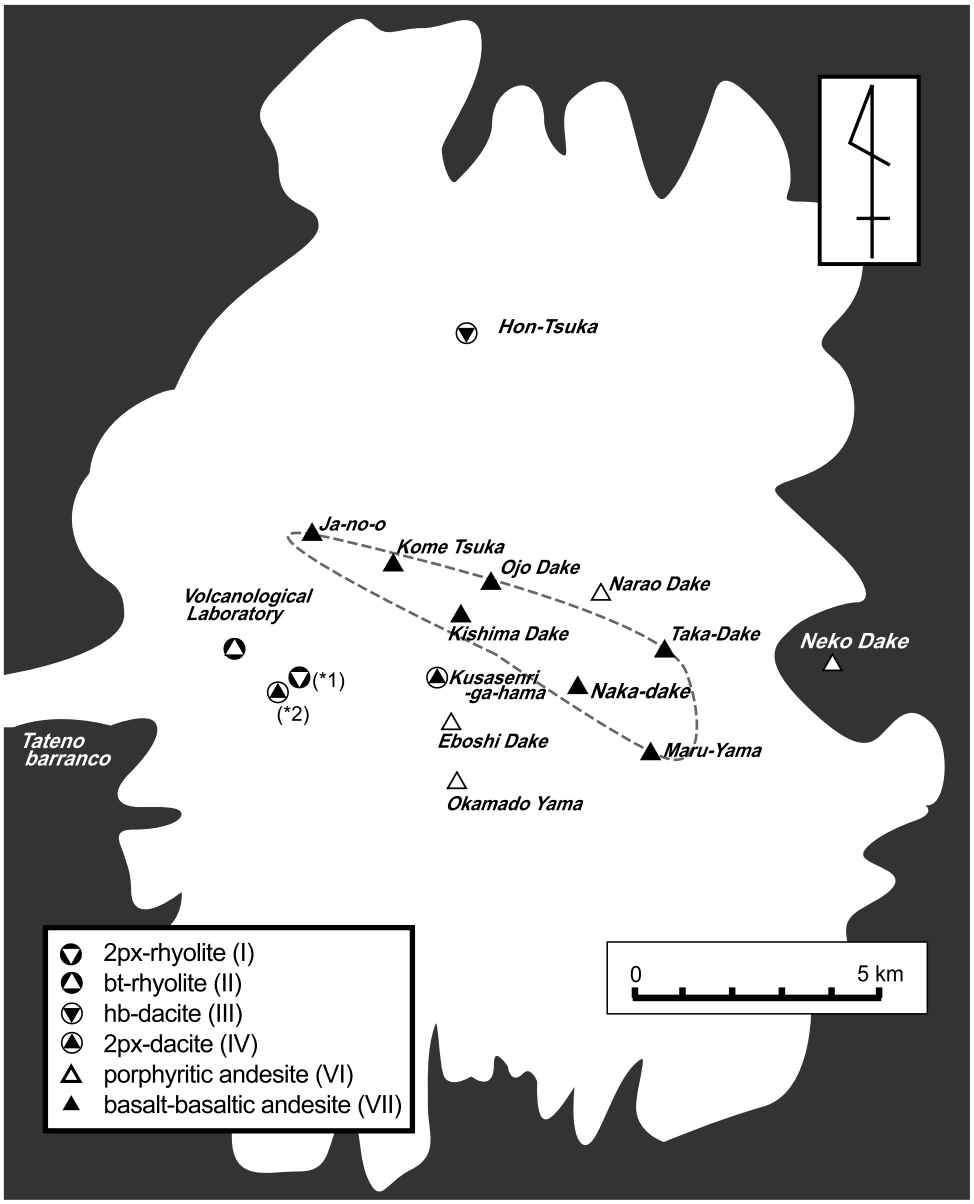

Fig. 2.31

Distribution map of the intra-caldera vents indicating that younger basaltic products were erupted from the central vents of the caldera area surrounded by dotted line. *1 indicates the possible vent of Otogase lava and *2 indicates the possible vent of Nagano lava, both as suggested by Miyabuchi et al. (2004).

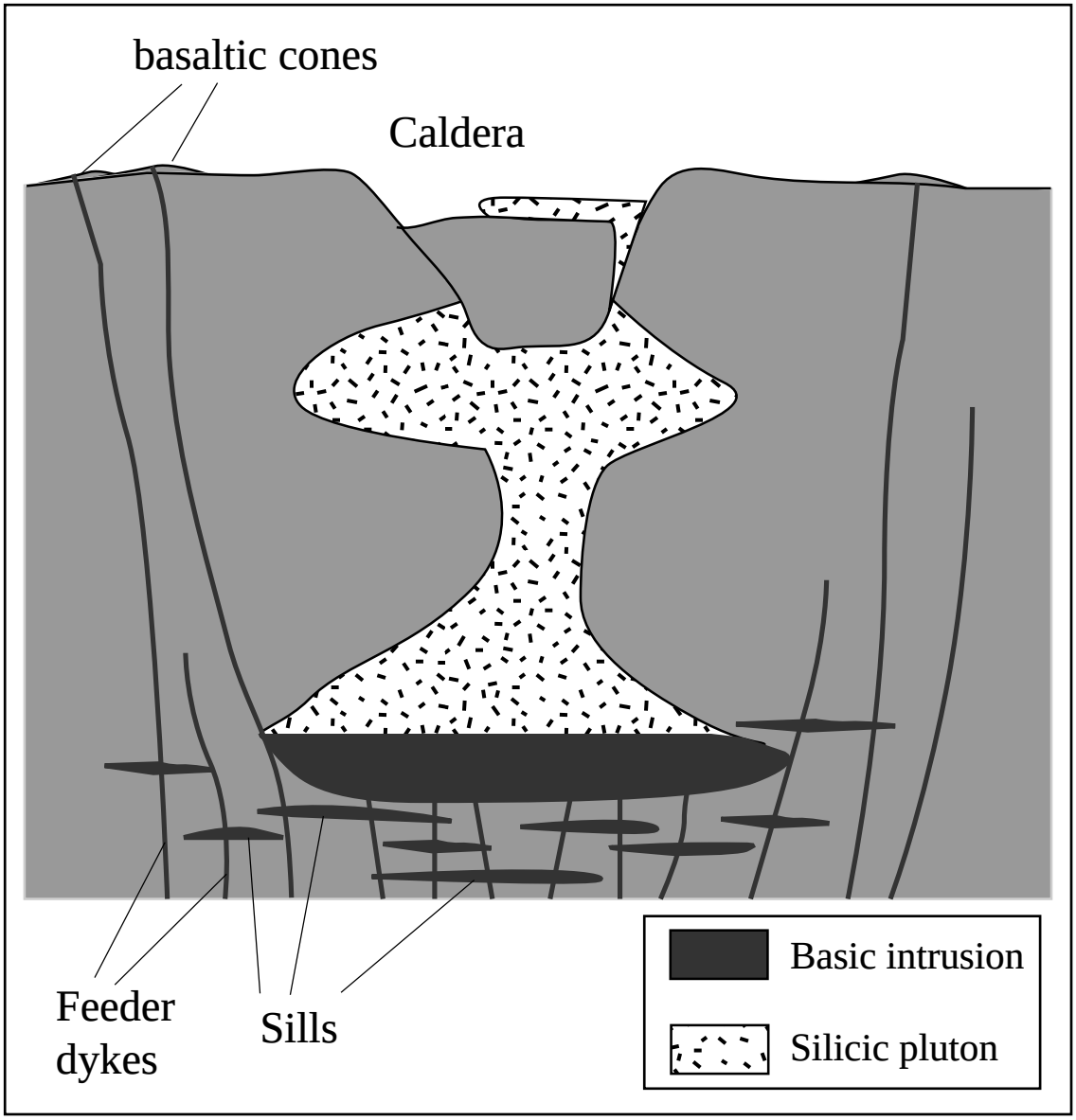

Fig. 2.32

A simplified schematic model for the magma-plumbing system beneath the caldera volcano which is proposed by Huppert and Sparks (1988). In this model, ascending basalts can still reach the surface in peripheral regions of the huge silicic magma chamber.

The relationship between the distributions of vents and the compositions of volcanic products

Fig. 2.31 shows the distributions of vents of the post-caldera lavas. The vents extruding basaltic magmas (group VII) are centered in the caldera, whereas those extruding other silicic magma (groups I, II, III, IV and VI) are distributed around them. If the huge single magma chamber, as assumed in the caldera-forming stage, exists beneath the caldera, the opposite distribution of the vents probably are observed. This is because the upwelled basaltic magma probably is trapped by this huge silicic magma chamber, and is modified the composition from basaltic to silicic. However, the basaltic magma which passed through around the silicic magma chamber probably erupts without the change in composition (Huppert and Sparks, 1988; Fig. 2.32). In this case, the expected distributions of the vents are as follows: the vents extruding the silicic magmas are centered; the vents extruding basaltic magmas are distributed around the silicic vents. Therefore, the existence of the huge silicic magma chamber is not consistent with the distributions of vents observed in the post-caldera volcanic stage. This probably indicates the multiple magma chambers coexisted after the caldera formation.

2.6.1-2 Compositional heterogeneity within the aphyric andesite lava flows: a case study of Aso Tochinoki lava

AS mentioned in the Chapter 2.5, the Tochinoki lava (group V: aphyric andesite) is divided into following two types on the basis of the phenocryst abundances and the bulk-rock composition: Silicic Tochinoki lava (ST) which contains more than 8 vol. % of phenocryst and 63 wt. % of silica content; Mafic Tochinoki lava (MT) which contains less than 7 vol. % of phenocryst and 62 wt. % of silica content (Fig. 2.16). Both ST and MT are commonly observed in the outcrop and borehole core samples. For convenience sake, I call those of the core samples as STC and MTC, and those of

the outcrop samples as STO and MTO.

Genetic relationship between coexisting mafic and silicic Tochinoki lavas within a composite lava flow in the borehole core sample

The Tochinoki lava found in the two borehole cores of Kyoto University (Fig. 2.15) is a composite lava flow which is formed by STC and MTC. The STC forms the upper part of the composite lava, whereas the MTC forms the lower part of it (Fig. 2.15). The compositional difference between the STC and MTC is not caused by the accumulation of phenocrysts, because the phenocryst abundance of STC is higher than that of MTC (Fig. 2.16).

The genetic relationship between the STC and MTC is examined by the mass-balance calculation of Bryan et al. (1969) by using the program of 'igpet99' (Carr, 1999). The sample which has the lowest silica contents in the MTC (ASK1920) is assumed as the parental magma. The assumed daughter magma is the sample which has the highest silica contents in the STC (AVL4-05). The result of the calculation is shown in Table 2.6. The compositions of the fractionated minerals are averaged values of the compositions of phenocrysts included in the parental magma (ASK1920). The MTC does not include the type-2 plagioclase (Fig. 2.18) which is disequilibrium with the host magma, hence the all fractionated minerals used in the mass-balance calculation are assumed to be equilibrium with the host magma. The result of the calculation (Table 2.6) indicates that the composition of daughter magma (AVL4-05) can be produced by the fractionation of the following minerals from the parental magma (ASK1920): 13 % of plagioclase, 2.6 % of clinopyroxene, 2.1 % of orthopyroxene and 4.1 % of magnetite.

In addition, the relationship is also examined by Rayleigh fractionation equation (see Chapter 2.5.1-1) by using the trace element data. The bulk distribution coefficients (D) of Rb, Zr, Nb and Sr are calculated by using their mineral-melt partition coefficients (Green, 1994; Rollinson, 1993) and the mass ratios of fractionated minerals (Table 2.6). The calculated D values of these trace elements are

Table 2.6. Results of least squares mixing calculations

	Fractionated minerals				Daughter (AVL4-05)	Parent (ASK1920)			residual
	cpx	opx	pl	mt	Obs.	Obs.	Calc.		(r)
SiO_2	51.06	52.83	53.18	0.09	65.93	60.68	61.09		-0.41
TiO_2	0.59	0.31	0.06	10.69	0.73	0.92	1.06		-0.14
Al_2O_3	1.88	1.12	27.87	3.08	15.91	16.29	16.34		-0.05
FeO*	8.81	17.03	0.64	77.93	4.44	7.54	7.56		-0.02
MnO	0.01	0.01	0.00	0.00	0.12	0.15	0.09		0.06
MgO	15.25	25.29	0.07	1.29	1.11	1.91	1.88		0.03
CaO	20.30	1.60	11.26	0.01	3.00	4.40	4.4		0.00
Na_2O	0.32	0.03	4.72	0.01	4.47	4.25	4.12		0.13
K_2O	0.01	0.00	0.45	0.01	4.00	3.40	3.19		0.21
P_2O_5	0.00	0.00	0.00	0.00	0.30	0.46	0.23		0.23
Total	98.22	98.22	98.24	93.11	100.00	100.00	99.96	r^2	0.31

Daughter + fractionated minerals = Parent

	Proportions of Phases	% Fractionated minerals
AVL4-05	0.782	
cpx	0.026	11.9
opx	0.021	9.7
pl	0.130	59.7
mt	0.041	18.7
ASK1920	1.000	

The compositions of fractionated minerals represent averaged compositions of each phenocryst in the parent mafic Tochinoki core sample ASK1920. Abbreviations of minerals: cpx = clinopyroxene; opx = orthopyroxene; pl = plagioclase; mt = magnetite.

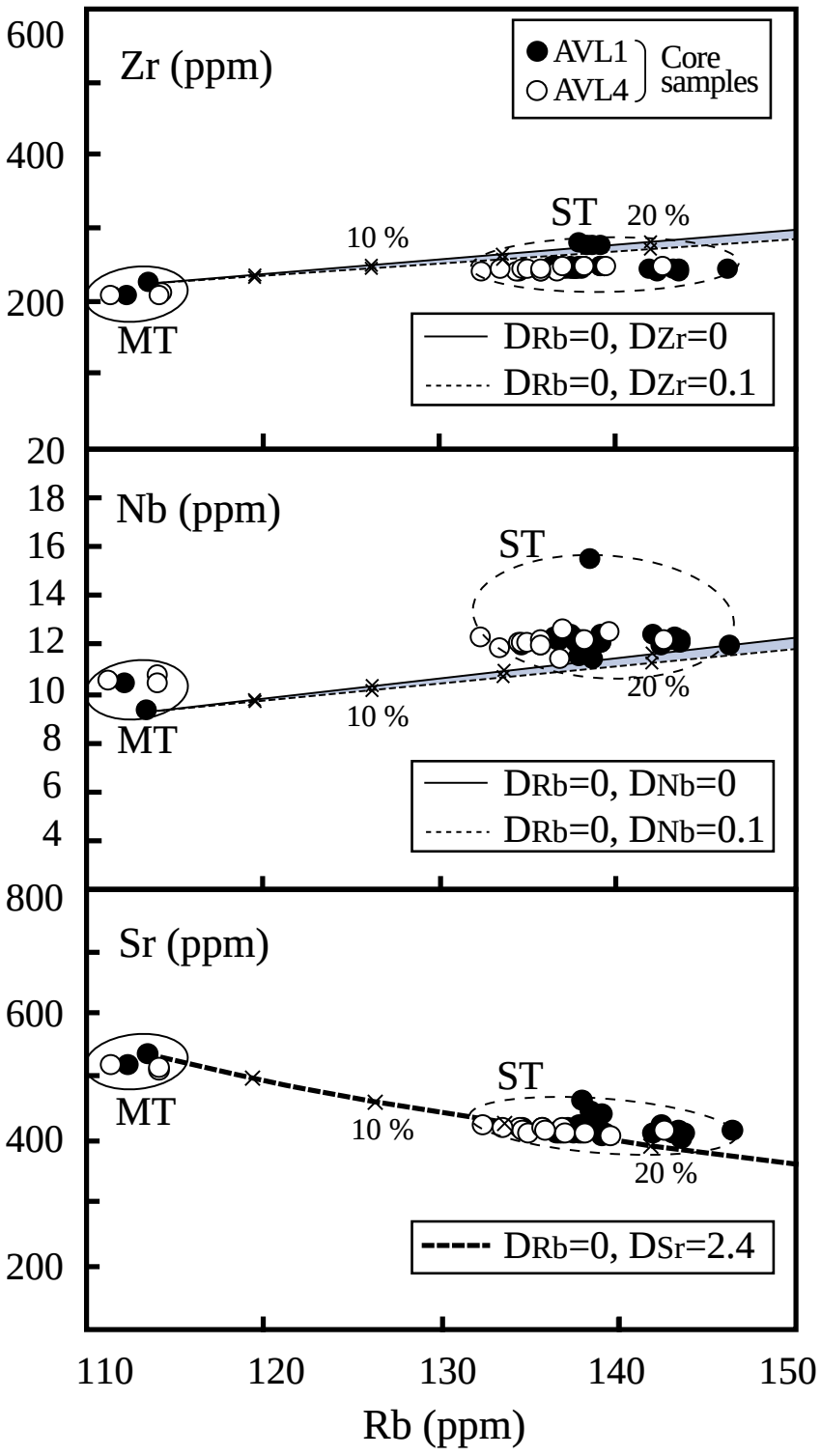

Fig. 2.33

Rb-Nb, Rb-Zr and Rb-Sr diagrams for Tochinoki core samples. Shaded areas show the compositional range predicted by the maximum fractional crystallization model. Numbers (%) represent a degree of fractionation.

as follows: D_{Rb}, D_{Zr} and $D_{Nb} < 0.1$, $D_{Sr} = 2.4$. The higher D value of Sr than other elements indicates that the Sr behaves a compatible element to plagioclase. The results of the Rayleigh fractionation equation are shown in the Fig. 2.33. The estimated trends of compositional variation formed by simple fractional crystallization of the parental magma are shown in the shaded areas and dotted line in the Fig. 2.33. These estimated trends correspond approximately to the observed trends. These results indicate that the STC is produced by the fractionation of 15–25 % minerals from the parental magma (Fig. 2.33). The estimated mass ratios of fractionated minerals are well consistent with the results of mass-balance calculation (Table 2.6). These results of these calculations indicate the main process which caused the compositional diversity observed in Tochinoki lava (group V) is the fractional crystallization.

The formation mechanism of the layered structure in composite lava flow

The massive part of the borehole core sample shows compositional layered structure which is composed of the lower mafic (MTC) and the upper silicic (STC) parts (Fig. 2.27). The lowermost part of the AVL1 core is composed of the brecciated lava of the STC. This silicic-over-mafic layered structure of Tochinoki lava is commonly observed in the other reported composite lava flows (Carrigan and Eichelberger, 1990; Carrigan, 1994; Watts et al., 1999). In addition, this layered structure is the inversion of the mafic-over-silicic layered pyroclastic fall-out deposits erupted from the compositionally zoned-magma chamber which has the silicic-over-mafic zonation (Smith, 1979). In particular, this layered structure is observed in the lava flow (silicic-over-mafic) and within the vent (mafic margin and silicic core parts) by the research drilling of the Inyo Obsidian Dome. The lowermost part of the lava flow is the basal breccia part which is formed by both mafic and silicic lava breccia (Carrigan and Eichelberger, 1990).

Carrigan and Eichelberger (1990) and Carrigan (1994) explained the formation mechanism of the layered structure observed in the composite lava flow on the basis of the result of analog fluid experiment as follows: If two types of fluids of differing

viscosity flow in the pipe, redistribution will occur. The lower-viscosity component (= mafic magma) migrates to the wall leaving the higher-viscosity component (= silicic magma) to occupy the core. Because the rate of energy dissipation is proportional to viscosity, dissipation in the system is minimized when the lower-viscosity component flows in the region of highest shear. In effect, the annular low-viscosity fluid lubricates the rise of the viscous core. The opposite zonation, with high-viscosity fluid in the annulus, has been found to be unstable, both by linear stability theory (Hickox, 1971) and by laboratory experiment (Blake and Campbell, 1986). This viscous segregation process is probably occurred within the vent of Inyo Obsidian Dome, and formed the silicic-over-mafic layered composite lava flow.

The layered structure observed in Tochinoki lava (Fig. 2.17 and 2.27) is very similar to that of the Inyo Obsidian Dome. Therefore, the Tochinoki composite lava is possibly formed by the viscous segregation of two different magmas. In addition, the basal breccia of the Inyo Obsidian Dome lava which has wide compositional range from mafic to silicic is interpreted as the lava-breccia of flow front of the composite lava (Carrigan and Eichelberger, 1990). The lowermost brecciated part of the Tochinoki lava which has silicic composition (STC) probably is the basal breccia of composite lava flow.

The possibility of coexistence of multiple flow units in Tochinoki lava

Miyabuchi et al. (2004) suggested that the possibility of the existence of the multiple flow units which have diverse compositions in the Tochinoki lava. Both core and outcrop samples are divided into two groups (MT and ST) on the basis of their phenocryst abundances and silica contents. The boundaries of these two groups are 7 vol. % of phenocryst abundances and 62 wt. % of silica contents (Fig. 2.16).

However, the following differences are observed between core and outcrop samples: 1) the clinopyroxene phenocrysts included in the MTO are commonly surrounded by the reaction-rim of Ca-poor pyroxene (Mg# = 61), however that is not included in the MTC; 2) the plagioclase phenocrysts in the outcrop samples (MTO and

STO) have wider range in composition than those in the core samples (Fig. 2.19). In addition, the outcrop samples have high abundances of the plagioclase phenocrysts which have Ca-rich cores (Fig. 2.18 and 2.19); 3) the bulk-rock compositions of the outcrop samples do not overlap with those of the core samples (Fig. 2.28).

These observations indicate that the petrological characteristics of the outcrop samples are not similar to those of the core samples. This implies that these core and outcrop samples are the different flow units. These two types of lava samples are included in the same stratigraphy, hence they probably are the contemporaneous different lava flow unites. The similar volcanism to this was observed in the Miyake-jima 1983 eruption. This volcanism produced compositionally diverse magmas from the multiple fissure vents (Soya et al., 1984). However, it is not clear whether the Tochinoki lava had the multiple vents, because the most of the distributional area of it is covered by the upper units of volcanic products from the post-caldera stage.

2.6.2 Cause of the temporal changes of mafic magma composition in Aso area

The magmatisms occurred in and around Aso volcano are divided into the following three stages on the basis of the geochemical characteristics of the basaltic and andesitic products: 1) 3.8 Ma: the activity of high-Mg andesite; 2) from 2.2 Ma to 290 ka: the coexistence of high-Al basalt, Island arc-type andesite and adakitic andesite; 3) after 290 ka: the activities of high-Al basalt and Island arc-type andesite. The stage-1 and -2 include the pre-caldera volcanism. The stage-3 includes both the caldera-forming and post-caldera volcanisms.

The origin of high-Mg andesite erupted in the stage-1 is probably similar to that of other northern Kyushu high-Mg andesite, because the eruption age and incompatible element compositions (Fig. 2.12) of this andesite overlap with those of the other northern Kyushu high-Mg andesite (8–3 Ma; Tatsumi et al., 1980; Shiraki et al., 2000).

High-Mg andesite magmas are generated by the partial melting of mantle materials under hydrous condition or the interaction between mantle and silicic slab melt in warm subduction zones (e.g. Tatsumi, 2003). The origin of high-Mg andesite is closely

associated with the anomalous tectonic settings such as subduction of young and hot oceanic plate and backarc opening (Tatsumi, 2003, 2006; Kimura et al., 2005). Most of the high-Mg andesite lavas in the Japan Island are distributed in Setouchi volcanic belt, from central Japan to eastern Kyushu (Tatsumi, 2003). Many geological and geochemical studies indicate that the Setouchi high-Mg andesite lavas erupted at about 13.6 ± 0.3 Ma from a number of K-Ar data (Tatsumi and Ishizaka, 1978, 1982; Shiraki, 1993; Shiraki et al., 1995).

The origin of Setouchi high-Mg andesite involves the subduction of young and hot Shikoku basin lithosphere (15–26 Ma; Okino et al., 1994) into the high-temperature upper mantle associated with the opening of Japan Sea. The isotope mixing calculations indicate that the Setouchi high-Mg andesite is a mixture of the silicic slab-melt and the mantle material (Tatsumi, 2003, 2006; Shimoda et al., 1998).

The origin of the northern Kyushu high-Mg andesite, including Aso high-Mg andesite, is probably different from that of the Setouchi high-Mg andesite. This is because the eruption ages of northern Kyushu high-Mg andesites (<8 Ma) are significantly younger than those of the Setouchi high-Mg andesites (13.6 Ma). In addition, Tatsumi et al. (1980) indicated the northern Kyushu high-Mg andesites contain higher alkali and Light Rare Earth Element (LREE) contents than those of Setouchi high-Mg andesites. The defining difference between the northern Kyushu and Setouchi high-Mg andesites are observed in their B contents (Fig. 2.12). The Setouchi high-Mg andesite is characterized by the high B contents. On the other hand, the northern Kyushu high-Mg andesites show the depletion of B in the Fig. 2.12.

Shiraki et al. (2000) and Kakubuchi et al. (1995) argued that the high-Mg andesites from Nagasaki and Hikosan areas are not involved by the slab-melt derived from the subducted Philippine Sea plate, because the Wadati-Benioff Zone is not detected beneath these areas. In addition, these high-Mg andesites are coincided with the OIB-type basalts. This probably indicates the subducted oceanic plate did not exist beneath these areas when the high-Mg andesites were active. These northern Kyushu high-Mg andesites are probably generated by the interaction between the upwelled high-temperature asthenospheric mantle and the pre-existed shallower metasomatized

mantle (Shiraki et al., 2000). Although the trigger of the upwelling of asthenospheric mantle is not constrained by the data obtained in this study, the most probable cause is the development of the Okinawa Trough (4-2 Ma). This development of the backarc basin is similar to the origin of the Setouchi high-Mg andesite (Tatsumi, 2003), however, the low B contents of the Aso high-Mg andesite does not indicate the interaction between the high-temperature mantle and oceanic slab. Therefore, the source region beneath Aso area probably was not metasomatized by the slab-derived fluid or melt released from the Philippine Sea plate, but was heated by the high-temperature asthenospheric mantle associated with the backarc opening in 3.8 Ma.

After 2.2 Ma, in the stage-2, the geochemical characteristics of the erupted magmas were drastically changed from the stage-1. The basaltic products erupted in this stage are the low-Mg high-Al basalts which are the typical basalts in the Island-arc setting (Kuno, 1960; Sisson and Grove, 1993b; Fig. 2.10). These basalts show the incompatible element pattern of the typical Island-arc basalts which have high LILE and low Nb contents (Fig. 2.12). Two types of andesitic rocks are observed in this stage-2, Island-arc type and adakitic andesites (group E) (Fig. 2.11). The adakitic magma is interpreted to be a partial melt of the oceanic slab with a garnet residue, and typically has high Sr/Y and low $^{87}Sr/^{86}Sr$ ratios (Defant and Drummond, 1990). In addition, the melting of the oceanic-slab probably occurs in the warm subduction zones (Defant and Drummond, 1990). The coexistence of the Island-arc type and adakitic andesites is also observed in the Yufu-Tsurumi volcano which is located in the 50 km northeast of Aso volcano (Fig. 1.2). Sugimoto et al. (2006) indicated that these two types of andesites observed in the Yufu-Tsurumi volcano is the mixture of the Island-arc type magma and slab melt on the basis of isotope mixing calculations. The andesitic products in this stage-2 are also possibly the mixtures of the Island-arc magma and the slab melt, because the petrography (hornblende-two pyroxene andesite), Y contents and Sr/Y ratios of these andesites (Y = 16–19 ppm, Sr/Y = 25–45) are similar to those of the Yufu-Tsurumi andesites (Y = 14–27 ppm, Sr/Y = 20–42). However, the B contents, B/Sm, B/Zr and B/Nb ratios of the group E (B = 7–17 ppm,

B/Sm = 2–5, B/Zr = 0.1–0.2, B/Nb = 1.2–2.8) is higher than those of the Yufu-Tsurumi andesites (B = 7–10 ppm, B/Sm = 1.7–2.8, B/Zr = 0.04–0.07, B/Nb = 0.6–1.2). This high B contents observed in the group E probably represents the high boron contents of the Island-arc type magma which is the end-member of the mixing with the slab-malt, because the largest amount of slab-derived fluid is transported to the mantle beneath Aso in the northern Kyushu (See Chapter 1). These observations probably indicate the slab-melting and slab-dehydration are occurred simultaneously beneath the Aso volcano in the stage-2.

After 290 ka, in the stage-3, the basaltic products are the low-Mg high-Al basalts which are the typical basalts in the Island-arc setting (Kuno, 1960; Sisson and Grove, 1993b; Fig. 2.24). These basalts show the incompatible element patterns of the typical Island-arc basalts which have high LILE and low Nb contents (Fig. 2.26). The andesites are also show the incompatible element patterns which is similar to those of the basalts. The adakitic andesite is not observed in this stage-3 (Fig. 2.25). These observations indicate the magmatism in the stage-3 is probably occurred in the typical arc-setting which is characterized by the cold oceanic plate subduction.

The source composition of the basaltic magma probably did not change largely from stage-2 to -3. On the other hand, the major differences between stage-2 and -3 are observed in the incompatible trace elements compositions of the silicic products (Fig. 2.2.2). The SiO_2 contents of the post-caldera dacite and rhyolite (64–73 wt. %) are similar to those of the pre-caldera dacite and rhyolite; however, the incompatible element (Ba, Rb, Zr, Nb and Y) contents of them are significantly higher than those of the pre-caldera dacite and rhyolite (Fig. 2.2.2). This major difference among them is not explained by the different degrees of partial melting and/or fractional crystallization of the same source. Hence the origin of the silicic magma probably changed between stage-2 and -3. Although the cause of this is not constrained by the data of this study, the predominance of the arc-type andesite and disappearance of the adakitic andesite may contribute to the change of the silicic magma compositions.

Fig. 2.34 shows the temporal changes of B/Sm, B/Zr and B/Nb ratios of the volcanic products from Aso area. In the stage-1, the B/Sm, B/Zr and B/Nb ratios of the

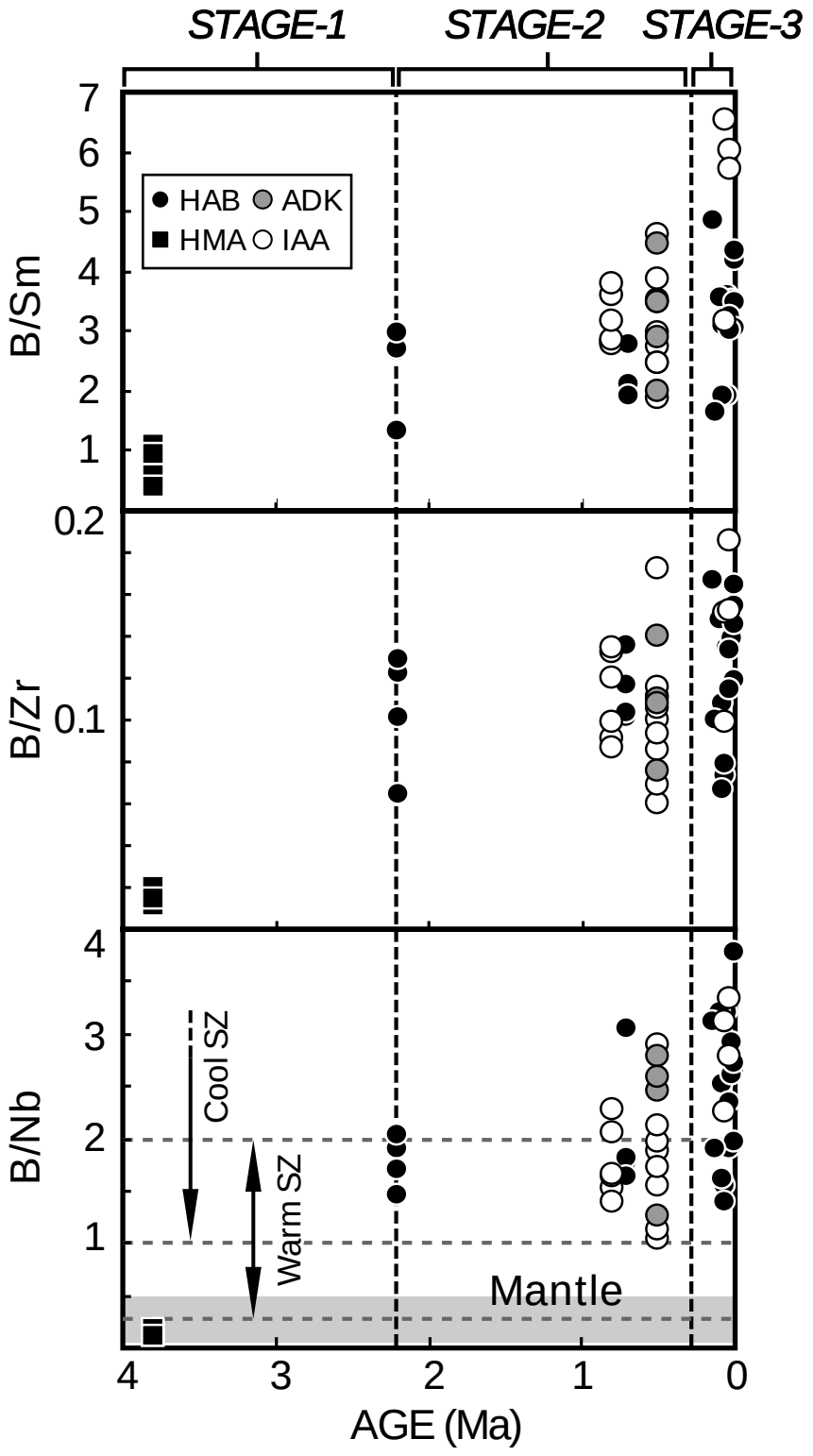

Fig. 2.34

K-Ar ages vs. B/Sm, B/Zr and B/Nb diagrams for the volcanic products from Aso area. Data for mantle: Ryan et al. (1996); Cool subduction zone (SZ) basalts: Moriguti et al. (2004) and Ishikawa and Tera (1997); Warm SZ: Leeman et al. (2004), Hochstaedter et al. (1996) and Hasenaka et al. (1993). Abbreviations: HAB = high-alumina basalt; HMA = high-magnesian andesite; ADK = adakitic andesite; IAA = Island-arc typr andesite.

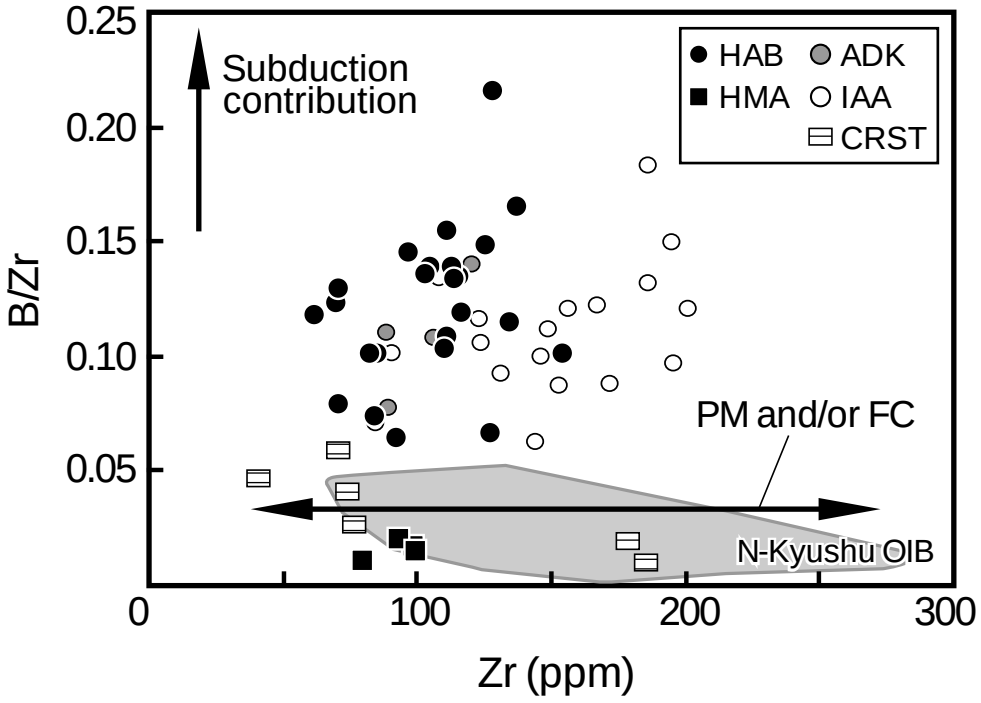

Fig. 2.35

Zr vs. B/Zr diagrams for volcanic products from Aso area. Up-arrow indicates involvement of subduction components. Right and left arrows show partial melting (PM) and/or fractional crystallization (FC) controlled processes. Abbreviations: HAB = high-alumina basalt; HMA = high-magnesian andesite; ADK = adakitic andesite; IAA = Island-arc typr andesite; CRST = crustal rocks. The shaded area shows the compositional range of the northern Kyushu OIB-type basalts. Data of these crustal rocks and OIB-type basalts are from Chapter 1.

high-Mg andesites (B/Sm = 0.4–1.0, B/Zr = 0.01–0.02, B/Nb = 0.1–0.2) are significantly lower than those of other volcanic products (1.8–4.5, 0.06–0.15, 1.0–3.3). In particular, the B/Nb ratios of the high-Mg andesites are the same as the mantle values (0.05–0.5: Ryan et al., 1996). On the other hand, the B/Sm, B/Zr and B/Nb ratios of the basaltic and andesitic products in the stage-2 are significantly higher than those of the high-Mg andesites. In this stage-2, the B/Nb ratios of the basaltic products are largely plotted in the field of the boundary between warm and cool subduction zone basalts (Fig. 2.34). In the stage-3, the basalts represent higher values and wider ranges of B/Sm, B/Zr and B/Nb ratios than those of the basalts in the stage-2. The andesitic products represent slightly higher values of B/Sm, B/Zr and B/Nb ratios than those of the andesites in the stage-2. Most of the stage-3 basalts are plotted in the field of the cool subduction zone basalts (Fig. 2.34).

These temporal changes of the B/Sm, B/Zr and B/Nb observed in the volcanic products from stage-1 to 3 probably indicate the increase of the subduction involvement. Fig. 2.35 shows the enrichments of B/Sm, B/Zr and B/Nb ratios observed in the volcanic products are not explained by the different degree of partial melting of source mantle material. The compositions of high-Mg andesites (B/Zr = 0.01–0.02) are similar to those of the northern Kyushu OIB-type basalts (B/Zr = 0.01–0.05). The fractional crystallization of these high-Mg andesites can not generate the high-alumina basalts and other andesites, because the B/Zr ratios of them are significantly higher than those of the high-Mg andesites. In addition, the enrichment of high-alumina basalts are not explained by the crustal assimilation processes of the most mafic sample, because the B/Zr ratios of the crustal rocks (0.01–0.06) are lower than the most mafic sample (0.07; Fig. 2.35).

As mentioned above, the temporal changes of petrography, major and trace element compositions observed in the Aso volcanic products probably indicate that the composition of magma source is entirely changed between stage-1 and -2. The cause of the drastic change of the composition of magma-source beneath Aso volcano probably is the commencement of subduction of the old segment of Philippine Sea plate. The geotherm was probably high in the stage-1; however, it was probably decreased by the

commencement of subduction. This major tectonic change probably provides a large amount of slab-derived fluid to the mantle beneath Aso volcano between 3.8 and 2.2 Ma.

2.7 Summary

1. The pre-caldera lavas are divided into the following eight groups on the basis of their phenocryst assemblages and SiO_2 contents: A) ol-cpx basalt; B) ol-opx-cpx andesite; C) opx-cpx andesite; D) ol-opx-cpx-hb andesite; E) opx-cpx-hb andesite; F) hb andesite; G) opx-cpx-hb dacite; H) hb-bt rhyolite.

The post-caldera volcanic products are divided into the following seven groups: I) 2px-rhyolite; II) bt-rhyolite; III) hb-dacite; IV) 2px-dacite; V) aphyric andesite; VI) porphyritic andesite; VII) basalt-basaltic andesite.

In addition, the high-Mg andesite lava erupted prior to the eight groups of the pre-caldera lavas is distributed in the western part of Aso caldera.

2. The results of the Rayleigh fractionation calculation indicate that at least four end-member magmas (I, V, VI and VII) for magma-mixing were existed in the post-caldera stage. In the present Aso, the mafic vents are distributed in the center of the caldera, and are surrounded by the silicic vents. These distributions do not indicate the existence of the huge single silicic magma chamber beneath caldera; however indicate the existence of multiple magma chambers.

3. Tochinoki lava (group V) is composed of two different lava types: silicic and phenocryst-rich lava (ST); mafic and phenocryst-poor lava (MT). The Tochinoki lava observed in the borehole core sample is the composite lava which is composed of these ST and MT.

The results of the mass-balance equations indicate that the major element composition of the most silicic core sample is produced by the fractionation of plagioclase, orthopyroxene, clinopyroxene and magnetite from the most mafic one. This result is well consistent with the results of the Rayleigh fractionation calculations.

The silicic-over-mafic layered structure observed in the core sample is the

inversion of the mafic-over-silicic layered pyroclastic fall-out deposits erupted from the compositionally zoned-magma chamber which has the silicic-over-mafic zonation. This layered structure is probably formed within the vent before eruption by the viscous segregation process of magma.

The whole-rock and mineral compositions of the core samples are different from those of the outcrop samples. This indicates that these core and outcrop samples probably are contemporaneous different lava flow units.

4. The magmatism in Aso area is divided into the following three stages on the basis of the petrological characteristics of the basaltic and andesitic products: 1) 3.8 Ma: the activity of high-Mg andesite; 2) from 2.2 Ma to 290 ka: the coexistence of high-Al basalt, Island arc-type andesite and adakitic andesite; 3) after 290 ka: the activities of high-Al basalt and Island arc-type andesite.

The origin of the high-Mg andesite is probably similar to that of other northern Kyushu high-Mg andesite, because the eruption age and incompatible element compositions of the former overlap with those of the latter. The B/Sm, B/Zr and B/Nb ratios of these high-Mg andesites are significantly low. In particular, the B/Nb ratio of the high-Mg andesite is similar to the mantle value. This indicates that the slab-derived material was not transported to the mantle beneath Aso area in the stage-1.

After 2.2 Ma, the activities of arc-type magmas are pronounced. The activity of adakitic andesite which erupted in the stage-2 probably indicates the subducted oceanic slab was partially molten. The volcanic products erupted after 2.2 Ma have significantly higher B/Sm, B/Zr and B/Nb ratios than those of the high-Mg andesite. These increases were probably caused by the fluid addition to the mantle beneath Aso area which is associated with the commencement of subduction of the Philippine Sea plate between 3.8 and 2.2 Ma.

Acknowledgements

I express my gratitude to Prof. Toshiaki Hasenaka for his supervise and encouragement.

I also express my gratitude to Dr. Hideaki Matsue, Mr. Hiroyuki Sawahata and Mr. Mitsunori Ishimoto for their help in organizing the prompt gamma-ray analysis at Japan atomic energy agency (JAEA). Technical support for XRF analysis was provided by Dr. Yasushi Mori at Kitakyushu Museum of Natural History and Human History. Mr. Takuya Matsuzaki is thanked for EPMA at Institute for Study of the Earth's Interior, Okayama University.

I am grateful to Dr. Yasuaki Sudo for access to the borehole core samples of Tochinoki lava. This study could not be performed without support of Mr. Shin Yoshikawa and other staffs of Aso Volcanological Laboratory, Kyoto University.

I am also grateful to Prof. Takaaki Fukuoka, Dr. Takashi Sano, Associate Prof. Shigeru Yamashita, Prof. William P. Leeman, Prof. Jun-Ichi Kimura, Dr. Akihiko Tomiya, Associate Prof. Masao Ban and Dr. Katsuya Kaneko for their helpful comments and critical suggestions on this study.

I thank Ms. Hitomi Kato for her PGA data, and Dr. Kuniyuki Furukawa, Dr. Taro Shinmura, Ms. Madoka Shimono, Mr. Kosuke Yatsuda Mr. Takuya Edamura and Ms. Maiko Morinaga for helping fieldwork. I also thank Mr. Takashi Nasu, Mr. Hideki Uemura, Ms. Yuka Takae and Ms. Yuko Sekiguchi for discussions in the seminar.

I would like to express my hearty thanks to my parents, Takashi Miyoshi, Hiromi Miyoshi and my dearest friend, Ms. Keiko Tanaka for their warm encouragement and support.

This work has been partially supported by the Fukada Geological Institute Foundation.

References

Abbey, S., 1983. Studies in "Standard Samples" of Silicate Rocks and Minerals 1969-1982. Canadian Geological Survey Paper 114, 83-15.

Bebout, C. E., Ryan J. G., Leeman, W. P., Bebout, A. E., 1999. Fractionation of trace elements by subduction-zone metamorphism: Effect of convergent-margin thermal evolution. Earth Planet. Sci. Lett. 171, 63-81.

Blake, S., Campbell, I.H., 1986. The dynamics of magma-mixing during flow in volcanic conduits. Contrib. Mineral. Petrol. 94, 72-81.

Brophy, J.G., Dreher S.T., 2000. The origin of composition gaps at South Sister volcano, central Oregon: implications for fractional crystallization processes beneath active calc-alkaline volcanoes. J. Volcanol. Geotherm. Res. 102, 287-307.

Bryan, W.B., Finger, L.W., Chayes, F., 1969. Estimating proportions in petrographic mixing equations by least-squares approximation. Science 163, 926-927.

Carmichael, I. S. E., 1967. The iron-titanium oxides of salic volcanic rocks and their associated ferromagnesian silicates. Contrib. Mineral. Petrol. 14, 36-64.

Carr, M., 1999. Program Igpet. Terra Softa Inc., Somerset, New Jersey, U.S.A.

Carrigan, R.C., 1994. Two-component magma transport and the origin of composite intrusions and lava flows. In Magmatic systems (Ryan, M. P. Ed). Academic Press, London, 319-354.

Carrigan, R.C., Eichelberger, J.C., 1990. Zoning of magmas by viscosity in volcanic conduits. Nature, 343, 248-251.

Chaussidon, M., Marty, B., 1995. Primitive boron isotope composition of the mantle. Science 269, 383-386.

Chaussidon, M., Jambon, A., 1994. Boron content and isotopic composition of oceanic basalts: Geochemical and cosmochemical implications. Earth Planet. Sci. Lett. 121, 277-291.

Chen, C. H., DePaolo, D. J., Nakada, S., Shieh, Y. N., 1993. Relationship between eruption volume and neodymium isotopic composition at Unzen volcano. Nature 362, 831-834.

Defant, M. J., Drummond, M. S., 1993. Mount St. Helens: Potential examples of the partial melting of the subducted lithosphere in a volcanic arc. Geology 21, 547-550.

Defant, M. J., Drummond, M. S., 1990. Derivation of some modern arc magmas by melting of young subducted lithosphere. Nature 347, 662-665.

Flanagan, F.J., 1976. Descriptions and Analysis of Eight New USGS Rock Standards. U.S. Geological Survey Professional Paper 840, 192.

Govindaraju, K., 1994. 1994 Compilation of Working Values and Descriptions for 383 Geostandards. Geostandards Newsletter 18, 1-158.

Green, T. H., 1994. Experimental studies of trace-element partitioning applicable to igneous petrogenesis—Sedona 16 years later. Chemical Geol. 117, 1-36.

Hasenaka, T., Yoshida, T., Aoki, K., 1993. Michoacan-Guanajuato volcanic field, Mexico: 1. Trace element geochemistry of alkaline and calc-alkaline rocks. Res. Rep. Lab. Nucl. Sci., Tohoku Univ. 26, 256-277.

Hickey-Vergas, R., 2006. Basalt and tonalite from the Amami plateau, northern west Philippine basin: new early Cretaceous ages and geochemical results, and their petrologic and tectonic implications. The Island Arc 14, 653-665.

Hickox, C. E., 1971. Instability due to viscosity and density stratification in axisymmetric pipe flow. Phys. Fluids. 14, 251-262.

Hilde, T. W.C., Lee, C. – S., 1984. Origin and evolution on the west Philippine basin: a new interpretation. Tectonophysics 102, 85-104.

Hoang, N., Uto, K., 2003. Geochemistry of Cenozoic basalts in the Fukuoka district (northern Kyushu, Japan): implications for asthenosphere and lithospheric mantle interaction. Chemical Geol. 198, 249-268.

Hochstaedter, A. G., Ryan, J. G., Luhr, J. F., Hasenaka, T., 1996. On B/Be ratios in the Mexican volcanic belt. Geochim. Cosmochim. Acta 60, 613-628.

Hunter, A.G., 1998, Intracrustal controls on the coexistence of tholeiitic and calc-alkaline magmaseries at Aso volcano, SW Japan. J. Petrol., 39, 1255-1284.

Huppert, H.E., Sparks, R.S., 1988. The generation of granitic magmas by intrusion of basalt into continental crust. J. Petrol. 29, 599-624.

Ishida, M., 1992. Geometry and relative motion of the Philippine Sea plate and Pacific plate beneath the Kanto-Tokai district, Japan. J. Geophys. Res. 97, 489-513.

Ikawa, T., Nagao, T., 1996. Genetic relationships between basalts and andesites in the Taradake volcanic area, Northwest Kyushu. J. Miner. Petrol. Econ. Geol. 91, 321-338 (in Japanese with English abstract).

Ishikawa, T., Tera, F., Nakazawa, T., 2001. Boron isotope and trace element systematics of the three volcanic zones in the Kamchatka arc. Geochim. Cosmochim. Acta 65, 4523-4537.

Ishikawa, T., Tera, F., 1999. Two isotopically distinct fluid components involved in the Mariana arc: Evidence from Nb/B ratios and B, Sr, Nd, and Pb isotope systematics. Geology 27, 83-86.

Ishikawa, T., Tera, F., 1997. Source, composition and distribution of the fluid in the Kurile mantle wedge: Constraints from across-arc variations of B/Nb and B isotopes. Earth Planet. Sci. Lett. 152, 123-138.

Ishikawa, T., Nakamura, E., 1994. Origin of the slab component in arc lavas from across-arc variation of B and Pb isotopes. Nature 370, 205-208.

Ishikawa, T., Nakamura, E., 1993. Boron isotope systematics of marine sediments. Earth Planet. Sci. Lett. 117, 567-580.

Iwamori, H., 2007. Transportation of H2O beneath the Japan arcs and its implications for global water circulation. Chem. Geol. doi:10.1016/j.chemgeo.2006.08.011.

Kakubuchi, S., Kido, M., Hikosan Collaborative Research Group, 1995. High-magnesian andesites from the northwestern margin of the Pliocene Kuju-Beppu Tectonic Basin, northern Kyushu, Japan. Mem. Geol. Soc. Japan. 44, 125-138.

Kakubuchi, S., Matsumoto, Y., 1990. Primitive tholeiitic basalt from the Yabakei district, Oita prefecture, Southwest Japan. J. Miner. Petrol. Econ. Geol. 85, 559-568 (in Japanese with English abstract).

Kakubuchi, S., Nagao, T., Kagami, H., 1994. Genetic relationship between tholeiite and alkali basalts of the Kitamatsuura basalts, northwestern Kyushu, Japan. J. Miner. Petrol. Econ. Geol. 89, 41-55 (in Japanese with English abstract).

Kamata, H., 1989. Volcanic and structural history of the Hohi volcanic zone, central Kyushu, Japan. Bull. Volcanol. 51, 315-332.

Kamata, H., 1985. Stratigraphy and eruption age of the volcanic rocks in the west of Miyanoharu area, Kumamoto prefecture—Age and distribution of the volcanic activity of central-north Kyushu, Japan—. J. Geol. Soc. Jpn. 91, 289–303.

Kamata, H., Kodama, K., 1994. Tectonics of an arc-arc junction: an example from Kyushu Island at the junction of the southwest Japan arc and Ryukyu arc. Tectonophysics 233, 69-81.

Kamata, H., Kobayashi, T., 1997. The eruptive rate and history of Kuju volcano in Japan during the past 15,000 years. J. Volcanol. Geotherm. Res. 76, 163-171.

Kaneoka, I., Ojima, M., 1970. On the radiometric ages of volcanic rocks from Japan. Bull. Volcanol. Soc. Jpn. 15, 10–21 (in Japanese with English abstract).

Kimura, J. - I., Stern, R. J., Yoshida, T., 2005. Reinitiation of subduction and magmatic responses in SW Japan during Neogene time. Geol. Soc. Amer. Bull. 117, 969-986.

Kita, I., Yamamoto, M., Asakawa, Y., Nakagawa, M, Taguchi, S., Hasegawa, H., 2001. Contemporaneous ascent of within-plate type and island-arc type magmas in the Beppu-Shimabara graben system, Kyushu island, Japan. J. Volcanol. Geotherm. Res. 111, 99-109.

Kobayashi, T., 1984. Geology of Yufu-Tsurumi volcanoes and their latest eruptions. Mem. Geol. Soc. Jpn. 24, 93-108 (in Japanese with English abstract).

Kuno, H., 1960. High-alumina basalt. J. Petrol. 1, 121–145.

Leeman, W. P., Sisson, V. B., 1996. Geochemistry of boron and its implications for crustal and mantle processes, in: E. S. Grew, L. M. Anovitz (Eds.), Boron: Mineralogy, Petrology and Geochemistry. Rev. Mineral. 33, Mineral. soc. Am., Washington, DC, pp. 645-707.

Leeman, W. P., Smith, D. R., Hildreth, W., Palacz, Z., Rogers, N., 1990. Compositional diversity of late Cenozoic basalts in a transect across the southern Washington Cascades: Implications for subduction zone magmatism. 95, 19561-19582.

Leeman, W. P., Tonarini, S., Chan, L. H., Borg, L. E., 2004. Boron and Lithium isotopic variations in a hot subduction zone — the southern Washington Cascades.

Chem. Geol. 212, 101-124.

Leeman, W. P., Lewis, J. F., Evarts, R. C., Conrey, R. M., Sttreck, M. J., 2005. Petrologic constraints on the thermal structure of the Cascades arc. J. Volcanol. Geotherm. Res. 140, 67-105.

LeMaitre, R. W., Bateman, P., Dudek, A., Keller, J., LameyreLeBas, M. J., Sabine, P, A., Schmid, R., Sorensen, H., Streckeisen, A., Woolley, A. R., Zanettin, B., 1989. A classification of igneous rocks and glossary of terms: Oxford, Blackwell.

MacDonald, G. A., Katsura, T., 1964. Composition and origin of Hawaiian lavas: J. Petrol. 5, 83-133.

Masuda, N., Watanabe, K., Miyabuchi, Y., 2004, Rhyolite to Dacite Lava Flows Newly-discovered on the Western Slope of Aso Central Cones, Southwestern Japan. Bull. Volcanol. Soc. Japan, 49, 119-128.

Matsui, T., Shibata, K., 1976. K-Ar ages of basalts in northwest Kyushu. Bull. Volcanol. Soc. Jpn. 21, 207 (in Japanese).

Matsumoto, H., Yamagata, S., Itaya, T., 1992. K-Ar ages and main chemical compositions of basaltic rocks from northern Kyushu and Shimonoseki city, southwest Japan. In: Ishida, S. (Ed.), Exploration of Volcanoes and Rocks in Japan, China and Antarctica. Yamaguchi Univ., Yamaguchi, Japan, pp. 247-264.

Matsumoto, A., Uto, K., Ono, K., Watanabe, K., 1991. K–Ar age determinations for Aso volcanic rocks—concordance with volcanostratigraphy and application to pyroclastic flows. Programme and Abstracts of Volcanol. Soc. Jpn. 1991, no. 2, p. 73 (in Japanese).

Miyabuchi, Y., Masuda, N., Watanabe, K., 2004, Geologic History of the Western Part of Post-caldera Central Cones of Aso Volcano, Southwestern Japan, Based on Stratigraphic Relationships between Lava Flows and Airfall Tephra Layers. Bull. Volcanol. Soc. Japan, 49, 267-282.

Moran, A. E., Sisson, V. B., Leeman, W. P., 1992. Boron depletion during progressive metamorphism: implications for subduction process, Earth Planet. Sci. Lett. 111, 331-349.

Mori, Y., Mashima, H., 2005. X-ray fluorescence analysis of major and trace elements

in silicate rocks using 1:5 dilution glass beads. Bulletin of the KitaKyushu museum of natural history and human history series A (Natural History) pp. 12.

Moriguti, T., Shibata, T., Nakamura, E., 2004. Lithium, boron and lead isotope and trace element systematics of Quaternary basaltic volcanic rocks in northeastern Japan: mineralogical controls on slab-derived fluid composition. Chem. Geol. 212, 81-100.

Nagamune, T., Tashiro, H., 1989. Shape of the Wadati-Benioff zone beneath Kyushu, Japan. J. Seismol. Soc. Jpn. 42, 13-19 (in Japanese with English abstract).

Nagao, T., Hase, Y., Nagamine, S., Kakubuchi, S., Sakaguchi, K., 1999. Late Miocene to middle Pleistocene Hisatsu volcanic rocks generated from heterogeneous magma sources: Evidence from temporal-spatial variation of distribution and chemistry of the rocks. J. Miner. Petrol. Econ. Geol. 94, 461-481 (in Japanese with English abstract).

Nagao, T., Sawai, O., Itaya, T., Kakubuchi, S., 1992. K-Ar ages and petrological characteristics of the tholeiitic basalts and high-magnesian andesite from Amakusa-Shimoshima, Kumamoto prefecture, SW Japan. J. Miner. Petrol. Econ. Geol. 87, 283-290 (in Japanese with English abstract).

Nakada, S., Kamata, H., 1991. Temporal change in chemistry of magma source under central Kyushu, southwest Japan: progressive contamination of mantle wedge. Bull. Volcanol. 53, 182-194.

Nakada, S., Motomura, Y., 1997. Magma chamber of Unzen volcano and origin of phenocrysts and enclaves. Bull. Volcanol. Soc. Jpn. 42, 167-174 (in Japanese with English abstract).

Ogata, M., Takaoka, N., 1991. K-Ar ages of volcanic rocks from the Taradake area. Bull. Volcano. Soc. Jpn. 36, 187-191 (in Japanese with English abstract).

Ohta, T., Hasenaka, T., Ban, M., Sasaki, M., 1992. Characteristic geology and petrology of non-arc type volcanism at Oninomi monogenetic volcano, Yufu-Tsurumi graben. Bull. Volcanol. Soc. Jpn. 37, 119-131 (in Japanese with English abstract).

Ohta, T., Hasenaka, T., Fujimaki, H., 1990. Geology and petrography of Yufu-Tsurumi

volcano group, Oita prefecture. J. Miner. Petrol. Econ. Geol. 85, 113-129 (in Japanese with English abstract).

Okino, K., Shimakawa, Y., Nagaoka, S., 1994. Evolution of the Shikoku basin. J. Geomag. Geoelectr. 46, 463-479.

Okuno, M., 2002, Chronology of tephra layers in southern Kyushu, SW Japan, for the last 30000 years. The Ouaternary Research (Daiyonki-Kenkyu) 41, 225-236.

Ono, K., Watanabe, K., 1985. Geological map of Aso volcano, 1: 50,000. Geological map of volcanoes 4. Geol. Surv. Jpn (in Japanese with English abstract).

Ono, K., Watanabe, K., 1983. The Aso caldera. The Earth Monthly 5, 73–82 (in Japanese).

Ono, K., 1965. Geology of the eastern part of Aso caldera, central Kyushu, southwest Japan. J. Geol. Soc. Japan 71, 541-553.

Peacock S. M., Herving, R. L., 1999. Boron isotopic composition of subduction-zone metamorphic rocks. Chemical Geol. 160, 281-290.

Peacock, S. M., Wang, K., 1999. Seismic consequences of warm versus cool subduction metamorphism: examples from southwest and northeast Japan. Science 286, 937-939.

Pitman III, W. C., R. L., Larson, E. M., Herron, 1974. Age of the ocean basins determined from magnetic anomaly lineations. Geol., Soc., Amer. Map and chart series, MC-6.

Rickwood, P.C., 1989. Boundary lines within petrologic diagrams which use oxides of major and minor elements. Lithos 22, 247–264.

Rollinson, H.R., 1993. Using geochemical data: evaluation, presentation, interpretation. Longman Singapore Publ. ltd. p. 352,

Ryan, J. G., Leeman, W. P., Morris, J. D., Langmuir, C. H., 1996. The boron systematics of intraplate lavas: Implications for crust and mantle evolution. Geochim. Cosmochim. Acta 60, 415-422.

Ryan, J. G., Langmuir, C. H., 1993. The systematics of boron abundances in young volcanic rocks. Geochim. Cosmochim. Acta 57, 1489-1498.

Sadeghi, H., Suzuki, S., Takenaka, H., 2000. Tomographic low-velocity anomalies in

the uppermost mantle around the northeastern edge of Okinawa trough, the backarc of Kyushu. Geophys. Res. Lett. 27, 277-280.

Sano T., Fukuoka, T., Hasenaka, T., 2004. Determination of chlorine contents in Geological Survey of Japan reference materials by prompt gamma neutron activation analysis. Geostandards and Geoanalytical Res. 28, 443-448.

Sano, T., 2002. Determination of major and trace element contents in igneous rocks by X-ray fluorescence spectrometer analysis. Bull. Fuji Tokoha Univ. pp. 59.

Sano, T., Hasenaka, T., Shimaoka, A., Yonezawa, C., Fukuoka, T., 2001. Boron contents of Japan Trench sediments and Iwate basaltic lavas, northeast Japan arc: estimation of sediment-derived fluid contribution in mantle wedge. Earth Planet. Sci. Lett. 186, 199-213.

Sano, T., 1995. Geology of Iki volcano group: Lava flow-stratigraphy mainly based on K-Ar dating. Bull. Volcanol. Soc. Jpn. 40, 329-347 (in Japanese with English abstract).

Sano, T., Fukuoka, T., Hasenaka, T., Yonezawa, C., Matsue, H., Sawahata, H., 1999. Accurate and efficient determination of boron content in volcanic rocks by neutron induced promptγ-ray analysis. J. Radioanal. Nucl. Chem. 239, 613-617.

Schmincke, H.U., 2004. Volcanism. Springer, Berlin, p. 324

Shibata, K., Mizuno, A., Yuasa, M., Uchida, S., Nakagawa, T., 1977. Further K-Ar dating of tonalite dredged from the Komahashi-Dani seamount. Bull. Geol. Surv. Jpn. 28, 1-4.

Shimoda, G., Tatsumi, Y., Nohda, S., Ishizaka, K., John, B.M., 1998. Setouchi high-Mg andesites revisited: geochemical evidence for melting of subducting sediments. Earth Planet. Sci. Lett. 160, 479–492.

Shinjo, S., Woodhead, J. D., Hergt, J. M., 2000. Geochemical variation within the northern Ryukyu Arc: magma source compositions and geodynamic implications. Contrib. Min. Petrol. 140, 263-282.

Shiraki, K., Miyamoto, M., Matsuo, H., Ueki, Y., Azuma, T., Nagao, T., Matsumoto, Y., Tajima, T., 2000. High-Mg andesites and basalts in the southern Nishisonogi peninsula, Nagasaki prefecture. Center of Instrumental Analysis, Yamaguchi Univ.

8, 24-37 (in Japanese with English abstract).

Shiraki, K., Yoshioka, K., Matsumoto, Y., 1995. Magnesian andesites in the Oono volcanic rocks, central Kyushu: westward continuation of the Setouchi volcanic belt. J. Geol. Soc. Jpn. 101, 387-392.

Shiraki, K., 1993. Generation of magnesian andesites in the Setouchi region. Mem. Geol. Soc. Jpn. 42, 255-266 (in Japanese with English abstract).

Sibuet, J. –C., Hsu, S. –K., Shyu, C. –T., Lin, C. –S., 1995. Structural and kinematic evolutions of the Okinawa Trough backarc basin, in Taylor, B., ed., Backarc basins: Tectonics and Magmatism: New York, Plenum Press, p. 347-379.

Sisson T.W. and Grove, T.L., 1993. Experimental investigations of the role of H_2O in calc-alkaline differentiation and subduction zone magmatism. Contrib. Mineral. Petrol. 113, 143-166.

Sisson, T.W., Grove, T.L., 1993b, Temperatures and H_2O contents of low-MgO high-alumina basalts. Contrib. Min. Petrol. 113, 167-184.

Smith, H. J., Spivack, A. J., Staudigel, H., Hart, S. R., 1995. The boron isotopic composition of altered oceanic crust. Chem. Geol. 126, 119-135.

Soya, T., Uto, K., Makimoto, H., Kamata, H., Okumura, K., Suto, S., 1984. Bulk and mineral chemistry of lavas and ejecta of the 1983 eruption of Miyakejima volcano. Bull. Volcanol. Soc. Jpn. 29, 283–296 (in Japanese with English abstract).

Sugimoto, T., Shibata, T., Yoshikawa, M., Takemura, M., 2006. Sr-Nd-Pb isotopic and trace element compositions of the Yufu-Tsurumi volcanic rocks: implications for the magma genesis of the Yufu-Tsurumi volcanoes, northeast Kyushu, Japan. J. Min. Petrol. Sci. 101, 270-275.

Sun, S. S., McDonough, W. F., 1989. Chemical and isotopic systematics of oceanic basalts: implications for mantle composition and processes, in: A. D. Saunders, M. J. Norry, (Eds.), Magmatism in the Ocean Basins. Geol. Soc. London. Spec. Publ. 42, pp. 315-345.

Takai, M., Miyachi, M., Hirano, I., 1984. Paleomagnetism and fission-track ages of Kinbo volcano, Southwest Japan. Rock Magnetism and Paleogeophys. 11, 21-25.

Tatsumi, Y., 2006. High-Mg andesites in the Setouchi volcanic belt, southwestern

Japan: analogy to Archean magmatism and continental crust formation? Annu. Rev. Earth Planet. Sci., 34, 467–499.

Tatsumi, Y., 2003. High-Mg andesitegenesis, continental crust formation and mantle evolution. University of Tokyo Press, p. 213.

Tatsumi, Y., 1995. Subduction zone magmatism—A contribution to whole mantle dynamics—. University of Tokyo Press, p. 186.

Tatsumi, Y., Ishizaka, K., 1982. Origin of high-magnesian andesites in the Setouchi volcanic belt, Southwest Japan: I, Petrographical and chemical characteristics. Earth Planet. Sci. Lett. 60, 293-404.

Tatsumi, Y., Torii, M., Ishizaka, K., 1980. On the age of the volcanic activity and the distribution of the Setouchi volcanic rocks —Age determination for Setouchi volcanic rocks, No. 5—. Bull. Volcanol. Soc. Jpn. 25, 171-179 (in Japanese with English abstract).

Tatsumi, Y., Ishizaka, K., 1978. K-Ar age of Sanukitoid from Yashima, Kagawa prefecture, Japan —Age determination for Setouchi volcanic rock series, No. 2—. J. Miner. Petrol. Econ. Geol. 73, 355-358 (in Japanese with English abstract).

Tonarini, S., Leeman, W. P., Civetta, L., D'Antonio, M., Ferrara, G., Necco, A., 2004. B/Nb and $\delta^{11}B$ systematics in the Phlegrean volcanic district, Italy. J. Volcanol. Geotherm. Res. 133, 123-139.

Uto, K., Hoang, N., Matsui, K., 2004. Cenozoic lithospheric extension induced magmatism in southwest Japan. Tectonophysics 393, 281-299.

Wang, Z., Zhao, D., 2006. Vp and Vs tomography of Kyushu, Japan: New insight into arc magmatism and forearc seismotectonics. Phys. Earth Planet. Inter. 157, 269-285.

Watanabe, K., Itaya, T., Ono, K., Takada, H., 1989. K-Ar ages of dike rocks in the southwestern region of Aso caldera, Kyushu, Japan. Bull. Volcanol. Soc. Jpn. 34, 189–195 (in Japanese with English abstract).

Watanabe, K., 2001. History and activity of Aso volcano (Japanese title "Aso kazan no oitachi"). Ichinomiya-cho, Japan. (in Japanese).

Watts, R.B., Silva, S.L., Rios, G.J., Croudace, I., 1999. Effusive eruption of viscous

silicic magma triggered and driven by recharge: a case study of the Cerro Chascon-Runtu Jarita dome complex in southwest Bolivia. Bull. Volcanol. 60, 241-264.

Wedepohl, K. H., 1995. The composition of the continental crust. Geochim. Cosmochim. Acta 59, 1217-1232.

Wells, P. R. A., 1977. Pyroxene thermometry in simple and complex systems. Contrib. Mineral. Petrol. 62, 129-139.

Wunder, B., Meixner, A., Romer, R. L., Wirth, R., Heinrich, W., 2005. The geochemical cycle of boron: Constraints from boron isotope partitioning experiments between mica and fluid. Lithos 84, 206-216.

Yokose, H., Yanashima, T., Kikuchi, W., Sugiyama, N., Shinohara, A., Takeuchi, T., Nagao, K., Kodama, K., 1999. Episodic magmatism since 5 Ma in the western part of Beppu-Shimabara graben, Kyushu, Japan. J. Miner. Petrol. Econ. Geol. 94, 338–348 (in Japanese with English abstract).

Yokose, H., Yamamoto, S., 1996. Crustal xenolith from the Kinbo volcanic rocks: Part 1 deep-crustal components of northwest Kyushu. J. Miner. Petrol. Econ. Geol. 91, 86–101 (in Japanese with English abstract).

Yonezawa, C., 1993. Prompt γ-ray analysis of elements using cold and thermal reactor guided neutron beams. Anal. Sci. 9, 185–193.

Zhao, D., Asamori, K., Iwamori, H., 2000. Seismic structure and magmatism of the young Kyushu subduction zone. Geophys. Res. Lett. 27, 2057-2060.

Zhao, D., Hasegawa, A., Horiuchi, S., 1992. Tomographic imaging of P and S wave velocity structure beneath Northeastern Japan. J. Geophys. Res. 97, 19909–19928.

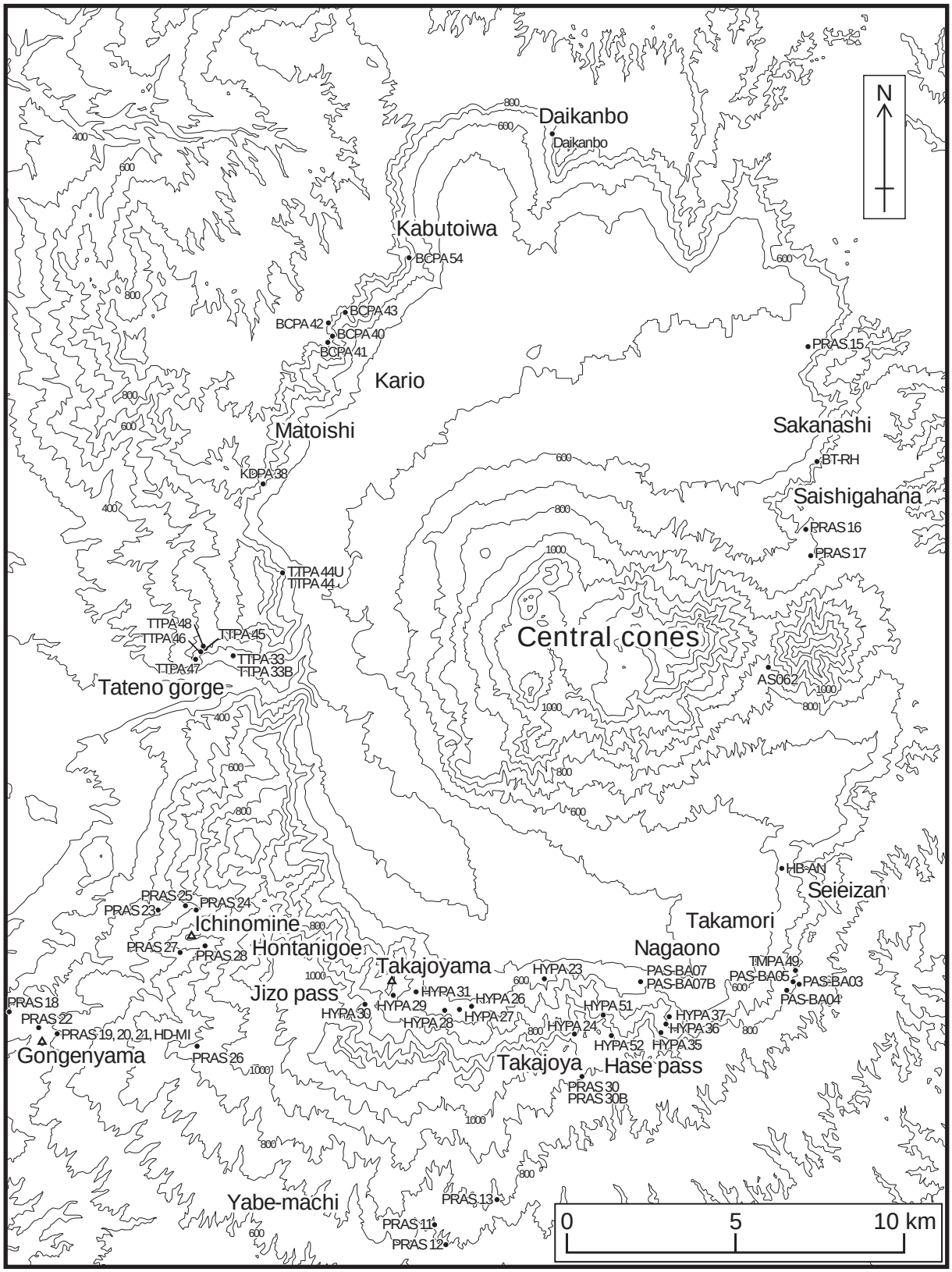

Appendix 1

Sample locality map of pre-caldera volcanic rocks.

Refereed papers

1. Masaya Miyoshi, Takaaki Fukuoka, Takashi Sano, Toshiaki Hasenaka, 2008. Subduction influence of Philippine Sea plate on the mantle beneath northern Kyushu, SW Japan: an examination of Boron contents in basaltic rocks. *Journal of Volcanology and Geothermal Research*, **171**, 73-87.

2. Masaya Miyoshi, Madoka Shimono, Toshiaki Hasenaka, Takashi Sano, Takaaki Fukuoka, 2008. Determination of boron contents in volcanic rocks by prompt-gamma ray analysis: an application to magma genesis in Kyushu island, SW-Japan. *Journal of Radioanalytical and Nuclear Chemistry*, in press.

3. Masaya Miyoshi, Takashi Nasu, Toshihiko Tajima, Michio Kido, Yasushi Mori, Toshiaki Hasenaka, Hidetoshi Shibuya, Keisuke Nagao, 2008. K-Ar ages of high-magnesian andesite lavas from northern Kyushu, Japan. *Journal of Mineralogical and Petrological Sciences*, in press.

4. Masaya Miyoshi, Toshiaki Hasenaka, Yasushi Mori, Shigeru Yamashita, 2007. Origin of compositional heterogeneity within Tochinoki andesite lava flow from the western part of Aso caldera. *Journal of Mineralogy, Petrology and Economic Geology*, **36**, 15-29 (in Japanese with English abstract).

5. Masaya Miyoshi, Toshiaki Hasenaka, Takashi Sano, 2005. Genetic relationships of compositionally diverse magmas from Aso post-caldera volcanism. *Bulletin of Volcanological Society of Japan*, **50**, 269-283 (in Japanese with English abstract).